How lipid specific T cells become effectors

A Dissertation

SUBMITTED TO THE FACULTY OF THE

UNIVERSITY OF MINNESOTA

BY

Haiguang Wang

IN PARTIAL FULFLIMENT OF THE REQUIREMENTS

FOR THE DEGREE OF

DOCTOR OF PHILOSOPHY

Adviser: Kristin A. Hogquist, Ph.D.

April 2019

Abstract

Invariant natural killer T (iNKT) cells are composed of at least three functionally distinct subsets, NKT1, NKT2 and NKT17. Through selective activation of these three iNKT effector subsets, iNKT cells can modulate immune responses and tissue homeostasis in different fashions. However, the developmental steps that drive iNKT cells into functional distinct subsets have not been elucidated, and thus their potential to be utilized in anti-cancer or autoimmune immunotherapies has not been realized, despite the fact that iNKT stimulatory lipids are well-tolerated in human trials. My dissertation research aims to fill this knowledge gap by investigating the following aspects of iNKT biology: 1) characterizing the multipotent progenitor for the iNKT effector subsets (in chapter 2); 2) isolating the critical factors that determine how individual iNKT subsets are derived, with a focus on NKT2 cells (in chapter 3); 3) characterizing how distinct iNKT effector subsets specifically modulate protective host immune responses (in chapter 2 & 3); and 4) technical improvement in advancing more accurate analysis of *ex vivo* iNKT cells (in chapter 4).

Firstly, in chapter 2, I demonstrate that the small proportion of thymic iNKT cells that express CCR7 represent a multi-potent progenitor pool that gives rise to effector subsets within the thymus. These $CCR7^{+}$ iNKT cells also emigrate from the thymus in a *Klf2* dependent manner, undergo further

maturation after reaching the periphery. Furthermore, *Ccr7* deficiency impaired differentiation of iNKT effector subsets and localization to the medulla. Parabiosis and intra-thymic transfer showed that thymic NKT1 and NKT17 were resident-they were not derived from and did not contribute to the peripheral pool. Finally, each thymic iNKT effector subset produces distinct factors that influence T cell development.

Secondly, previous studies showed IL-4 is produced by NKT2 cells in the thymus, where it conditions $CD8^+$ T cells to become “memory like” amongst other effects in the steady state. However, the signals that cause NKT2 cells to constitutively produce IL-4 remain poorly defined, where in the chapter 3, these signals were investigated. Using histocytometry, IL-4 producing NKT2 cells were localized to the thymic medulla, suggesting medullary signals might instruct NKT2 cells to produce IL-4. Moreover, NKT2 cells receive and require TCR stimulation for continuous IL-4 production at steady state, since NKT2 cells lost IL-4 production when intra-thymically transferred into *Cd1d* deficient recipients. In bone marrow chimeric recipients, only hematopoietic, but not stromal APC, provided such stimulation. Furthermore, using different Cre-recombinase transgenic mouse strains to specifically target CD1d deficiency to various APC, together with the use of diphtheria toxin receptor (DTR) transgenic mouse strains to deplete various APC, we found that macrophages were the predominant cell to stimulate NKT2 IL-4 production.

Lastly, it has been recently shown that high extracellular ATP concentrations or NAD-mediated P2RX7 ribosylation by the enzyme ARTC2.2 can induce P2RX7 pore formation and cell death. Because both ATP and NAD are released during tissue preparation for analysis, cell death through these pathways may compromise the analysis of iNKT. The expression of ARTC2.2 and P2RX7 on distinct iNKT subsets is unclear, however, as is the impact of recovery from other nonlymphoid sites. Therefore, in the chapter 4, I showed NKT1 cells express high levels of both ARTC2.2 and P2RX7 compared with NKT2, NKT17 cells. Furthermore, I demonstrated that ARTC2.2 blockade enhanced NKT1 recovery from nonlymphoid tissues during cell preparation. Moreover, blockade of this pathway was essential to preserve functionality, viability, and proliferation of iNKT cells. Therefore, short-term *in vivo* blockade of the ARTC2.2/P2RX7 axis permits much improved flow cytometry–based phenotyping and enumeration of murine iNKT from nonlymphoid tissues, and it represents a crucial step for functional studies of this population.

Altogether, I believe the findings here provide a clearer understanding of how the lipid specific iNKT cells become effector subsets as well as a technical improvement for accurate analysis of these cells.

Acknowledgement

First and foremost, I want to thank my advisor, Kris Hogquist. She is an excellent scientist and very nice person, I have highest respect for her. Best mentor ever, I am honored and grateful for being one of her students, I wouldn't be what I am without her. Also, thanks to Steve Jameson, for his input and support for my research.

Thanks to all past and present members in Hogquist and Jameson labs (Jamequist lab), for their encouragement, support and helpful feedback. Especially, You Jeong Lee, for his guidance and help during my rotation in the lab; Jane Ding, our lab manger, for keeping the lab running smoothly as well as encouragement and parties; Henrique Borges da Silva, Lily J. Qian, for all the help and support, greatly appreciate it; Elise Breed, Katie Block, Hristo Georgiev, Oscar Salgado, Thera Lee, Changwei Peng, Emily Truckenbrod, Daniel Walsh, Kristina Burrack, Kristin Renkema and Roland Ruscher were all essential parts of such a fun and motivating lab. People in the Center for Immunology (CFI), for their discussions, feedback and willingness to help. My graduate program, Lisa Hubinger, Mike Murtaugh, Mark Rutherford and Kent Reed were a tremendous support system. Moreover, I received generous help from my collaborators for the thesis projects, Mark Anderson and Corey Miller in UCSF. I also want to express my gratitude for members in my thesis committee, Bruce Walcheck, David Masopust and Jim Lokensgard, I

appreciate all your advice and guidance, it has been helpful for shaping me into a better scientist.

Most of all, I want to thank my parents, for their enormous love and support. I can’t make it through without them.

Dedication

For the loved ones.

Table of Contents

List of Tables

List of Figures

Chapter 1

Introduction

Natural killer T cells (NKT) were named because they express T cell receptor (TCR)–CD3 complexes as well as the natural killer (NK) cell receptor NK1.1 (CD161) (1, 2). Later, research discovered that NKT cells express a semi-invariant TCR, characterized by a Vα14-Jα18 TCRα chain coupled with a limited Vβ repertoire (Vβ2, Vβ7, or Vβ8.2) in mice, and an invariant Vα24-Jα18 paired with Vβ11 in humans (3, 4). Owning to this semi-invariant TCR, invariant natural killer T (iNKT) cells recognize self- and foreign-lipid antigens presented by the CD1d molecule and could be specifically detected using CD1d tetramer loaded with a cognate lipid antigen.

iNKT cells originate in the thymus, but in contrast to the conventional peptide specific $CD4^+$ or $CD8^+$ T cells, which are positively selected by cortical thymic epithelial cells, the positive selection of iNKT cells solely relies on the interactions among cortical double-positive (DP) thymocytes (5-8). DP thymocytes expressing the rearranged Vα14-Jα18 TCR recognize high-affinity lipid antigens presented by CD1d molecules on neighboring DP thymocytes (4). iNKT cells highly express the transcription factor promyelocytic leukemia zinc finger protein PLZF (*zbtb46*), which is essential for their effector program (9, 10), for specifying the tissue-resident properties of iNKT cells, and for their ability to produce cytokines early after stimulation (9-11).

It has been realized that iNKT cells are a heterogenous population, and recent evidence from various groups suggest that there are three major functional

iNKT subsets at steady state according to their expression of lineage-specific transcription factors and cytokine-producing potential. The three iNKT subsets are designated NKT1, NKT2, and NKT17, in analogy to the classical CD4 T helper lineages. NKT1 cells are PLZF^{low} T-bet^{+} and produce both IFN-γ and low amounts of IL-4 after stimulation. They express NK1.1 and other NK receptors and represent the subset that "NKT" cells were named after. NKT2 and NKT17 cells, in contrast, do not express NK1.1. NKT2 cells are PLZF^{high} and produce high amounts of IL-4 at steady state and after stimulation. NKT17 cells are PLZF^{intermediate} ROR-γt^{+} and produce IL-17 after stimulation (12). Through intra-thymic transfer and fetal thymic organ culture (FTOC), previous studies demonstrated that each iNKT subset (NKT1, NKT2, and NKT17) is terminally differentiated; i.e., do not give rise to other cell subsets (12-14). iNKT cells play diverse roles in immunity due in part to the existence of these three functional subsets.

The Development and Differentiation of iNKT Cells

Initial Positive Selection

Like the conventional CD4^{+} and CD8^{+} T cells, iNKT cells originate from precursors undergoing TCR gene rearrangement in the thymus. A lineage tracing study using transgenic mice (ROR-γt–Cre × ROSA26^{lsl}-EGFP) in which ROR-γt triggers permanent expression of green fluorescent protein (GFP) confirmed that iNKT cells were derived from ROR-γt^{+} DP thymocytes in

the thymus (5) (Figure 1-1 “Selection”), while a minor population could arise from DN thymocytes bypassing DP stage (15). Moreover, ROR-γt itself is essential for iNKT cell generation, in that, it supports DP survival through regulating Bcl-xL expression, allowing for optimal rearrangement of Vα14-Jα18 TCR chains (16). Similarly, an E protein transcription factor, HEB, promotes survival of DP thymocytes through regulating both ROR-γt and Bcl-xL expression, which opens the window of time to allow distal Jα rearrangement (17). Downstream of the initial selection of DP thymocytes, c-Myc has been shown to control the maturation of iNKT cells (18, 19). Moreover, c-Myb has also been shown to play a central role in this process, as it supports long half-life of DP thymocytes to allow Vα14 to Jα rearrangement (20).

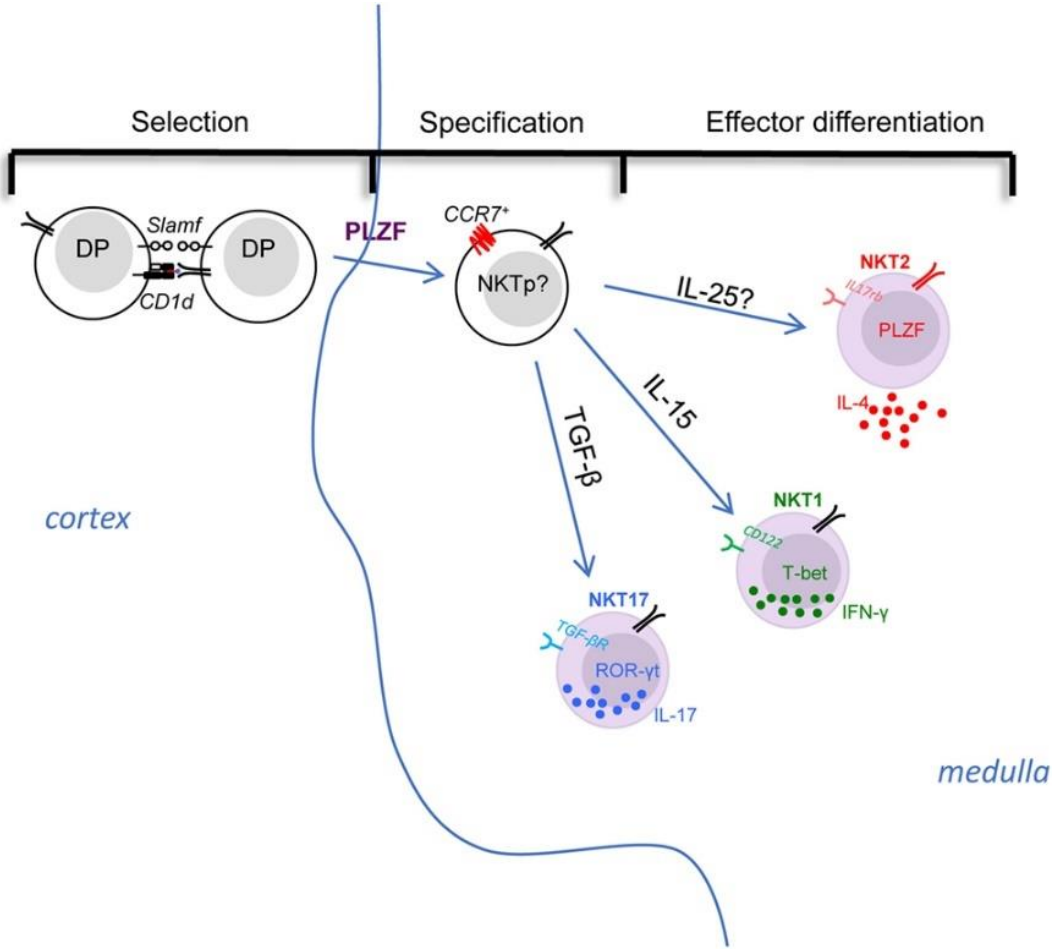

Figure 1-1. The selection, specification, and effector differentiation of invariant natural killer T (iNKT) cells in the thymus. The initial positive selection of iNKT cells depends on the interaction among double-positive thymocytes in cortex. Then, with the upregulation of PLZF and the chemokine receptor CCR7, the multi-potent iNKT common precursors migrate to thymic medulla and specify their fate into different effector subsets. The effector differentiation into NKT1, NKT2, and NKT17 are influenced and directed by various factors. For instance, cytokine signals play essential roles in differentiation: IL-15 is critical for CD122 expressing NKT1 cell differentiation, whereas TGF-β is required for TGF-βR-expressing NKT17 cells, while NKT2 cells express IL-17 RB (IL-25 receptor), although the role of IL-25 requires evaluation. iNKT subsets are poised in an effector state, but only NKT2 cells are

actively producing cytokine (IL-4) at steady state, while NKT1 and NKT17 cells maintain potential to produce IFN-γ or IL-17, respectively, after stimulation.

Immediate post-selection precursor iNKT cells are characterized as CD1d tetramer^{+} CD44^{-} CD24^{+} CD69^{+}, termed as “stage 0” iNKT cells. The strong TCR signal during iNKT selection was directly demonstrated using a reporter mouse in which a GFP cassette was inserted in the Nur77 locus (an immediate-early gene upregulated by TCR stimulation), wherein the GFP level indicates the TCR signal strength (21). In these mice, stage 0 iNKT cells express a high level of GFP indicating they received strong TCR signal during selection (21). Beside this strong TCR signal, the development of iNKT cells also relies on a “second signal” generated through homotypic interactions between signaling lymphocyte activation molecule family (SLAMF) receptors, SLAMF1 and SLAMF2, expressed on the DP thymocytes (22). In addition to supporting a long half-life in DP thymocytes, c-Myb also promotes the expression of CD1d and SLAMFs, which are essential for positive selection of iNKT cells (20). Deficiency of c-Myb completely abrogates the generation of iNKT cells, as CD24^{+} stage 0 iNKT cells were NOT detected (20).

Historically, in B6 mice, the maturation of iNKT cells beyond stage 0 was described as a stepwise linear model from stage 1 to 3 based on expression of CD44 and NK1.1. In this model, the stage 0 iNKT cells develop into CD24^{-} CD44^{-} NK1.1^{-} stage 1 cells, then upregulate CD44 to become stage 2 cells, and finally acquire NK1.1 expression to become stage 3 cells in a linear fashion (23). This model fits some but not all the available data. For example,

NKT17 cells were known to express CD44 but not NK1.1 (stage 2), never become NK1.1^{+} (stage 3) (13). Alternatively, based on the expression of transcription factors, PLZF, Gata3, T-bet, and ROR-γt, CD24^{-} iNKT cells could be very well categorized into three distinct subsets, NKT1, NKT2, and NKT17 as described above. Similar to NKT17 cells, intra-thymic transfer of “stage 2” IL-4 producing NKT2 cells (IL-4^{+} IL-17RB^{+} CD4^{+}) showed that they do not give rise to T-bet^{+} NK1.1^{+} “stage 3” cells either (12). Therefore, a revised lineage-diversification model for iNKT cell development, in which a common progenitor gives rise to the distinct lineages of NKT1, NKT2, and NKT17 cells (Figure 1-1) was suggested. We herein discuss the promoting and inhibitory factors for selection, specification, and differentiation of iNKT cells, which are summarized in Table 1-1.

Promoting factors	**Selection**	**Specification**	**Effector differentiation**		
			NKT1	**NKT2**	**NKT17**
	ROR-γt	PLZF	CD122/IL-15	IL-17RB/IL-25 ?	TGF-βRII/TGF-β
	HEB	Runx1	Let-7	Lin28	
	c-Myc	CUL3	Pak2		
	c-Myb	CCR7/CCL21a	Hobit	T cell receptor (TCR) binding half-life	
	SLAMF1 and SLAMF2	Egr2	UTX	KLF13	
	miR-181a	NKAP	T cell factor 1		
	TCR signaling strength	Histone deacetylase 3	Lymphoid enhancer factor 1 (preferentially promote NKT2)		
		Dicer/microRNAs			
Inhibitory factors			Lin28	Let-7	
			TCR binding half-life	Kruppel-like factor 2	TET2/TET3
				Jarid2	
				Ezh2	

Table 1-1. Genetic factors influence development of iNKT subsets.

Specification

Stage 0 iNKT cells arise from DP thymocytes in the thymic cortex (6). However, in CD1d tetramer-based immunofluorescence and histocytometric analysis, thymic iNKT subsets were found to be predominantly localized in the thymic medulla (24) (Figure 1-1). Consistent with this, the thymic medullary environment was reported to impact the functional maturation of iNKT cells (25). Therefore, the nature and localization of the common progenitor that directly gives rise to distinct subsets is unclear. Furthermore, the signals that drive their migration from cortex to medulla, as well as the medullary factors that control the differentiation of iNKT subsets has not yet been reported. A previous study demonstrated that the chemokine receptor CCR7, which responds to the chemokines CCL21, is important for thymocytes trafficking from the cortex to the medulla (26). Additionally, the number of iNKT cells was significantly reduced in $CCR7^{-/-}$ mice (27). Interestingly, single cell RNA-seq analysis of thymic iNKT cells suggested that $PLZF^{high}$ iNKT cells might comprise a progenitor population (28). Previous work showed IL-4^{-} $PLZF^{high}$ iNKT cells could further differentiate into T-bet^{+} NKT1 cells when sorted and intra-thymically transferred into thymus (12), suggesting they maintain precursor potential. Further analysis of this IL-4^{-} $PLZF^{hi}$iNKT cell population by RNA-seq and PCA analysis confirmed they have the least similarity to the three effector subset (29). Taken together, it could be inferred

that CCR7^{+} cells within PLZF^{high} iNKT cells might serve as the common progenitor for iNKT subsets (Figure 1-1 “Specification”).

Factors Involved in Specification and/or Effector Differentiation

Cytokines

IL-15, TGF-β, and IL-25

Numerous studies have demonstrated cytokines produced in the local environment play central roles in determining the differentiation of CD4^{+} T helper subsets (Th1, Th2, and Th17) (30). Similarly, the differentiation of iNKT subsets is heavily influenced by different cytokine signals (Figure 1-1 “Effector differentiation”). For instance, it’s been shown that NKT1 cells highly express CD122 (IL2Rβ), and CD122-mediated IL-15 signaling is essential for the differentiation of NKT1 cells (31). Likewise, the absence of TGF-β signaling (CD4-Cre × TGF-βRII$^{flox/flox}$ and CD4-Cre × Smad4$^{flox/flox}$) led to complete loss of ROR-t^{+} NKT17 cells (32). Both NKT2 and NKT17 cells express IL-17RB (IL-25 receptor), which was essential for the production of IL-13, IL-9, IL-10, and IL-17 after stimulation with αGalCer (14), demonstrating that the cytokine production of activated iNKT cells is influenced by a signal through this receptor. It was further shown that such effect was dependent on E4BP4, a transcription factor that regulates IL-10 and IL-13 production in CD4^{+} T and iNKT cells (33, 34). Interestingly, E4BP4 seems to be upregulated in iNKT cells only after stimulation with IL-25 or αGalCer (14, 34), but not expressed

by thymic or most peripheral iNKT cells in the steady state (except the adipose iNKT cells) (14, 34, 35). Though inferred by the data, iNKT subsets defined by transcription factor expression as NKT1, 2, and 17 were not directly evaluated in the study (14). Thus, whether the development of NKT2 and/or NKT17 cells is controlled by the IL-17RB/IL-25 axis remains or be defined. In a scenario where IL-25 signaling controls differentiation of NKT cells, it would be important to define the source of IL-25 in the thymus (Figure 1-1; Table 1-1). A recent study demonstrated that a type of specialized epithelial cells, called tuft cells, are the solely source of IL-25 in the gut (36). It will be interesting to check the thymus for this lineage of epithelial cells as well.

Transcription Factors

Egr2

Strong TCR signaling in stage 0 iNKT cells commits their fate to iNKT lineage, as it leads to elevated expression of the transcription factors Egr1 and Egr2, which influence further development of iNKT cells (37). In agreement with Egr2 directly binding the PLZF promoter, Egr1 and Egr2 together are critical for PLZF induction, which indicates that Egr1 and Egr2 may be upstream of PLZF in determining iNKT lineage fate (37). In addition, Egr2-deficient iNKT cells failed to express CD122, indicating that elevated Egr2 expression not only specifies iNKT lineage at an early stage but its sustained expression may

also further influence differentiation of iNKT subsets (37). In addition, a cytoskeletal remodeling protein, P21-activated kinase 2 (Pak2) also influences the development of iNKT cells, especially NKT1 and NKT2 cells, possibly through regulation of the two critical transcription factors, Egr2 and PLZF (38).

KLF Family Factors

The transcription factor Kruppel-like factor 2 (KLF2) is essential for T cells egress from thymus and lymph node, because it's required for the expression of sphingosine 1 phosphate receptor type 1 (S1P1) in T cells (39). Unexpectedly, thymocytes in KLF2-deficient mice (CD4-Cre × $KLF2^{flox/flox}$) displayed a memory phenotype ($CD44^{high}$ $CXCR3^{+}$ $CD122^{+}$) that was shown to be an IL-4-dependent cell-nonautonomous effect (40). Furthermore, this effect was due to the expansion of IL-4-producing $PLZF^{high}$ T cells (mostly NKT2 cells), showing that KLF2 negatively regulates the differentiation of NKT2 cells (41). Another member of the Kruppel-like family, KLF13, plays the opposite role. KLF13 deficiency ($KLF13^{-/-}$) led to a diminished population of IL-4-producing $PLZF^{high}$ iNKT cells (42).

Hobit

Though serving as an important factor that instructs the tissue retention program in iNKT cells and resident memory T cells (Trm) (43), the transcription factor Hobit was also shown to regulate the differentiation of iNKT cells (44). Hobit expression is high in $CD44^{high}$ $NK1.1^{+}$ iNKT cells (mostly

NKT1 cells), but low in CD44^{low} NK1.1^{-} and CD44^{high} NK1.1^{-} iNKT cells (mostly NKT17 and NKT2 cells) (44). Accordingly, the number of CD44^{high} NK1.1^{+} iNKT cells was significantly reduced in Hobit-deficient mice, while the abundance of CD44^{low} NK1.1^{-} and CD44^{high} NK1.1^{-} iNKT cells remained intact (44). Though the iNKT subsets were not distinguished in the study, it could be inferred from the data that Hobit promotes the differentiation and/or thymic retention of NKT1 cells.

Lymphoid Enhancer Factor 1 (LEF1) and T Cell Factor 1 (TCF1)

The transcription factors LEF1 and TCF1 are essential for T cell development including early commitment to the T cell fate, transition from DN to the DP thymocytes, as well as following CD4/CD8 choice (45). The critical role of LEF1 and TCF1 in the differentiation of iNKT subsets has also been shown. Deletion of TCF1 at DP stage (CD4-Cre × Tcf7$^{flox/flox}$) led to a severe defect in all three iNKT subsets (46). In addition, iNKT cell development was similarly impaired in absence of LEF1 (Vav-Cre × Lef1$^{flox/flox}$) (47). LEF1 was required for the proliferation and survival of iNKT cells, especially the massive expansion after stage 0 (47). Interestingly, though it influenced the development of all three iNKT subsets, LEF1 showed a preference in promoting the differentiation of NKT2 cells (47).

Chromatin Modifiers

Epigenetic modifications also regulate development and differentiation of iNKT

cells. The TET-family dioxygenases, TET1, TET2, and TET3, oxidize 5-methylcytosine (5mC) to 5-hydroxymethylcytosine (5hmC), which is an important DNA modification critical for various biological processes (48-50). Simultaneous deletion of *Tet2* and *Tet3* resulted in uncontrolled TCR-mediated expansion of NKT17 cells through suppression of T-bet and ThPOK (51). Jarid2, a component of polycomb repressive complex 2 that methylates histone 3 lysine 27 (H3K27), is also involved in iNKT cells development. Upregulated after TCR stimulation, Jarid2 directly binds to the PLZF promotor as a transcriptional repressor. Therefore, deficiency of Jarid2 led to significant expansion of $PLZF^{high}$ NKT2 cells (52). In addition, the transcriptional repressor NKAP was shown to be required for the development of iNKT cells, as the iNKT development was completely abrogated at stage 0 in mice deficient of NKAP (CD4-Cre × $NKAP^{flox/flox}$) (53). How NKAP regulates iNKT cell development is not clear, but its interaction with the histone deacetylase 3 (Hdac3) may be important, as NKAP is known to associate with Hdac3 and a similar defect of iNKT cells was observed in Hdac 3 conditional knockout mice (CD4-Cre × $Hdac3^{flox/flox}$) (54). A recent report demonstrated that the H3K27me3 histone demethylase UTX is essential for iNKT cell development, especially the differentiation of NKT1 cells, as there was considerably fewer T-bet^{+} NKT1 cells in UTX-deficient mice while NKT2 and NKT17 cells were not affected (55). UTX not only directly binds to the promoters of T-bet and CD122

genes but also influences the epigenetic landscape and transcription of PLZF-activated genes (55).

MicroRNAs (miRNAs)

MicroRNAs are small noncoding single-strand RNAs (~22 nt) that modulate the stability and transcriptional activities of messenger RNAs (mRNAs) and *via* this mechanism influence the transcriptomes of various cells, leading to further effects on cellular proliferation, apoptosis, lineage commitment, and differentiation (56). Perhaps not surprisingly, complete loss of mature iNKT cells was observed in mice lacking Dicer (CD4-Cre × $Dicer^{flox/flox}$), which are incapable of generating functional miRNAs in T cells, thus demonstrating that miRNAs are essential for the development of iNKT cells (57). miR-181a is abundant in DP thymocytes and could augment TCR signaling strength *via* enhancing the basal activation of TCR signaling molecules, such as increased basal phosphorylation level of Lck and ERK (58). Deletion of miR-181a (miR-181a/b-$1^{-/-}$ mice) completely blocked iNKT cell development at the DP/Stage 0, which was presumably due to reduced responsiveness to TCR signals as exogenous agonistic ligand (αGalCer) could rescue iNKT cell generation (59). The miR-17–92 family cluster is also critical for the development of iNKT cells, in that absence of miRNAs of the miR-17–92 family cluster (triple knockout of three paralogs miR-17–92, miR-106a–363, and miR-106b–25 clusters) resulted in almost complete ablation of the three

iNKT effector subsets (60). Excessive TGF-β signaling was seen in the remaining triple knockout iNKT cells, but it did not solely account for the impaired iNKT cell development, because deletion of TGF-βRII did not fully restore the hemostasis of iNKT cells (60). It was further found that the Let-7 family miRNAs, the most abundant family of miRNAs in mammals, tightly controls the differentiation of iNKT subsets (61, 62). Let-7 miRNAs are abundant in NKT1 cells while low in NKT2 and NKT17 cells, targeting *Zbtb46* mRNAs and inhibiting PLZF expression, therefore, directing iNKT cell differentiation into $PLZF^{low}$NKT1 lineage (62). Moreover, Lin28 inversely regulates Let-7 miRNAs, and Lin28 transgenic mice, which are practically deficient in Let-7 miRNAs, showed significantly increased NKT2 and NKT17 cells (62). miR-150 is expressed in lymphocytes (B, T, and NK cells) and has been implicated in their maturation. Correspondingly, miR-150 expression is expressed in iNKT cells after stage 0 (63, 64). In a mixed bone marrow chimera system, cell-intrinsic deficiency of miR-150 mildly affected iNKT cell development (63, 64), while overexpression of miR-150 substantially blocked maturation of iNKT cells beyond stage 0 (63). This suggests that fine-tuning of miR-150 level might be critical for iNKT cell development. Though the molecular pathway underlying this miR-150-dependent iNKT cell development is unclear, regulation of c-Myb by miR-150 could be involved (63, 64).

Cellular Protein Degradation System

While playing a central role in iNKT cell development, PLZF is initially induced in the stage 0 iNKT cells, and its expression can be regulated by the transcription factor Runx1 through direct binding to a critical enhancer of PLZF gene (65). Using Chip-Seq analysis, PLZF was shown to bind and regulate multiple genes, especially a broad set of immune effector genes expressed in iNKT cells (66). Beside directly regulating the expression of various genes, PLZF was also shown to transport an E3 ubiquitin ligase, cullin 3 (CUL3), from cytosol to nucleus, which would induce unique and essential ubiquitination patterns in iNKT cells (67). The number of iNKT cells was dramatically decreased in mice lacking CUL3 (CD4-Cre × $CUL3^{flox/flox}$), further substantiating the importance of PLZF–CUL3 interaction in the development of iNKT cells (67). In line with its association with CUL3, PLZF has also been reported to interact with enhancer of zeste homolog 2 (Ezh2) methyltransferase (68). Moreover, Ezh2 directly methylates PLZF, causing its ubiquitination and subsequent degradation. Deletion of Ezh2 leads to sustained expression of PLZF and substantial expansion of $PLZF^{high}$ $NK1.1^{-}$ iNKT cells (mostly IL-4-producing NKT2 cells) (68).

Endogenous Selecting Lipid-Ligand and TCR Specificity

The generation of iNKT cells depends on recognition of lipid antigen presented by CD1d molecules on DP thymocytes. This antigen is most likely

to be a self-lipid(s), because iNKT cells emerge early in life (6, 69), before stable colonization of commensal bacterial. Moreover, the phenotype and function of thymic and most peripheral iNKT cells (except pulmonary and intestinal iNKT cells) are normal in germ-free mice (70, 71). Regulated lipid metabolism in DP thymocytes is critical for thymic selection of iNKT cells, and the transcription factor Bcl11b plays a vital role in this process (72). Bcl11b-deficient (CD4-Cre × $Bcl11b^{flox/flox}$) thymocytes showed deficient presentation of endogenous lipid antigens, dysregulated endo-lysosomal compartment, and alterations in genes involved in lipid metabolism (72). Moreover, in a mixed bone marrow chimera system, Bcl11b-deficient DP thymocytes (TCR-$\alpha^{-/-}$/CD4-Cre × $Bcl11b^{flox/flox}$) failed to support selection of iNKT precursors in Bcl11b-sufficient DP thymocytes ($\beta2m^{-/-}$/Bcl11b-Wt) (72). CD1d molecules can traffic between cell membrane and cytosolic organelles, surveying the endo-lysosomal compartment (73). A mouse model that expresses CD1d with a truncated cytoplasmic tail showed a severe defect in intracellular trafficking, and the number of iNKT cells was significantly reduced, suggesting the selection of iNKT cells relies on endosomal trafficking of CD1d molecule (74). Though a great effort has been made to understand the stimulatory thymic self lipid(s), controversy remains, as reviewed elsewhere (23, 75, 76). Briefly, iGb3, an endogenous lysosomal glycosphingolipid, though thought to be presented by LPS-activated dendritic cells that activate iNKT cells (77), is

unlikely to be a major selecting ligand for iNKT cells given that the development and function of iNKT cells are normal in isoglobotrihexosylceramide (iGb3)-deficient mice (78). Instead, glycosphingolipids (GSL) have been implicated in the development of iNKT cells as mice deficient of GSL-synthesizing enzyme glucosylceramide (GlcCer) synthase (GSC) in hematopoietic cells (Vav-Cre × $GCS^{flox/flox}$) showed mild reduction of iNKT cells in both thymus and periphery (79). While stage 0 iNKT cells were not examined in the study, it remains unclear whether GSL are involved in the positive selection of iNKT cells. A recent report demonstrated the selecting ligands likely to be α-linked glycosylceramides (80). Since all glycosylceramides in mammals were believed to be β-anomers due to that mammalian glycosylceramide synthases are β-transferases (81), this finding is somewhat surprising. Earlier studies pioneered by the Brenner group showed, though initially thought to be a potent lipid self-antigen for iNKT cells, that β-glucopyranosylceramide (β-GlcCer) actually does NOT possess antigenic activity to iNKT cells (82, 83). The observed activity of β-GlcCer is likely due to inclusion of an α-GlcCer species (83). These observations suggested the possibility that α-glycolipids are endogenous antigenic lipids for iNKT cells (83). However, nuclear magnetic resonance spectroscopy analysis at the time did not render a definitive identity (83). It is possible that an unknown alternative enzymatic pathway, unfaithful enzymatic

activities, or unique stressed cellular environments could confer production of small amounts of α-linked glycolipids, though the exact mechanism remain to be discovered (80, 84). The peroxisome-derived ether lipids seem to be partially involved in the iNKT cell development, as mice deficient in the peroxisomal enzyme glyceronephosphate O-acyltransferase (GNPAT) harbor moderately reduced iNKT cells and GNPAT$^{-/-}$ thymocytes are unable to support maturation of iNKT cells (85). However, the number of stage 0 iNKT cells are NOT changed in GNPAT$^{-/-}$ mice (85), suggesting that peroxisome-derived lipids may not be the predominant selecting ligands for iNKT cells, but rather influence later developmental events of iNKT cells. The lysosomal phospholipase A2 (LPLA2), which modifies lysophospholipids in the lysosome, has been shown to play a role in thymic selection of iNKT cells, as both CD1d endogenous antigen presentation and iNKT cell numbers were negatively affected in the absence of LPLA2 (86). Taken together, considering that maturation of iNKT cells after positive selection of stage 0 iNKT cells requires the presence of CD1d in the thymus (87), it is possible that the endogenous lipid ligands for iNKT cells are presented in both thymic cortex and medulla and are displayed by different antigen-presenting cells (APCs). In this fashion, they may influence both selection (in the cortex) and effector differentiation (in the medulla) of iNKT cells (Figure 1-2).

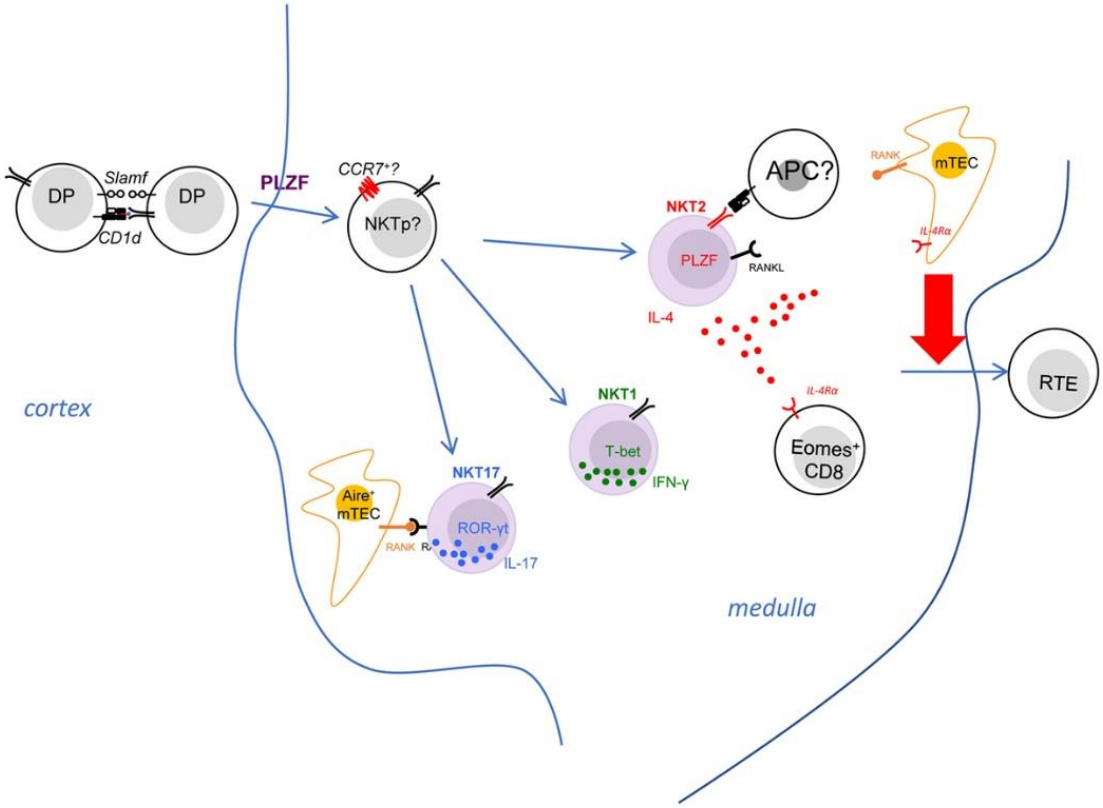

Figure 1-2. **The invariant natural killer T (iNKT) effector subsets modulate immune homeostasis in the thymic medulla.** The iNKT effector subsets predominantly reside in the thymic medullary area. Both NKT2 and NKT17 cells express RANK ligand, which interacts with RANK on medullary thymic epithelial (mTEC) to induce Aire expression. NKT2 cells also produce IL-4 at steady state, which has a striking effect on $CD8^+$ single positive thymocytes—causing them to upregulate Eomes and adopt memory-like phenotype and function. The iNKT-derived type 2 cytokines, IL-4 and IL-13, also influence mTEC to promote emigration of mature thymocytes, through and as-yet undefined mechanism. The activation requirements for NKT2 cells are poorly defined, although they do need T cell receptor stimulation to produce IL-4 in the medulla.

Consistent with a potential role of specific self-lipids in effector differentiation, it was noted that the three iNKT subsets express distinct but stable Vβ repertoires (12, 88, 89). For example, NKT2 cells show a higher usage of Vβ7 (12). Thus, a few studies have raised the hypothesis that differential TCR signaling events due to biased TCR Vβ gene usage could impact the differentiation of iNKT subsets (88, 89). Through generation of retrogenic mice expressing different CDR3β to manipulate iNKT TCR β chain *in vivo*, a recent study clearly demonstrated the half-life of TCR-Ag-CD1d interaction governs the frequency of different iNKT subsets in a cell-intrinsic manner. The number of NKT2 cells strongly correlated with the $t_{1/2}$ of tetramer binding (90). As mentioned above, a high level of Nur77GFP was seen in NKT2 cells in the steady state, suggesting continuous TCR signaling in NKT2 cells (12). However, it is less clear whether such continuous TCR stimulation is required for the steady-state production of IL-4 in NKT2 cells and/or the development of PLZF^{high} NKT2 cells (Figure 1-2). Since NKT2 cells reside in the thymic medulla, further efforts are required to elucidate where and how TCR binding kinetics of NKT2 cells might control their differentiation (Figure 1-2).

iNKT Cells Modulate Tissue Homeostasis

Major Role of iNKT-Derived IL-4

Thymus

Using KN2 mice, in which a human CD2 cassette was knocked into the IL-4

gene locus, and human CD2 expression on cell surface indicates active secretion of IL-4, a previous study demonstrated that thymic NKT2 cells produce abundant IL-4 at steady state (12). Another group showed thymic iNKT cells may also produce IL-13 at steady state in IL-13GFP mice (91). Because iNKT cells are predominantly localized in the medulla, IL-4 produced by NKT2 cells could influence a variety of immune events in that environment (Figure 1-2). Indeed, steady-state production of IL-4 selectively activates STAT6 in medullary $CD8^+$ single-positive thymocytes, which drives them to become memory phenotype ($CXCR3^+$ $CD122^+$ $Eomes^+$) (12, 41). This population of IL-4-induced memory T cells has been categorized as innate memory T cells (92), and they maintain greater function compared to naïve $CD8^+$ T cells. They are well equipped to produce IFN-γ in response to TCR stimulation and showed much better expansion after infection with *listeria monocytes* (LM) (41). Moreover, the developmental exposure to IL-4 is critical for $CD8^+$ T cells to mount robust Th1 responses to acute or chronic lymphocytic choriomeningitis virus infection (93, 94). Therefore, innate memory T cells are beneficial to the host for their functional superiority (95). Nevertheless, we do not yet understand, in the bigger picture, why iNKT cells recognition of medullary self-lipids should control this process.

IL-4 impacts other immune cells beyond CD8 T cells in thymic medulla. A recent study demonstrated that the type 2 cytokines (IL-4/13) produced by

iNKT cells could influence in the thymic emigration of mature thymocytes (91). IL-4Rα$^{-/-}$ mice showed accumulation of mature T cell in the thymus and reduced recent thymic emigrants in the periphery (91). Medullary thymic epithelial (mTEC) cells express IL-4Rα and can respond to the type 2 cytokines, as pSTAT6 level went up in mTEC of FTOC when IL-4 and IL-13 were added in the culture (91). Moreover, disorganization of the thymic medulla was observed in mice deficient of IL-4Rα, that the medulla contained some epithelial-free areas revealed by the ERTR5 staining (91). It was speculated that IL-4/13 signaling in mTEC might promote the egress of mature T cells from thymus, though the specific mechanism remains to be uncovered (91). While the S1p–S1p1 axis remains intact in the IL-4Rα$^{-/-}$ mice (91), it is possible that the IL-4/13 produced by NKT2 cells serve as a novel regulator of thymic emigration of T cells.

Periphery

In the periphery, iNKT cells are critical for restoring homeostasis under stressed conditions. The regulatory role of iNKT cells has been implicated in the type 1 diabetes, where iNKT cells are less frequent and biased toward Th1 cytokine production in diabetic siblings than in their non-diabetic siblings (96). The protective role of iNKT cells has been shown in the mouse model for type 1 diabetes [non-obese diabetes (NOD) mouse], as CD1d$^{-/-}$ NOD mice, lacking iNKT cells, have a higher risk and earlier onsets of diabetes compared

to $CD1d^{+/+}$ counterparts (97). Such protection is dependent on the IL-4 production by iNKT cells (98, 99), and activation of iNKT cells to produce IL-4 by cognate lipid antigen α-Galcer prevents diabetes in NOD mice (100, 101). Recent studies highlighted the key role of iNKT cells in regulating the pathogenesis of graft-versus-host disease (GvHD), a severe immunological dysregulation that frequently occurs after allogeneic hematopoietic stem cell transplantation (102, 103). Higher frequency of iNKT cells in patients correlated with lower risk of GvHD (103). In murine studies, stimulation with α-Galcer or adoptive transfer of iNKT cells confer substantial protection against GvHD (104, 105). Furthermore, the iNKT cell-derived IL-4 and following regulatory T cells expansion seem to be critical for optimal suppression of GvHD (103-105). These data point iNKT cells as promising therapeutic regimen for GvHD patients.

Invariant natural killer T cells are rare in most peripheral sites (0.1–1% of lymphocytes), but highly enriched in the liver, representing nearly 30% of hepatic lymphocytes (24). They are actively involved in restoring tissue homeostasis after sterile liver injury as demonstrated in a recent report (106). Shown by intravital microscopy, iNKT cells randomly patrol the sinusoids within liver in the steady state, while they rapidly move toward the injury site after injury (106, 107). Arrested at the injury site due to TCR stimulation and IL-12/18 signals, iNKT cells produce IL-4 to promote a series of events that

are vital for optimal tissue repair, including increased proliferation of hepatocytes, the switch of monocyte subtypes from $CCR2^{high}$ $CX3CR1^{low}$ to $CCR2^{low}$ $CX3CR1^{high}$, as well as reduced collagen deposition (106). Altogether, these studies demonstrated that iNKT cells are potent regulator in immunity, largely due to their ability to produce abundant cytokines. Most of the studies implicated iNKT cell-derived IL-4 as the critical factor in restoring tissue homeostasis. Therefore, to unleash the therapeutic potential of iNKT cells, it will be important to have better understanding of the underlying mechanisms, especially the relevant APCs and the precise stimulatory lipid antigens that activate iNKT cells to produce IL-4.

Role of Other iNKT Subsets

Invariant natural killer T cells also have strong potential to produce other cytokines (IFNγ by NKT1 and IL-17 by NKT17). However, the role of these subsets and cytokines on tissue homeostasis has not been deeply explored, although it should be noted that NKT17 are abundant in the lung. iNKT cells also express a variety of other stimulatory or inhibitory molecules; therefore, they might influence immune homeostasis through direct cell contact. One of the molecules expressed by iNKT cells is RANK ligand (RANKL) (25). Signals through tumor necrosis factor family receptors (TNFRSF) RANK promotes Aire expression in mTEC (108). While iNKT cells express RANKL, and $Aire^{+}$ mTECs were significantly reduced in $CD1d^{-/-}$ mice (25). It strongly

suggests that iNKT cells could regulate the development of mTEC through direct cross-talk to induce RANK signals. Further RNA-Seq analysis demonstrates that only NKT2 and NKT17 cells highly express RANKL (29), suggesting that iNKT subsets may have unique effects in modulating tissue homeostasis in the thymus (Figure 1-2).

Nevertheless, despite increasing knowledge of iNKT cell development and functions, crucial questions regarding iNKT biology remain. The developmental steps that drive NKT cells into functional distinct subsets have not been elucidated. In thesis research, I aim to address this question through investigation of the following aspects: (1) Is there a progenitor for iNKT subsets, and what is the characteristic of it if there is one? In chapter 2, I showed definitively that $CCR7^{+}$ iNKT cells serve as multipotent precursors for three iNKT subsets in thymus and periphery. (2) What are the critical factors that determine how individual iNKT subsets are derived. In chapter 3, I focused on the differentiation of NKT2 cells in thymus because they are the major source of IL-4 in the steady state and help shape thymic development in myriad ways. In this chapter, I demonstrated that TCR signaling in NKT2 cells stimulated by macrophages is required for the steady state IL-4 production in NKT2 cells. (3) Whether and how tissue resident iNKT effector subsets regulate tissue homeostasis? Using a novel technique to visualize endogenous iNKT cells within the tissues, iNKT effector subsets showed

selective tissue distribution, predominantly localized in medulla in the thymus. In chapter 2 and 3 collectively, I showed iNKT subsets shape thymic development through distinct mechanisms. (4) During thesis research, I made an important discovery that short term *in vivo* ARTC2.2 blockade enhanced NKT1 recovery from nonlymphoid tissues during cell preparation and was essential to preserve functionality, viability, and proliferation of iNKT cells. These findings were described in detail in chapter 4, which is a technical improvement that permits much improved flow cytometry–based phenotyping and enumeration of murine iNKT cells from nonlymphoid tissues, and it represents a crucial step for functional studies of this population.

Chapter 2

CCR7 defines a precursor for murine iNKT cells in thymus and periphery

Overview

The precise steps of iNKT subset differentiation in the thymus and periphery have been controversial. We demonstrate here that the small proportion of thymic iNKT and mucosal associated invariant T cells that express CCR7 represent a multi-potent progenitor pool that gives rise to effector subsets within the thymus. Using intra-thymic labeling, we also showed that $CCR7^{+}$ iNKT cells emigrate from the thymus in a *Klf2* dependent manner, and undergo further maturation after reaching the periphery. *Ccr7* deficiency impaired differentiation of iNKT effector subsets and localization to the medulla. Parabiosis and intra-thymic transfer showed that thymic NKT1 and NKT17 were resident—they were not derived from and did not contribute to the peripheral pool. Finally, each thymic iNKT effector subset produces distinct factors that influence T cell development. Our findings demonstrate how the thymus is both a source of iNKT progenitors and a unique site of tissue dependent effector cell differentiation.

Introduction

Invariant natural killer T (iNKT) cells are αβ T cells expressing semi-invariant T cell receptors (TCR) that respond to self-lipids or foreign-lipids presented by the MHC-I like antigen-presenting molecule CD1d (23). They are numerically less abundant than conventional peptide recognizing CD4 and CD8 T cells but profoundly important, secreting a variety of cytokines early after stimulation or in the steady state to influence immune responses and tissue homeostasis (12, 24, 109, 110). Previous work has demonstrated that despite being monospecific, iNKT cells display substantial functional heterogeneity (14, 32, 111-115), being composed of three predominant effector subsets, NKT1, NKT2 and NKT17 according to the expression of key transcription factors and cytokine production (12, 116). For instance, NKT1 cells are T-bet^{+} PLZF^{low} and produce IFN-γ; NKT17 cells are ROR-γt^{+} PLZF^{int} and produce IL-17; while NKT2 cells are PLZF^{high}, and produce IL-4 (12, 116). Through the selective activation and distinct localization of various iNKT effector subsets, iNKT cells can modulate immune responses and tissue homeostasis in different fashions (24, 109, 117). iNKT cells are positively selected in the thymus, in response to agonist interactions with self-lipid/CD1d expressing double positive thymocytes (DP) in the thymic cortex (5, 8, 21). At this point the cells express a high level of CD24, and are considered the most immature, or ‘stage 0’. In contrast, matured functionally competent effector iNKT cells localize

predominantly in the thymic medulla (24), and thymic medullary epithelial cells impact their functional maturation (25). Nonetheless, the developmental steps from stage 0 iNKT cells to mature iNKT effector subsets have remained unclear. Previous work used CD44 and NK1.1 to define 'stages' of iNKT development. However, more recent work showed that these markers are heterogeneously expressed on the mature cytokine producing iNKT effector subsets (14, 32, 111-115). Therefore, the field lacks precise identification of an iNKT multipotent precursor cell. Previous work in our lab, using T-bet and IL-4 reporter mice, identified T-bet^{+} NKT1, ROR-γt^{+} NKT17, and IL-4^{+} PLZF^{hi} NKT2 cells as terminally differentiated (12). However, IL-4^{-} PLZF^{hi} iNKT cells still retained precursor potential, and could convert to T-bet^{+} NKT1 cells in the thymus (12). These results suggest there is heterogeneity within the PLZF^{hi} iNKT cell population, and led us to hypothesize that there exists a population of progenitor cells within the PLZF^{hi} iNKT cells. Indeed, transcriptional profiling by RNA-Seq indicated IL-4^{-} PLZF^{hi} iNKT cells had low similarity with the three effector subsets, including IL-4 producing PLZF^{hi} iNKT cells (29). Single cell RNA-Seq analysis from another group also suggested there might be a progenitor population within the PLZF^{hi} iNKT cells (28). Here we identify a previously unknown sub-population of PLZF^{hi} CCR7^{+} iNKT cells as precursors for all three iNKT effector subsets. CCR7^{+} iNKT cells efficiently emigrate from the thymus in a *Klf2* dependent manner and then

undergo further maturation on site. However, some iNKT cells maintain residency in the thymus where they undergo differentiation without circulating. The thymic and peripheral pools of iNKT effector subsets do not exchange and therefore depend on CCR7^{+} iNKT cells for their establishment. In addition to marking the precursor pool, CCR7 also directs iNKT progenitor cells to localize to the thymic medulla and is required for differentiation of iNKT effector subsets. We further establish that thymic iNKT cells influence T cell development and thymic tissue homeostasis.

Results

CCR7$^+$ iNKT and MAIT cells are at an early stage of development and represent a precursor pool for effector subsets in the thymus

To identify iNKT cells at an early stage of development in the thymus, we used mice that express green fluorescent protein (GFP) under the control of the recombination-activating gene 2 (*Rag2*) promoter via a bacterial artificial chromosome transgene (*Rag2*^{GFP}), in which GFP expression indicates the 'age' of cells (118, 119). We found most thymic iNKT cells were *Rag2*^{GFP} negative, while a small proportion of iNKT cells express *Rag2*^{GFP} (Figure 2-1 A). The iNKT cells with the highest GFP also express CD24 and high level of CD69, indicating they are stage 0 iNKT cells that are immediate after agonist selection (Figure 2-1 A). Since we identified CCR7 as a potential progenitor specific gene (29), and a small population of CCR7$^+$ iNKT cells could be specifically detected (Figure 2-2 A), we further examined CCR7 expression in iNKT cells in *Rag2*^{GFP} mice. CCR7$^+$ iNKT cells expressed high to intermediate amounts of GFP, suggesting they are immature and recently derived from stage 0 iNKT cells (Figure 2-1 A and Figure 2-2 A). Whereas, the *Rag2*^{GFP} lowest cells (most mature) did not express CCR7 (Figure 2-1 A). According to the conventional 'staging' system of iNKT cells in B6 mice, CCR7$^+$ iNKT cells were predominantly NK1.1$^-$ CD44^{lo} (stage 1) but also included some NK1.1$^-$ CD44$^+$ cells (stage 2)

(Figure 2-1 B), although most NK1.1^{-} CD44^{+} (stage 2) cells were not CCR7^{+} as this gate mostly included functionally mature NKT2 and NKT17 cells, and NKT1 cells were NK1.1^{+} CD44^{+} (stage 3) (Figure 2-1 B). Furthermore, most CCR7^{+} iNKT cells did not express T-bet, ROR-γt, IL-4 (human CD2) (Figure 2-1 C). Rather, CCR7^{+} iNKT cells expressed abundant PLZF and LEF1 (Figure 2-1 C), which are both essential for iNKT cells development and proliferation (9, 10, 47).

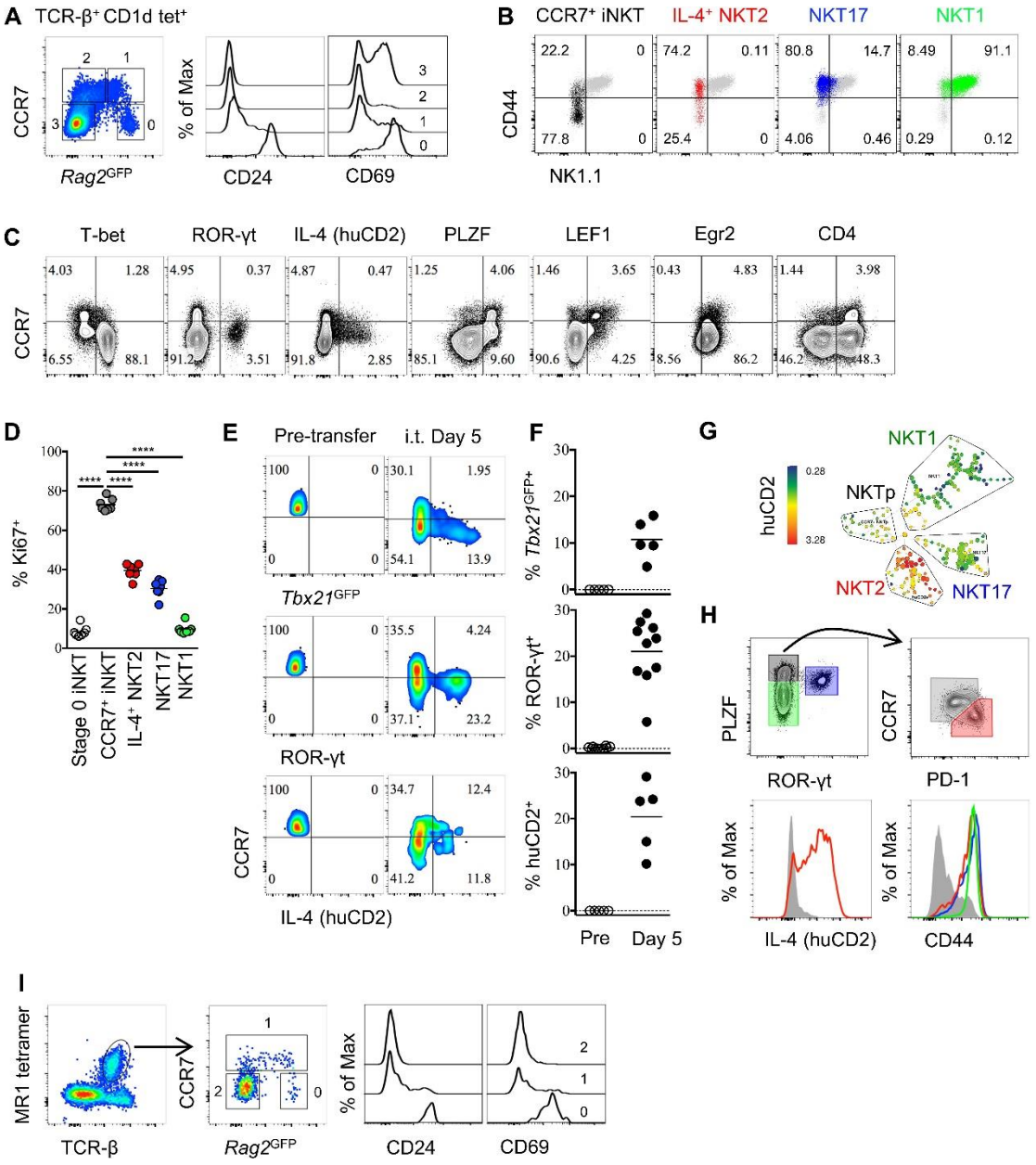

Figure 2-1. Thymic CCR7⁺ iNKT and MAIT cells are at an early developmental stage and give rise to distinct effector subsets in the thymus.

(**A**) Expression of *Rag2*^{GFP} and CCR7 in thymic iNKT cells (TCR-β⁺ CD1d-PBS57⁺) (left column), and of CD24 (middle column) and CD69 (right column) on cells with different levels of *Rag2*^{GFP}. Data are representative of 3 independent experiments with 3–4 mice in each. (**B**) Expression of NK1.1 and CD44 in thymic CCR7⁺ iNKT (black dots), IL-4⁺ (human CD2⁺) NKT2 (red dots), ROR-γt⁺ NKT17 (blue dots), T-bet⁺ NKT1 (green dots) cells together with

total thymic iNKT cells (grey dots). Numbers in quadrants indicate percent cells in each for CCR7^{+} iNKT (black dots), IL-4^{+} (human CD2^{+}) NKT2 (red dots), ROR-γt^{+}NKT17 (blue dots) and T-bet^{+} NKT1 (green dots) cells. Data are representative of 4 independent experiments with 2–3 mice in each. (**C**) Expression of T-bet, ROR-γt, huCD2, PLZF, LEF1, Egr2 and CD4 with CCR7 in thymic iNKT cells (TCR-β^{+} CD1d-PBS57^{+} CD24^{-}). Data are representative of 3 independent experiments with 2–3 mice in each. Numbers in quadrants indicate percent cells in each (throughout). (**D**) Frequency of Ki67^{+} cells in each population of thymic iNKT cells. Data are pooled from three independent experiments with 2–3 mice in each. $^{****}p<0.0001$ (one-way ANOVA, Tukey's multiple comparisons test) Each symbol represents an individual mouse; small horizontal lines indicate the mean. (**E**) Expression of *Tbx21*^{GFP}, ROR-γt and human CD2 in CCR7^{+} iNKT cells sorted from BALB/c *Tbx21*^{GFP} KN2 mice before intra-thymic transfer (left column) or 5 days after transfer in the thymus of congenic BALB/c recipient mice (right column). (**F**) Frequency of *Tbx21*$^{GFP+}$, ROR-γt^{+} or human CD2^{+}cells in donor cells before or 5 days after intra-thymic transfer into the thymus of congenic BALB/c recipient mice. Each symbol represents an individual recipient mouse; small horizontal lines indicate the mean. (**G**) SPADE analysis of thymic iNKT cells from B6 KN2 mice supports that CCR7^{+} NKTp are a distinct lineage from the effector subsets, NKT1, NKT2 and NKT17. Representative figure shows differential expression of human CD2 in each population of iNKT cells. (**H**) CCR7 and PD-1 distinguish two cell populations (top row, right column) within PLZF^{hi} iNKT cells (top row, left column), and expression of human CD2 and CD44 in CCR7^{+} NKTp (grey), NKT1 (green), NKT2 (red) and NKT17 (blue) are shown as overlays (bottom row). Data are representative of 3 independent experiments with 3 mice in each. (**I**)

Expression of *Rag2*^{GFP} together with CCR7 (middle column) in thymic MAIT cells (far left column), and expression of CD24 and CD69 in CCR7^{+} and CCR7^{-} MAIT cells with different level of *Rag2*^{GFP} (far right two columns). Data are representative of 2 independent experiments with 3 mice in each.

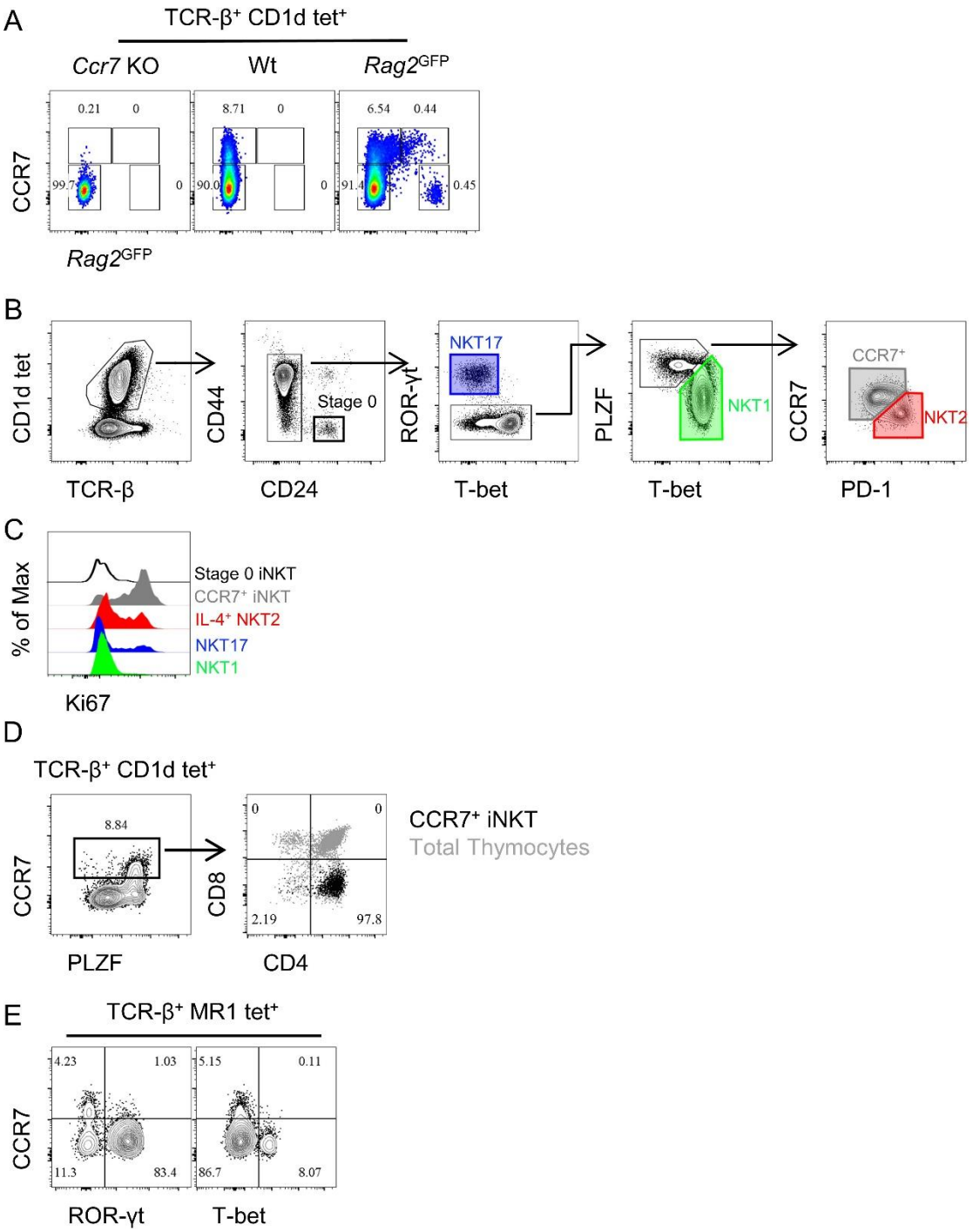

Figure 2-2. Specific CCR7 staining in iNKT cells and gating strategy of iNKT subsets and CD4/CD8 profile of CCR7$^+$ iNKT and CCR7$^+$ MAIT cells.

(**A**) Representative flowcytometry profile of CCR7 staining in thymic iNKT cells enriched from *Ccr7*$^{-/-}$, Wt and *Rag2*^{GFP} mouse. (**B**) Gating strategy to identify enriched thymic iNKT cells as well as various subpopulations of iNKT cells, stage 0 iNKT (heavy black line),

CCR7^{+} iNKT (grey polygon), NKT1 (green polygon), NKT2 (red polygon) and NKT17 cells (purple rectangle). (**C**) Representative staining of Ki67 in various subpopulations of iNKT cells, stage 0 iNKT (black), CCR7^{+} iNKT (grey), NKT1 (green), NKT2 (red) and NKT17 cells (purple). Data are representative of three independent experiments with 2–3 mice in each. (**D**) CD4/CD8 profile of thymic CCR7^{+} iNKT cells. Identification of CCR7+ cells in enriched thymic iNKT cells (left column), and CD4/CD8 profile of CCR7+ iNKT cells (black dots) relative to the total thymocytes (grey dots) from the same mouse (right column). Number indicates percent cells in each gate. (**E**) Expression of T-bet and ROR-γt with CCR7 in thymic MAIT cells (TCR-β^{+} CD1d-PBS57^{+}). Data are representative of 2 independent experiments with 2 mice in each.

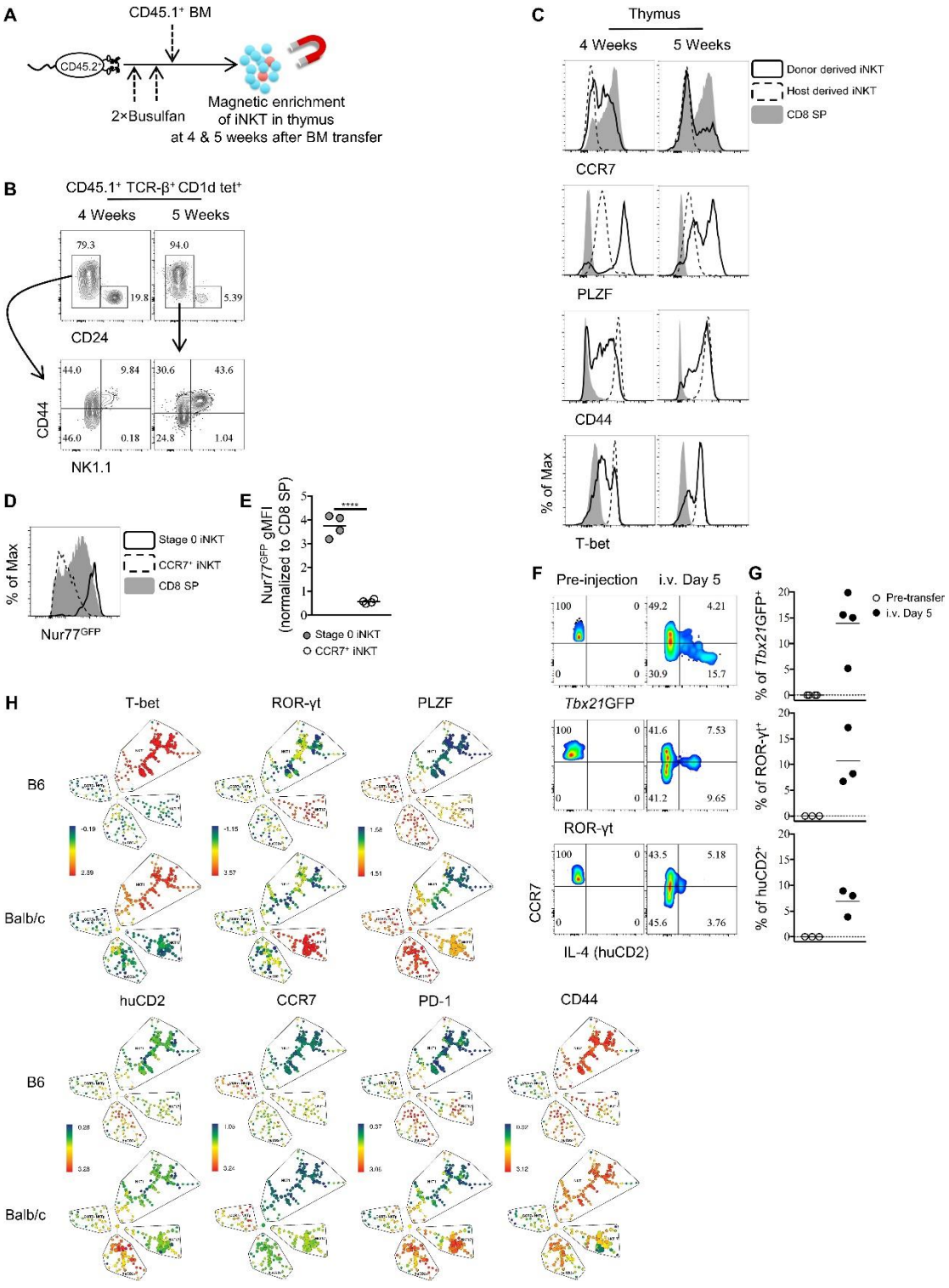

Figure 2-3. Thymic CCR7⁺ iNKT cells are enriched at an early timepoint in busulfan induced BM chimera.

(**A**) Experimental scheme to generate busulfan induced bone marrow chimeras and evaluate iNKT phenotype. (**B**) Frequency of $CD24^+$ $CD44^-$ stage 0 iNKT cells among total iNKT cells (TCR-β^+ CD1d tet^+) (top row) and expression of NK1.1 and CD44 in the $CD24^-$ iNKT cells (bottom row) in the thymus at indicated time point after bone marrow chimera induction. (**C**) Expression of CCR7, PLZF, CD44 and T-bet in donor derived iNKT, host derived iNKT and total CD8 SP cells in the thymus at indicated time point after bone marrow chimera induction. (**D**) Expression of $Nur77^{GFP}$ in Stage 0 iNKT cells (TCR-β^+ CD1d tet^+ $CD44^-$ $CD24^+$), $CCR7^+$ iNKT cells and CD8 SP thymocytes. Data are representative of 2 independent experiments with two mice in each. (**E**) Normalized gMFI of $Nur77^{GFP}$ in stage 0 iNKT and $CCR7^+$ iNKT cells. Data are pooled from two independent experiments with two mice in each. $^{****}p<0.0001$ (unpaired two tailed *t* test). Each symbol represents an individual mouse; small horizontal lines indicate the mean. (**F**) Expression of $Tbx21^{GFP}$, ROR-γt and human CD2 in $CCR7^+$ iNKT cells sorted from BALB/c $Tbx21^{GFP}$ or BALBc KN2 mice before intravenous injection (left column) or 5 days after injection of congenic BALB/c recipient mice, in the spleen (right column). (**G**) Frequency of $Tbx21^{GFP+}$, ROR-γt^+ or human $CD2^+$ cells in donor derived iNKT cells before or 5 days after intravenous injection of congenic BALB/c recipient mice, in the spleen. Each symbol represents an individual recipient mouse; small horizontal lines indicate the mean. (**H**) SPADE analysis of thymic iNKT cells from B6 and BALB/c KN2 mice shows $CCR7^+$ NKTp is a distinct lineage from the effector subsets, NKT1, NKT2 and NKT17. Representative figure shows differential expression of T-bet, ROR-γt, PLZF, huCD2, CCR7, PD-1 and CD44 in each population of iNKT cells.

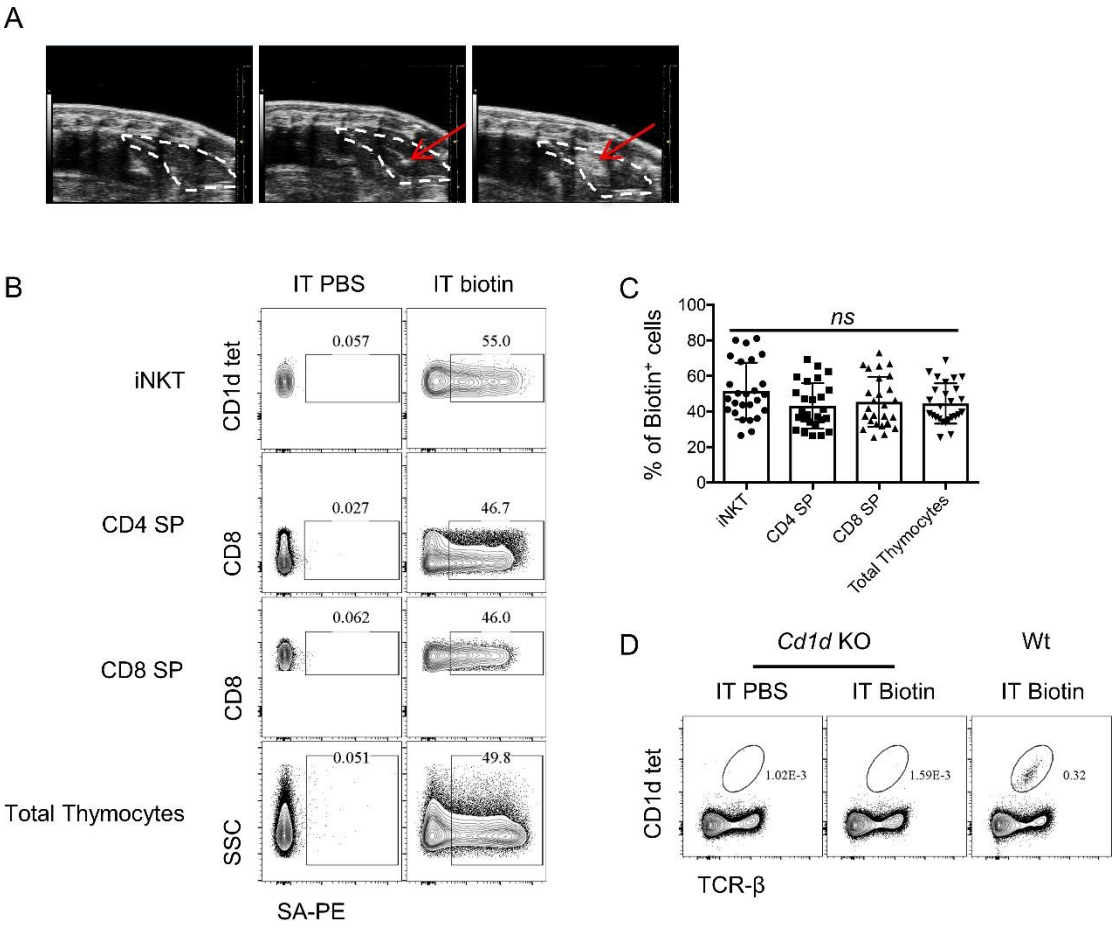

Figure 2-4. Ultrasound imaging guided intra-thymic injection.

(**A**) Representative ultrasound image of mouse chest area, the thymus is outlined by white dotted line (left column), the red arrow indicates the needle tip in thymus before injection (middle column), after injection the red arrow indicates the injected NHS-biotin contained in the thymus (right column). (**B**) Representative flowcytometry profile and (**C**) frequency of biotinylated cells revealed by streptavidin-PE staining in various cell populations (iNKT, CD4 SP, CD8 SP and total thymocytes) in the thymus 24 hr later after intra-thymic injection of PBS or NHS-biotin. Data are pooled from six independent experiments with 2–6 mice in each. *ns*, not significant, p>0.05 (one-way ANOVA). Each symbol represents an individual mouse;

Mean ± SD. (**D**) Representative flowcytometry profile of CD1d tetramer staining in thymocytes of *Cd1d* KO or Wt mouse received intra-thymic injection of PBS or NHS-biotin.

To confirm that the CCR7^{+} iNKT cells were at an early developmental stage, we sought to track a 'wave' of developing iNKT cells using busulfan induced bone marrow chimeras (Figure 2-3 A). We showed that, within CD45.1^{+} donor derive CD1d tetramer^{+} iNKT cells, the immature CD24^{+} CD44^{-} stage 0 iNKT cells were enriched at an early time point (4 weeks) and contracted at a later time point (5 weeks), while the NK1.1^{+} CD44^{+} mature iNKT cells were scarce at 4 weeks but abundant at 5 weeks (Figure 2-3 B), suggesting this approach tracks the developmental steps of iNKT cells. With this approach, CCR7^{+}iNKT cells (with lower CD44 and T-bet) were abundant at the early time point (4 weeks) after bone marrow introduction and decreased at the later time point (5 weeks) (with increased CD44 and T-bet) (Figure 2-3 C).

As CCR7^{+} iNKT cells expressed a high level of LEF1 (Figure 2-1 C), a transcription factor that is essential for iNKT cells proliferation, we examined Ki67 expression. Most CCR7^{+} iNKT cells expressed Ki67 (>75%) compared to the three effector subsets or the stage 0 iNKT cells (Figure 2-1 D, Figure 2-2 B, C), suggesting they are highly proliferative. Stage 0 iNKT cells received strong TCR signal during agonist selection which could be indicated by the level of *Nr4a1*using *Nr4a1*^{GFP} mice (also known as Nur77^{GFP} mice which will be used throughout the manuscript) (21). Highly proliferative as CCR7^{+} iNKT cells are, the Nur77^{GFP} could be diluted were they not continuously receiving TCR stimulation. We showed CCR7^{+} iNKT cells had much lower level of

Nur77^{GFP} than stage 0 iNKT cells (Figure 2-3 D, E). A previous study suggested that the transcription factor Egr2 controls the development of iNKT cells and is highly expressed in iNKT thymic precursors (37). Consistently, we observed a high expression of Egr2 in CCR7^{+} iNKT cells while most thymic iNKT cells were positive for Egr2 expression (Figure 2-1 C). Moreover, consistent with a previous report that iNKT cells go through the CD4^{+} stage after stage 0 iNKT cells (6), we showed CCR7^{+} iNKT cells indeed exclusively expressed CD4, but not CD8 (Figure 2-1 C, Figure 2-2 D).

These data raise the possibility that CCR7^{+} iNKT cells serve as progenitors for differentiation into effector subsets. We then directly assessed the potential of CCR7^{+} iNKT cells to develop into iNKT effector subsets by sorting CCR7^{+} thymocytes (CD4^{+} *Tbx21*$^{GFP-}$ huCD2^{-} CD24^{-} CD8^{-}) from *Tbx21*^{GFP}/KN2 mice and injecting them intra-thymically into congenic hosts. We used an ultrasound guided imaging technique to obtain accurate and efficient intra-thymic injection (Figure 2-4 A). Five days after intra-thymic transfer, all three effector subsets, NKT1, NKT2 and NKT17 cells were detected (Figure 2-1 E, F). To test the precursor potential of thymic CCR7^{+} iNKT cells in the periphery, we also injected the sorted CCR7^{+} thymocytes intravenously into congenic hosts and detected substantial differentiation of NKT1, NKT2 and NKT17 cells in the spleen (Figure 2-3 F, G), demonstrating that iNKT progenitors do not require the thymus for effector

differentiation.

To better identify markers that can distinguish the precursor cells from cytokine producing NKT2 effector cells, we performed Spanning-tree Progression Analysis of Density-normalized Events (SPADE analysis) on total thymic iNKT cells based on a range of key transcription factors, surface markers and cytokines. Importantly, $CCR7^+$ iNKT cells were clearly separated from the three major effector subsets, (Figure 2-1 G, Figure 2-3 H). Within the $PLZF^{hi}$ iNKT cells, CCR7 and PD-1 best distinguished progenitors from effectors, and only $PLZF^{hi}$ $PD\text{-}1^+$ iNKT cells produced IL-4 (human $CD2^+$) in the steady state (Figure 2-1 H).

Previous reports suggested that the two lineages of innate-like T cells—iNKT cells and mucosal associated invariant T (MAIT) cells—have similarities in aspects of their phenotype and functions, such that developmental parallels might exist between the two (71, 120). Indeed, similar to $CCR7^+$ iNKT cells (Figure 2-1 A), $CCR7^+$ MAIT cells also had high to intermediate *Rag2*^{GFP} expression while being low for CD24 and CD69 expression, suggesting they are also at an early stage of development after agonist selection (Figure 2-1 I). Mature MAIT cells are composed of only two distinct effector subpopulations, ROR-γt$^+$ and T-bet$^+$ MAIT cells (71). $CCR7^+$ MAIT cells did not express T-bet or ROR-γt (Figure 2-2 E). Together, these data suggest that both $CCR7^+$iNKT cells and $CCR7^+$ MAIT cells are

progenitor populations that give rise to their corresponding iNKT and MAIT effector cells.

CCR7^{+} iNKT cells are the predominant emigrating iNKT cells and they depend on *Klf2* for thymic emigration

To investigate the phenotype of iNKT cells emigrating from the thymus, we performed intra-thymic injection of a biotinylating agent (NHS-biotin) to label thymocytes (Figure 2-4 A) and analyze peripheral lymphoid organs 24 hr later (Figure 2-5 A). This technique showed robust and unbiased labeling of nearly 50% of all thymocytes (Figure 2-4 B, C) and did not interfere with the specificity of CD1d tetramer staining (Figure 2-4 D). Due to the low frequency of recent thymic emigrants (RTE) amongst total peripheral T lymphocytes (118, 119), we performed magnetic enrichment of biotin^{+} cells in the spleen. These two techniques combined offers a tool to accurately detect RTEs in periphery, as biotin^{+}splenic CD4^{+} or CD8^{+} T cells are predominantly *Rag2*$^{GFP+}$ (Figure 2-6 A, B). Using this tool, recent thymic emigrant iNKT cells (called 'RTE iNKT') could be readily detected (Figure 2-5 A), while biotin^{-} iNKT cells within the unbound fraction are largely (>97%) 'old' iNKT cells—those cells already residing in the periphery before intra-thymic labeling (Figure 2-5 A). As expected, the RTE iNKT cells have higher *Rag2*^{GFP} compared to biotin^{-} iNKT cells (Figure 2-6 C). We further

found that RTE iNKT cells were highly enriched for $CCR7^+$ cells compared to thymic or $biotin^-$ iNKT cells (Figure 2-5 B). Moreover, within the RTE iNKT cells, the $CCR7^+$ cells expressed higher *Rag2*^{GFP} than $CCR7^-$ cells (Figure 2-6 D). In agreement with these data, *Rag2*$^{GFP+}$ splenic iNKT cells were predominantly $CCR7^+$, while most *Rag2*$^{GFP-}$ splenic iNKT cells did not express CCR7 (Figure 2-6 E).

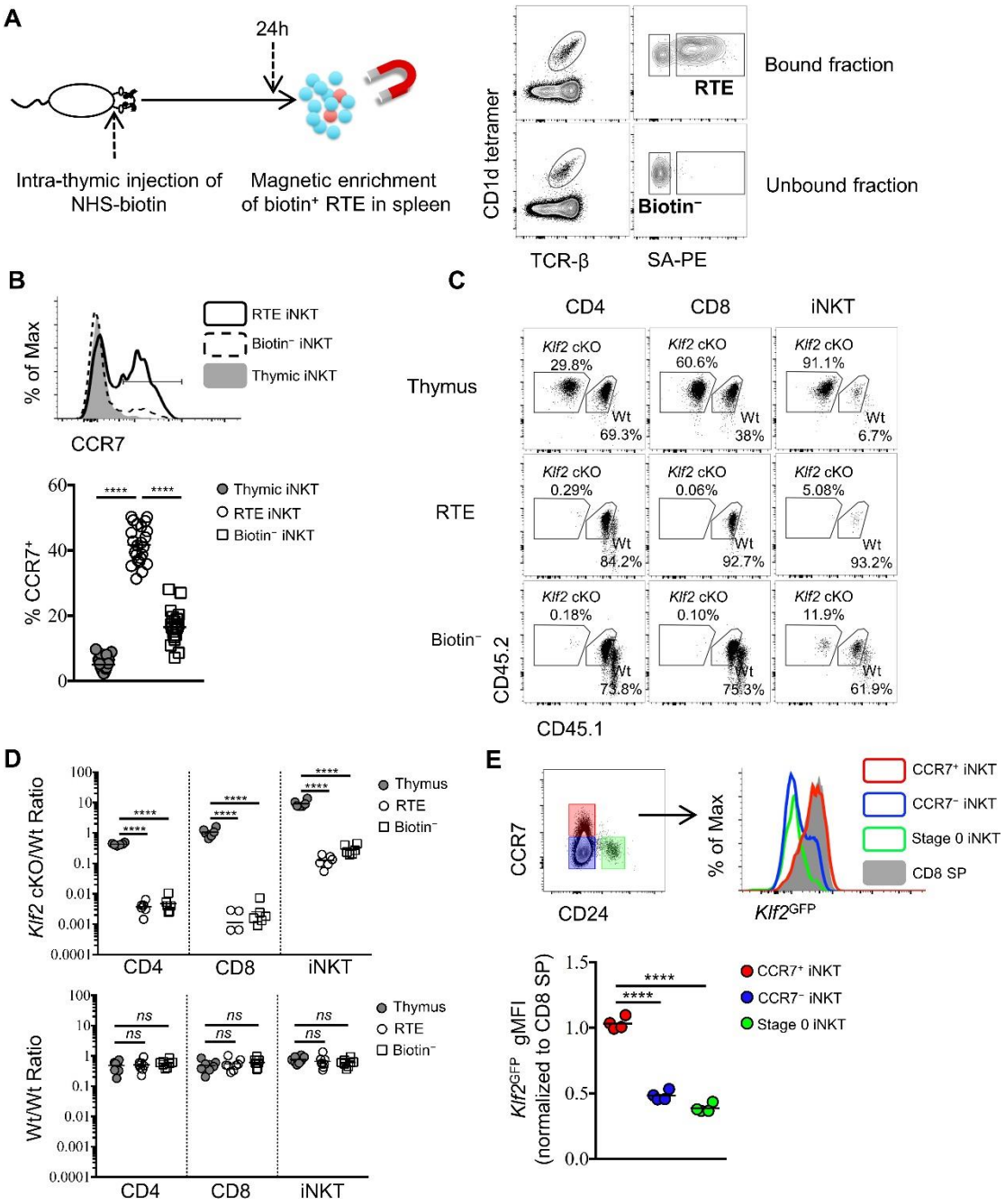

Figure 2-5. CCR7⁺ iNKT cells are enriched in the emigrating iNKT population and depend on *Klf2*.

(**A**) Experimental scheme to track recent thymic emigrants (RTE) through intra-thymic injection of NHS-biotin (left column) followed by enrichment of biotin⁺ splenic cells 24 hr after intra-thymic labeling, compared to 'old' cells (biotin⁻ cells from spleen) (right column). (**B**) Expression of CCR7 in thymic, RTE and biotin⁻ iNKT cells, the grey shade represents thymic

iNKT cells, the solid black line represents RTE iNKT cells, the dashed black line represents biotin$^-$ iNKT cells (top row); frequency of CCR7$^+$ cells in thymic, RTE and biotin$^-$ iNKT cells, the solid grey circle represents thymic iNKT cells, the open circle represents RTE iNKT cells, the open square represents biotin$^-$ iNKT cells (bottom row). Data are pooled from 5 independent experiments with 3–6 mice in each. $^{****}p<0.0001$ (one-way ANOVA) Each symbol represents an individual mouse; small horizontal lines indicate the mean. (**C**) Mixed bone marrow chimeras were generated with 25:75 ratio of donor bone marrow cells using CD45.2$^+$ CD45.2$^+$ B6 *Klf2*cKO cells and CD45.1$^+$ CD45.2$^+$ B6 Wt cells, or with 50:50 ratio of donor bone marrow cells using CD45.2$^+$ CD45.2$^+$ B6 Wt cells and CD45.1$^+$ CD45.2$^+$ B6 Wt cells. Eight weeks later, chimeras received intra-thymic labeling with NHS-biotin to track RTE among CD4, CD8 and iNKT cells. Data are representative of 2 independent experiments with 4–8 mice in each. (**D**) Statistical analysis of thymic, RTE and biotin$^-$ CD4 T cells, CD8 T cells and iNKT cells in 8-week-old BM chimeras reconstituted with *Klf2*cKO and Wt cells (top row) or with Wt and Wt cells (bottom row). Data are pooled form 2 independent experiments with 4–8 mice in each. Numbers indicate the ratio between the cells derived from each donor source. $^{****}p<0.0001$ (one-way ANOVA). *ns*, not significant, $p>0.05$ (one-way ANOVA). Each symbol represents an individual mouse; small horizontal lines indicate the mean. (**E**) Expression of *Klf2*^{GFP} in CCR7$^+$ iNKT, stage 0 iNKT, CCR7$^-$ iNKT cells and CD8 SP cells (top row). Normalized gMFI of *Klf2*^{GFP} in CCR7$^+$ iNKT, stage 0 iNKT, CCR7$^-$ iNKT cells (bottom row). Data are pooled from 2 independent experiments with 2 mice in each. $^{****}p<0.0001$ (one-way ANOVA). Each symbol represents an individual mouse; small horizontal lines indicate the mean.

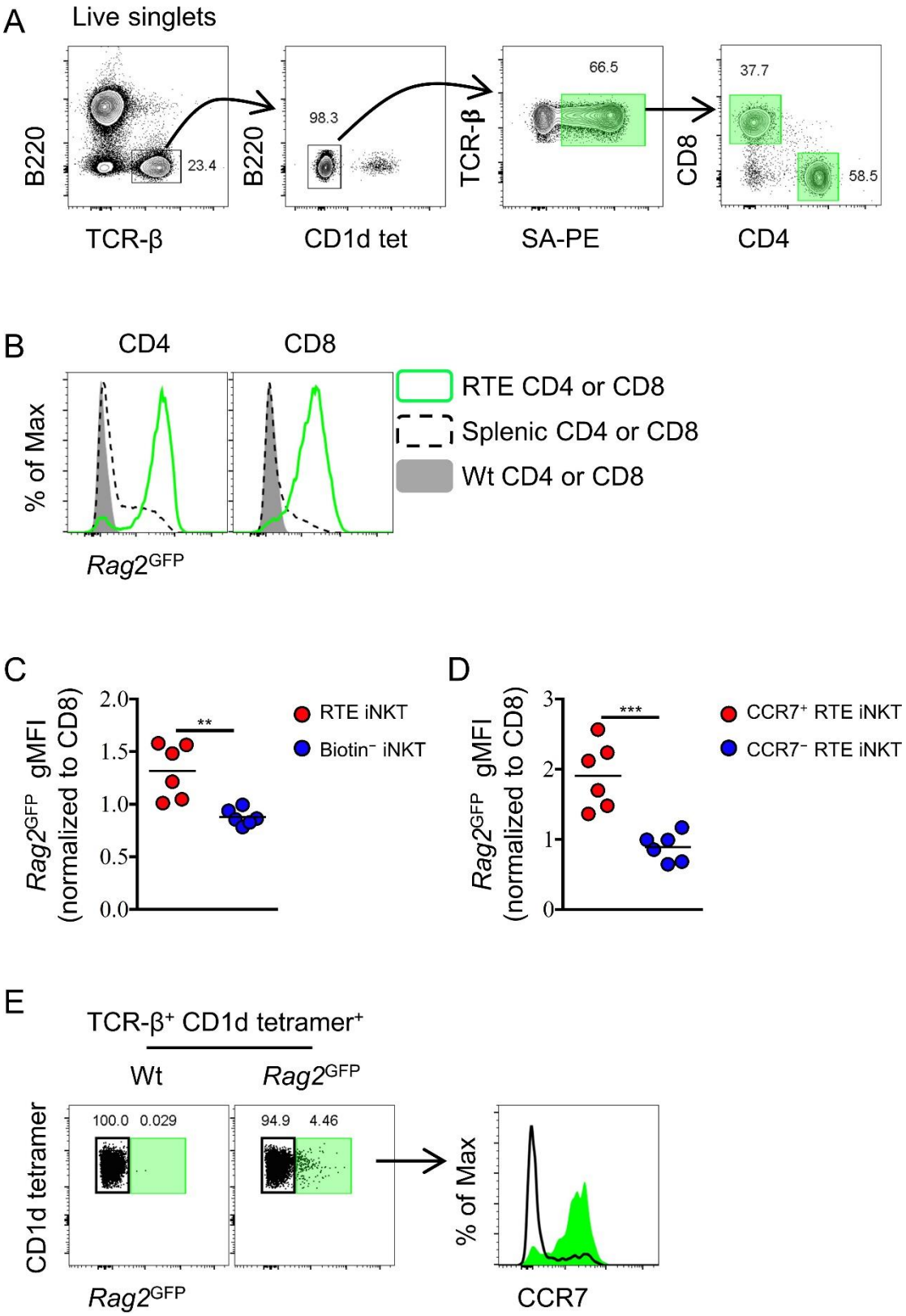

Figure 2-6. Intra-thymic labeling with NHS-biotin to identify RTEs in the periphery and *Rag2*$^{GFP+}$ splenic iNKT cells are CCR7^{+}.

(**A**) Gating strategy to identify RTEs of CD4 and CD8 T cells in spleen. (**B**) Expression of *Rag2*^{GFP} in RTE CD4 or CD8 T cells, total splenic CD4 or CD8 T cells, and Wt total splenic CD4 or CD8 T cells. Data are representative of two independent experiments with three mice in each (**C**) Normalized *Rag2*^{GFP} gMFI of RTE iNKT cells and biotin^{-} iNKT cells in spleen. Data are pooled from two independent experiments with three mice in each. $^{**}p$=0.0025 (unpaired two tailed *t* test). Each symbol represents an individual mouse; small horizontal lines indicate the mean. (**D**) Normalized *Rag2*^{GFP} gMFI of CCR7^{+} RTE iNKT cells and CCR7^{-} RTE iNKT cells in spleen. Data are pooled from two independent experiments with three mice in each $^{***}p$=0.0006 (unpaired two tailed *t* test). Each symbol represents an individual mouse; small horizontal lines indicate the mean. (**E**) *Rag2*$^{GFP+}$ iNKT cells predominantly express CCR7 (right column) when identified in spleen from B6 *Rag2*^{GFP} mice (left column), green shade indicates *Rag2*GFP^{+}iNKT cells and black line indicates *Rag2*$^{GFP-}$ iNKT cells.

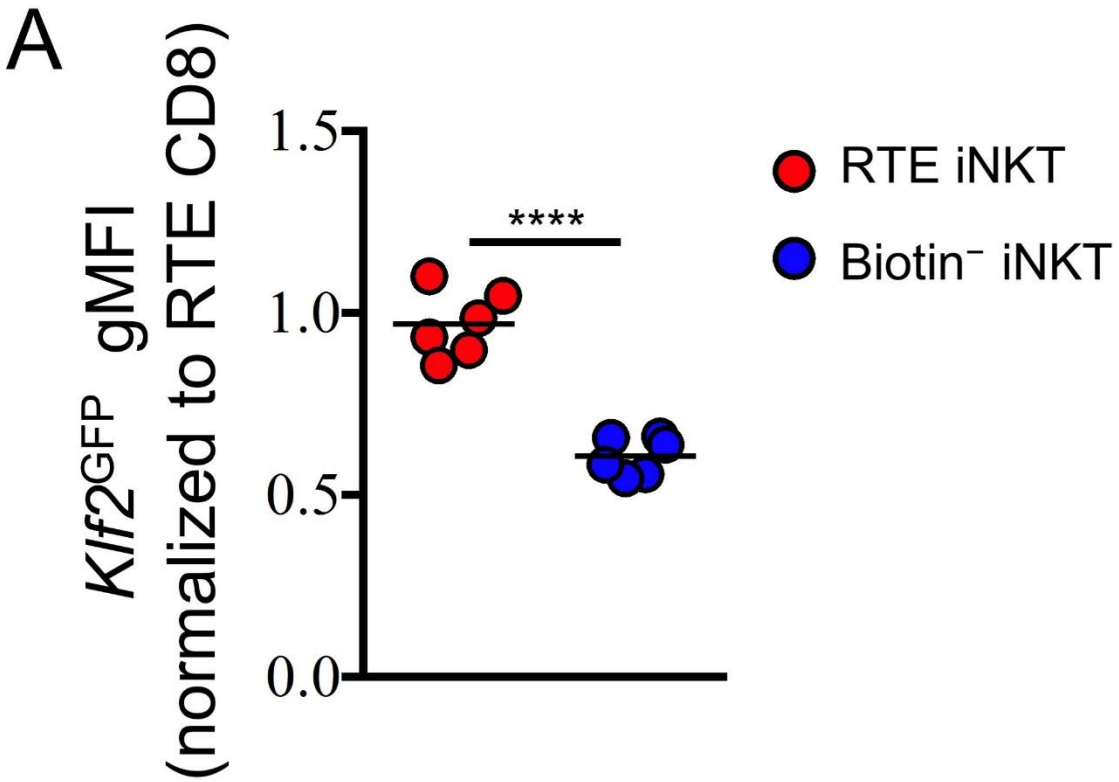

Figure 2-7. RTE iNKT cells express high level of *Klf2*^{GFP}.

(**A**) Normalized *Klf2*^{GFP} gMFI of RTE iNKT cells and biotin^{-} iNKT cells. Data are pooled from two independent experiments with 2–4 mice in each. $^{****}p<0.0001$ (unpaired two tailed *t* test). Each symbol represents an individual mouse; small horizontal lines indicate the mean.

The transcription factor Kruppel-like factor 2 (*Klf2*) is crucial for the thymic egress of conventional CD4 and CD8 lymphocytes (39). However, its role in thymic emigration of iNKT cells is currently unknown. To test whether thymic egress of iNKT cells was dependent on *Klf2*, we analyzed mixed bone-marrow chimeras with wild type and *Klf2*-deficient bone marrow. We performed intra-thymic labeling to track RTE. As expected, *Klf2*-deficient conventional CD4 and CD8 T cells were enriched in the thymus and underrepresented amongst peripheral cells (Figure 2-5 C, D). Similarly, *Klf2*-deficient iNKT cells were also enriched in the thymus and underrepresented amongst RTE and biotin$^-$ iNKT cells populations (Figure 2-5 C, D), suggesting thymic emigration of iNKT cells is dependent on *Klf2*. As *Klf2* regulates expression of S1PR1 (39), this is consistent with the previously reported requirement for S1PR1 in iNKT cell thymic egress (121). Next, we sought to assess *Klf2* expression in thymic and RTE iNKT cells using *Klf2*^{GFP} reporter mice. The majority of thymic iNKT cells did not express *Klf2*, though thymic CCR7$^+$ iNKT cells or RTE iNKT cells highly expressed *Klf2*comparable to mature thymic CD8 single positive (SP) thymocytes or RTE CD8 T cells, respectively (Figure 2-5 E, Figure 2-7 A). Altogether, these results suggest that CCR7$^+$ iNKT cells are the predominant thymic emigrating iNKT cell, and they do so in a *Klf2* dependent manner.

RTE iNKT are functionally immature and undergo further differentiation

in the periphery

In further characterizing RTE iNKT cells, we observed that T-bet$^+$, and ROR-γt$^+$ cells were substantially underrepresented amongst RTE iNKT cells compared to total thymic iNKT cells (Figure 2-8 A, B), suggesting that both T-bet$^+$ NKT1 and ROR-γt$^+$NKT17 cells may be resident in the thymus. This is consistent with the previously reported long-term retention of thymic NK1.1$^+$ iNKT cells (122). Similarly, thymic NKT2 cells that produce high levels of IL-4 (human CD2) were also less likely to be found amongst RTE (Figure 2-8 B). Though CCR7$^+$ iNKT cells were predominant within the RTE population, a small proportion of T-bet$^+$ NKT1 cells were still observed (Figure 2-8 A, B). However, cells within this small population failed to express Qa2, while the thymic T-bet$^+$ NKT1 and splenic biotin$^-$ T-bet$^+$NKT1 cells both expressed high level of Qa2 (Figure 2-8 C, D). As Qa2 has commonly been used to mark the most mature thymocytes, this suggests that RTE NKT1 cells were recently derived from progenitors, as opposed to emigrating as a mature cell. Indeed, in cells collected 72 hr after intra-thymic labeling, we observed a progressive increase in Qa2 in RTE NKT1 cells (Figure 2-8 C, D). Furthermore, RTE T-bet$^+$ NKT1 expressed significantly higher PLZF at 24 hr, while the expression was down regulated over 72 hr (Figure 2-8 D). Taken together, these results strongly suggested that RTE T-bet$^+$ NKT1 cells were not directly derived from mature thymic NKT1 cells, but more likely recently differentiated from

precursors. To further support this hypothesis, we sorted CCR7^{+} thymocytes (CD4^{+} *Tbx21*$^{GFP-}$ huCD2^{-}CD24^{-} CD8^{-}) from *Tbx21*^{GFP}/KN2 mice and injected them intra-thymically into congenic hosts (Figure 2-9 A). Five days later, all three effector subsets, NKT1, NKT2 and NKT17 cells were detected in the spleen (Figure 2-9 B, C), indicating CCR7^{+} iNKT cells rapidly emigrate to the periphery and serve as precursors that give rise to iNKT effector subsets.

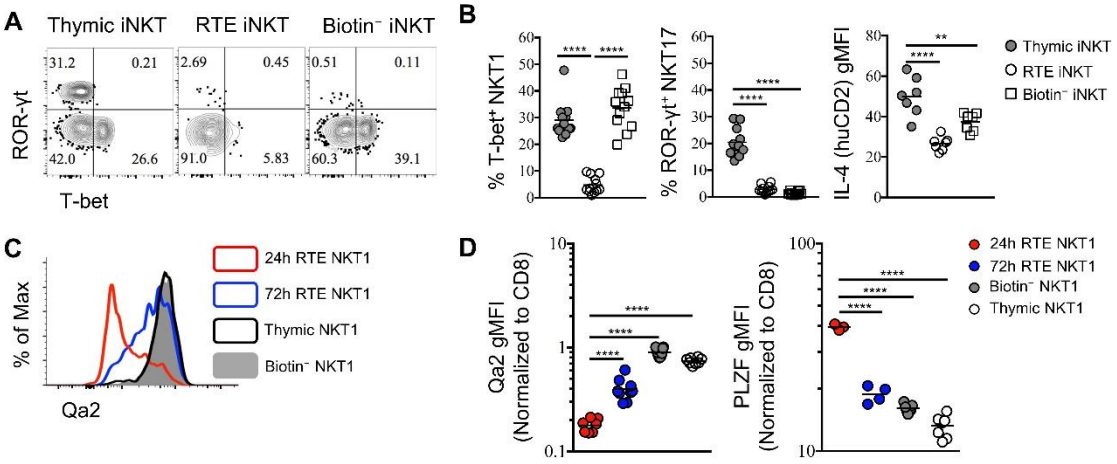

Figure 2-8. RTE iNKT cells are immature and undergo further differentiation after reaching periphery.

(**A**) Expression of T-bet and ROR-γt in thymic, RTE and splenic biotin⁻ iNKT cells. Number in quadrants indicates percent cells in each (throughout). Data are representative of 3 independent experiments with 2–6 mice in each. (**B**) Frequency of T-bet⁺ NKT1, ROR-γt⁺ NKT17 cells and normalized gMFI of IL-4 (human CD2) in thymic, RTE and splenic biotin⁻ iNKT cells. The solid grey circle represents thymic iNKT cell, the open circle represents RTE iNKT cells, the open square represents biotin⁻ iNKT cells. $^{**}p$=0.0048, $^{****}p$<0.0001 (one-way ANOVA). Data are pooled from 3 independent experiments with 2–6 mice in each. Each symbol represents an individual mouse; small horizontal lines indicate the mean. (**C**) Expression of Qa2 in thymic, 24 hr RTE, 72 hr RTE and splenic biotin⁻ T-bet⁺ NKT1 cells. Data are representative of 3 independent experiments with 2–3 mice in each. (**D**) Normalized gMFI of Qa2 in thymic, 24 hr RTE, 72 hr RTE and biotin⁻ T-bet⁺ NKT1 cells (left column). Normalized gMFI of PLZF in thymic, 24 hr RTE, 72 hr RTE and splenic biotin⁻ T-bet⁺ NKT1 cells (right column). $^{****}p$<0.0001 (one-way ANOVA). Data are pooled from 3 independent experiments with 2–3 mice in each. Each symbol

represents an individual mouse; small horizontal lines indicate the mean.

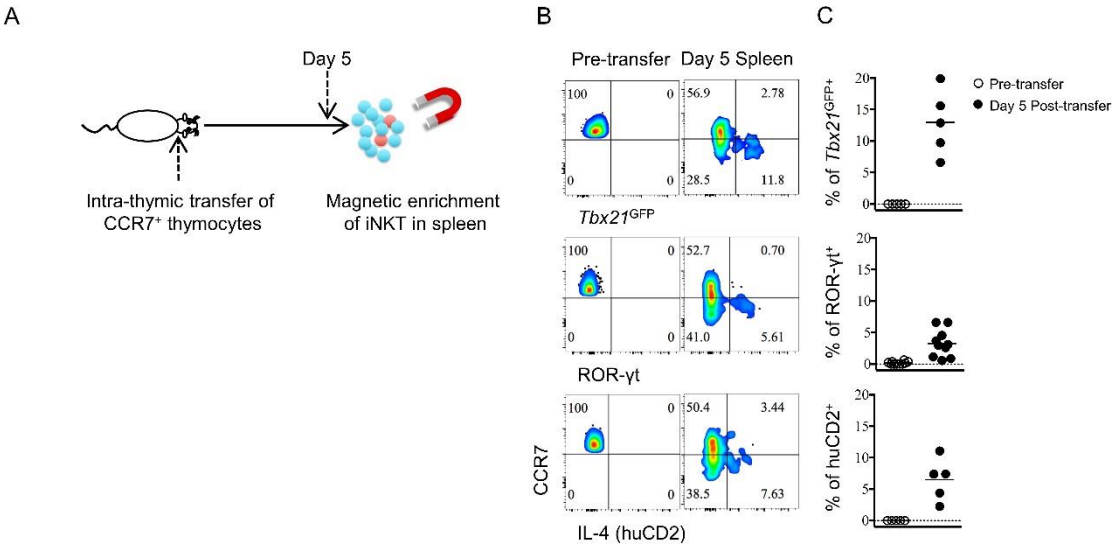

Figure 2-9. Thymic CCR7⁺ iNKT emigrate to the periphery and undergo further development into effector subsets.

(**A**) Experimental scheme for intra-thymic transfer of sorted CCR7⁺ thymocytes (CD4⁺ *Tbx21*^{GFP}⁻huCD2⁻ CD24⁻ CD8⁻) from *Tbx21*^{GFP}/KN2 mice into congenic hosts. The phenotype of donor derived iNKT cells was examined in the spleen after 5 days. (**B**) Expression of *Tbx21*^{GFP}, ROR-γt and human CD2 in CCR7⁺ iNKT cells sorted from BALB/c *Tbx21*^{GFP} KN2 mice before intra-thymic transfer (left column) or 5 days after transfer into congenic BALB/c recipient mice (right column). (**C**) Frequency of *Tbx21*$^{GFP+}$, ROR-γt⁺ or human CD2⁺ cells in donor cells recovered in the spleen, before or 5 days after intra-thymic transfer into the thymus of congenic BALB/c recipient mice. Each symbol represents an individual recipient mouse; small horizontal lines indicate the mean.

Ccr7 deficiency impairs differentiation of iNKT effector subsets and their localization to the thymic medulla

As CCR7$^+$ iNKT cells serve as progenitors for all three subsets of iNKT cells in the thymus, we sought to evaluate whether CCR7 itself might regulate the differentiation of thymic iNKT cells. To test this, we created mixed bone-marrow chimeras with wild type and *Ccr7*-deficient bone marrow cells, and analyzed the phenotype of thymic iNKT cells derived from both donors. As expected, the generation of double positive (DP) thymocytes was not affected by the absence of CCR7, while iNKT cells derived from the *Ccr7*-deficient donors showed substantially impaired differentiation of all three iNKT effector subsets (Figure 2-10 A, B). Similar to CCR7$^+$ iNKT cells, CCR7$^+$ MAIT cells were at early stage of development (Figure 2-1 I) and distinct from effector MAIT cells (Figure 2-2 E), which suggested the possibility of a similarly important role of CCR7 in the development of MAIT cells. In mixed bone marrow chimeras with wild type and *Ccr7*-deficient bone marrow cells, MAIT cell differentiation was also severely impaired when lacking cell-intrinsic CCR7 (Figure 2-11 A–C).

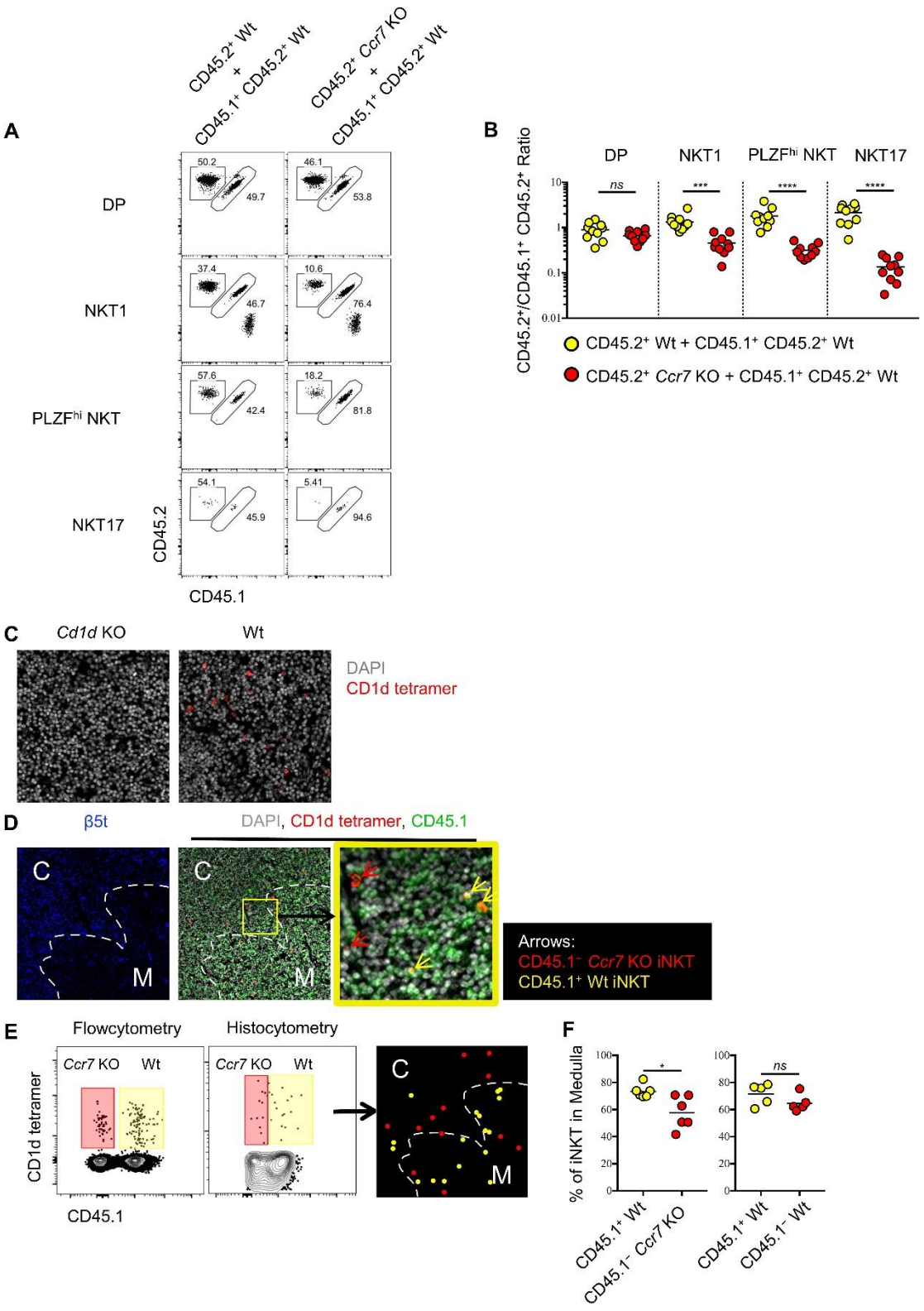

Figure 2-10. *Ccr7* deficiency impairs iNKT subsets differentiation and medullary localization.

(**A**) Mixed bone marrow chimeras were generated with 50:50 ratio of donor bone marrow cells using CD45.2$^+$ CD45.2$^+$ B6 *Ccr7* KO cells and CD45.1$^+$ CD45.2$^+$ B6 Wt cells, or with 50:50 ratio of donor bone marrow cells using CD45.2$^+$ CD45.2$^+$ B6 Wt cells and CD45.1$^+$ CD45.2$^+$ B6 Wt cells. Eight weeks later, the frequency of thymic iNKT effector subsets and thymocytes derived from different donor source were analyzed. Data are representative of 3 independent experiments with 4–10 mice in each. Numbers adjacent to outlined areas indicate percent cells in each, throughout. (**B**) Statistical analysis of thymic iNKT subsets and DP thymocytes in 8-week-old BM chimeras reconstituted with *Ccr7* KO and Wt cells or with Wt and Wt cells. Numbers indicate the ratio between the cells derived from each donor source. $^{***}p$=0.0001 (unpaired two tailed *t* test). $^{****}p$<0.0001 (unpaired two tailed *t* test). *ns*, not significant, p>0.05 (unpaired two tailed *t* test). Data are pooled from 3 independent experiments with 4–10 mice in each. Each symbol represents an individual mouse; small horizontal lines indicate the mean. (**C**) Thymic sections of *Cd1d* KO (left column) and Wt (right column) B6 mice were stained with CD1d tetramer (red) and the DNA-binding dye DAPI (grey) to visualize iNKT cells *in situ*. (**D**) Thymic sections of BM chimeras 8 weeks after reconstituted with *Ccr7* KO and Wt cells were stained for the cortical-thymic-epithelial-cell-associated proteasomal subunit β5t (blue), CD1d tetramer (red), CD45.1 (green) and the DNA-binding dye DAPI (grey) to visualize and distinguish cortex, medulla, CD45.1$^-$*Ccr7* KO iNKT and CD45.1$^+$ Wt iNKT cells. Yellow outline (middle column) indicates magnified area (right column); Arrows indicate CD45.1$^-$*Ccr7* KO iNKT cells (red), CD45.1$^+$ Wt iNKT cells (yellow). C: Cortex; M: Medulla. (**E**) Flowcytometry analysis of thymocytes (left column), histocytometry analysis of immunofluorescence image (middle column) and

localization of CD45.1⁻ *Ccr7* KO iNKT cells (red dot), CD45.1⁺ Wt iNKT cells (yellow dot) as determined by histocytometry (right column). (**F**) Frequency of iNKT cells localized in thymic medulla from 8-week-old BM chimeras reconstituted with *Ccr7* KO and Wt cells (left column) or with Wt and Wt cells (right column). $^{*}p$=0.0141, *ns*, not significant, p=0.1775 (unpaired two tailed *t* test). Each symbol represents an individual mouse; small horizontal lines indicate the mean.

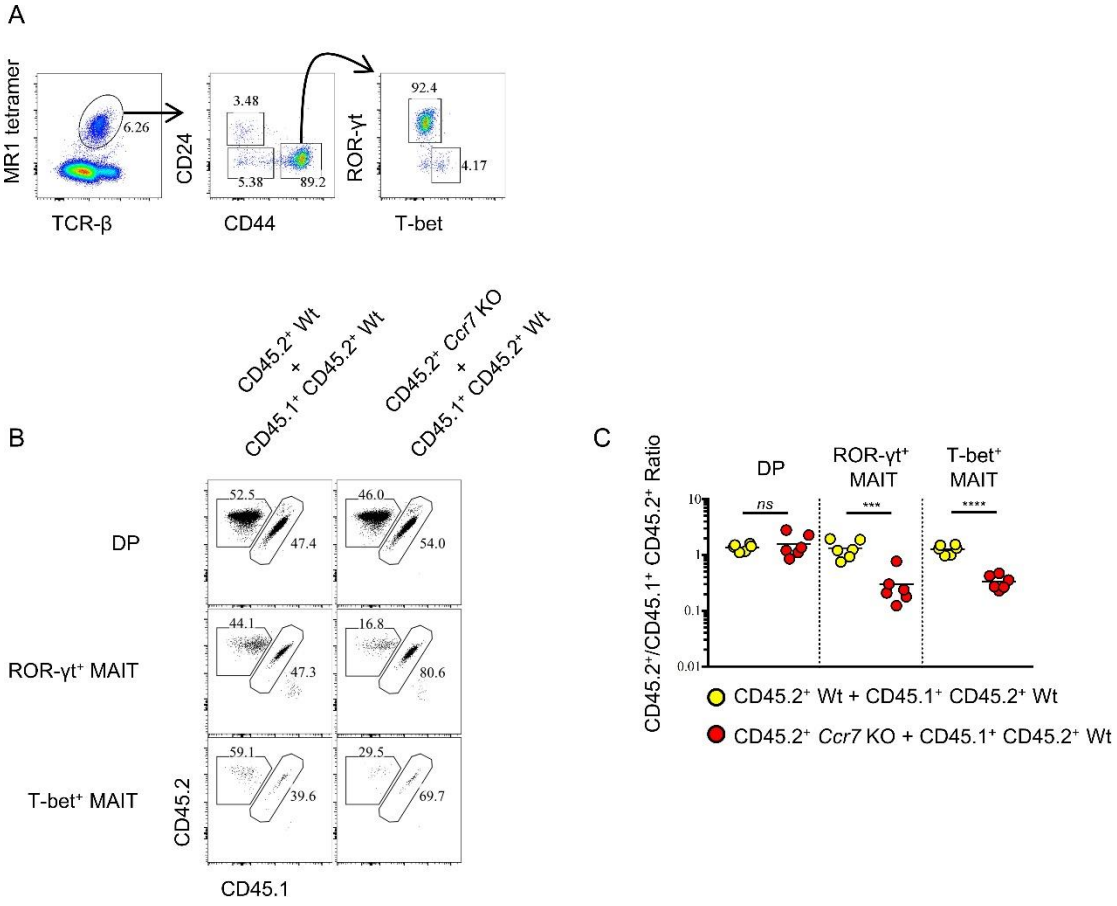

Figure 2-11. *Ccr7* deficiency impairs MAIT cells differentiation.

(**A**) Gating strategy to identify enriched thymic MAIT cells and mature ROR-γt⁺ and T-bet⁺ MAIT cells. (**B**) Mixed bone marrow chimeras were generated with a 50:50 ratio of donor bone marrow cells using CD45.2⁺ CD45.2⁺ B6 *Ccr7* KO cells and CD45.1⁺ CD45.2⁺ B6 Wt

cells, or with 50:50 ratio of donor bone marrow cells using CD45.2$^+$ CD45.2$^+$ B6 Wt cells and CD45.1$^+$ CD45.2$^+$ B6 Wt cells. Seven weeks later, the frequency of thymic MAIT mature subsets and thymocytes derived from different donor source were analyzed. Numbers adjacent to outlined areas indicate percent cells in each throughout. Data are representative of 3 independent experiments with 2–6 mice in each. (**C**) Statistical analysis of thymic MAIT mature subsets and DP thymocytes in 7-week-old BM chimeras reconstituted with *Ccr7* KO and Wt cells or with Wt and Wt cells. Numbers indicate the ratio between the cells derived from each donor source. Data are pooled from 3 independent experiments with 2–6 mice in each. $^{***}p$=0.0009 (unpaired two tailed *t* test). $^{****}p$<0.0001 (unpaired two tailed *t* test). *ns*, not significant, p>0.05 (unpaired two tailed *t* test). Each symbol represents an individual mouse; small horizontal lines indicate the mean.

It was recently shown that CCR7 responds to CCL21a produced in the thymic medulla and is essential for migration of thymocytes from the cortex to medulla (26). To directly assess whether CCR7 directs the medullary localization of thymic iNKT cells, we performed CD1d tetramer based immunofluorescence and histocytometry analysis in the mixed bone-marrow chimeras reconstituted with wild type and *Ccr7*-deficient bone marrow donors. CD1d tetramer based immunofluorescence could specifically detect the CD1d restricted iNKT cells in the thymus (Figure 2-10 C). Moreover, *Ccr7*-deficient iNKT cells showed significantly reduced localization in the thymic medulla compared to wild type iNKT cells (Figure 2-10 D–F). These data suggest that, CCR7 not only plays an indispensable role in differentiation of thymic iNKT effector subsets, but also directs iNKT cells to localize in thymic medulla.

Thymic iNKT effector subsets are resident and influence thymic tissue homeostasis

To gain insight into the potential tissue residency of thymic iNKT effector subsets, we generated parabiotic mice, which share blood circulation through surgical joining (Figure 2-12 A). Congenically distinct $CD45.1^+$ and $CD45.2^+$ mice were surgically connected for 30 days. Splenic CD4 or CD8 T cells were present at 50:50 ratios in parabiotic pairs consistent with their known circulation patterns (Figure 2-12 B, C). In contrast, ~80% of splenic

iNKT cells were of host origin (Figure 2-12 B, C), confirming that the majority of splenic iNKT cells are not circulating (11). Remarkably, >95% of thymic iNKT cells were of host origin (Figure 2-12 B, C). Considering that thymic iNKT effector subsets are negative for *Rag2*^{GFP} (Figure 2-1 A), these data suggest that iNKT cells in the thymus are largely tissue-resident.

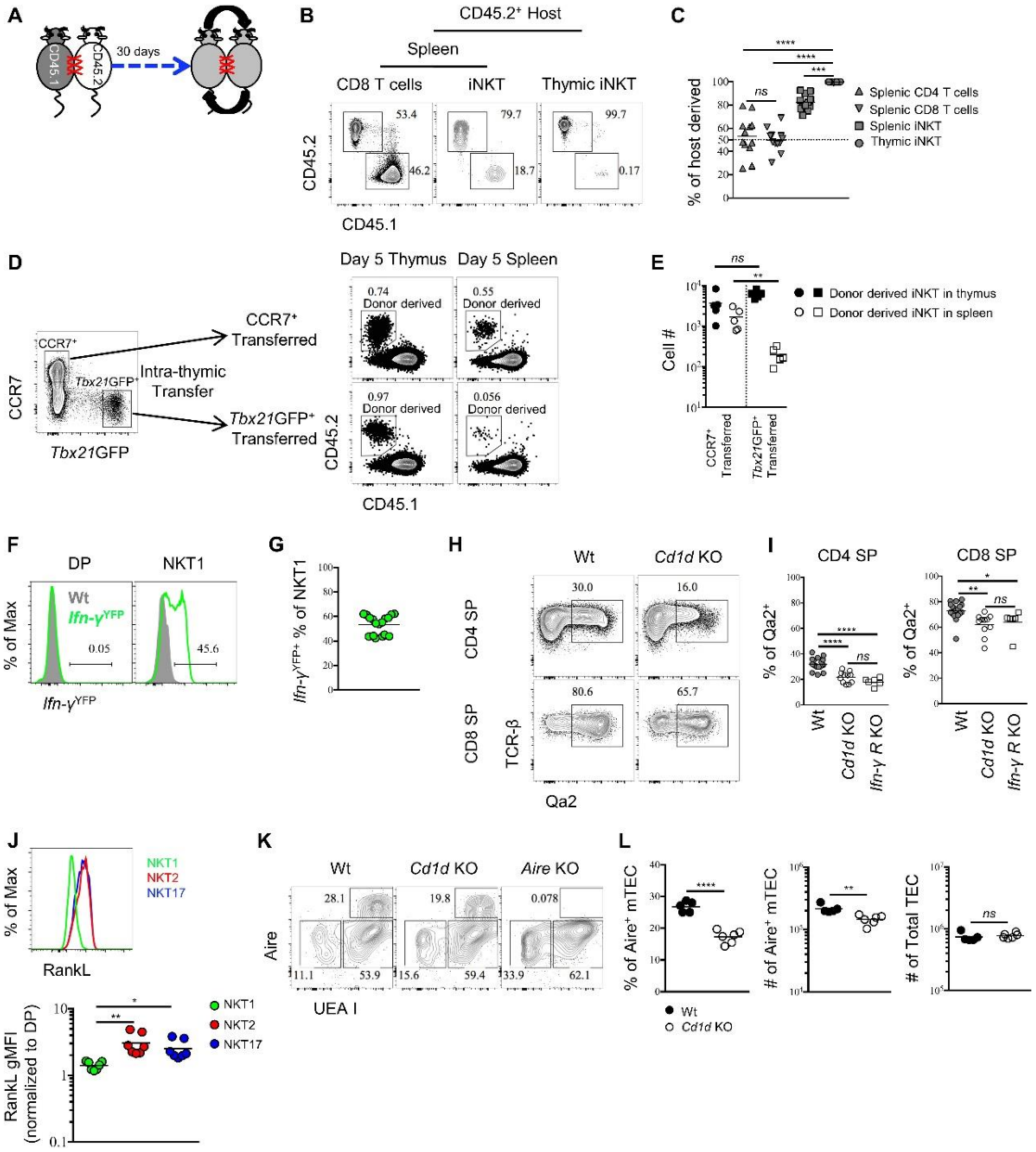

Figure 2-12. Thymic iNKT effector subsets are predominantly resident and may influence thymocytes maturation.

(**A**) Experimental scheme of parabiosis surgery. (**B**) Representative flowcytometry profile of spleen and thymus from the CD45.2⁺ host of a parabiotic pair after 30 days of parabiosis surgery, the number indicates the frequency of CD45.2⁺ (host) and CD45.1⁺ (parabiotic counterpart) cells in CD8 T cells and iNKT cells. Numbers adjacent to outlined areas indicate percent cells in each throughout. Data are representative of 2 independent experiments with 3

parabiotic pairs in each. (**C**) The frequency of cells derived from the host parabiont in splenic $CD4^+$ T, $CD8^+$ T and iNKT cells as well as thymic iNKT cells. Data are pooled from 2 independent experiments with 3 parabiotic pairs in each. *ns*, not significant, p=0.8722 (one-way ANOVA). $^{***}p$=0.0009, $^{****}p$<0.0001 (one-way ANOVA). Each symbol represents an individual mouse; small horizontal lines indicate the mean. (**D**) $CCR7^+$ *Tbx21*$^{GFP-}$ and $CCR7^-$ *Tbx21*$^{GFP+}$thymocytes were sorted from BALB/c *Tbx21*^{GFP} mice and intra-thymically transferred to congenic BALB/c recipients (left column). After 5 days, the donor derived iNKT cells were recovered in thymus and spleen from mice received $CCR7^+$ *Tbx21*$^{GFP-}$ thymocytes or $CCR7^-$ *Tbx21*$^{GFP+}$ thymocytes (right column). Numbers adjacent to outlined areas indicate percent cells in each throughout. Data are representative of 5 independent experiments. (**E**) Cell number of donor derived iNKT cells recovered in thymus and spleen from mice that received $CCR7^+$ *Tbx21*$^{GFP-}$ thymocytes or $CCR7^-$ *Tbx21*$^{GFP+}$thymocytes. Data are pooled from 5 independent experiments with 2 mice in each. *ns*, not significant, p=0.1508 (unpaired two tailed *t* test). $^{**}p$=0.0079 (unpaired two tailed *t* test). Each symbol represents an individual mouse; small horizontal lines indicate the mean. (**F**). Expression of YFP in DP thymocytes (left column) or thymic NKT1 cells ($NK1.1^+$ $CD44^+$) (right column), the grey shade represents cells from Wt mice, the solid green line represents cells from *Ifn-γ*^{YFP} mice; Numbers adjacent to solid black line indicate percent of *Ifn-γ*$^{YFP+}$ cells from *Ifn-γ*^{YFP} mice; Data are representative of 4 independent experiments with 3–5 mice in each. (**G**) Frequency of *Ifn-γ*$^{YFP+}$ cells within thymic NKT1 cells. Data are pooled from 4 independent experiments with 3–5 mice in each. Each symbol represents an individual mouse; small horizontal lines indicate the mean. (**H**) Expression of Qa2 in CD4 SP or CD8 SP thymocytes from Wt or *Cd1d* KO mice. Numbers

adjacent to outlined areas indicate percent cells in each throughout. Data are representative of 5 independent experiments. (**I**) Frequency of $Qa2^+$ cells in CD4 SP or CD8 SP thymocytes from Wt, *Cd1d* KO and *Ifn-γR*^{KO} mice. Data are pooled from 5 independent experiments, n = 18 (Wt), n = 11 (*Cd1d* KO), n = 6 (*Ifn-γR*^{KO}). $^{*}p$=0.0426, $^{**}p$=0.0023, $^{****}p$<0.0001 (one-way ANOVA). *ns*, not significant, p=0.2676 (CD4 SP), p=0.8848 (CD8 SP) (one-way ANOVA). Each symbol represents an individual mouse; small horizontal lines indicate the mean. (**J**) Expression of RankL in thymic NKT1, NKT2 and NKT17 cells (upper panel). Normalized gMFI of RANKL in thymic NKT1, NKT2 and NKT17 cells (bottom panel). Data are representative of 3 independent experiments with 2–3 mice in each. $^{**}p$=0.0027 (NKT1 *vs* NKT2), $^{*}p$=0.0391 (NKT1 *vs* NKT17) (one-way ANOVA). (**K**) Expression of Aire in TEC from Wt, *Cd1d* KO or Aire KO mice. Numbers adjacent to outlined areas indicate percent cells in each throughout. Data are representative of 4 independent experiments. (**L**) Frequency and number of $Aire^+$ mTEC (left and middle column), number of total TEC (right column) from Wt and *Cd1d* KO mice. Data are representative of 4 independent experiments, n = 5 (Wt), n = 6 (*Cd1d* KO). $^{****}p$<0.0001, $^{**}p$=0.0032, ns, not significant, p=0.5209 (unpaired two tailed *t* test). Each symbol represents an individual mouse; small horizontal lines indicate the mean.

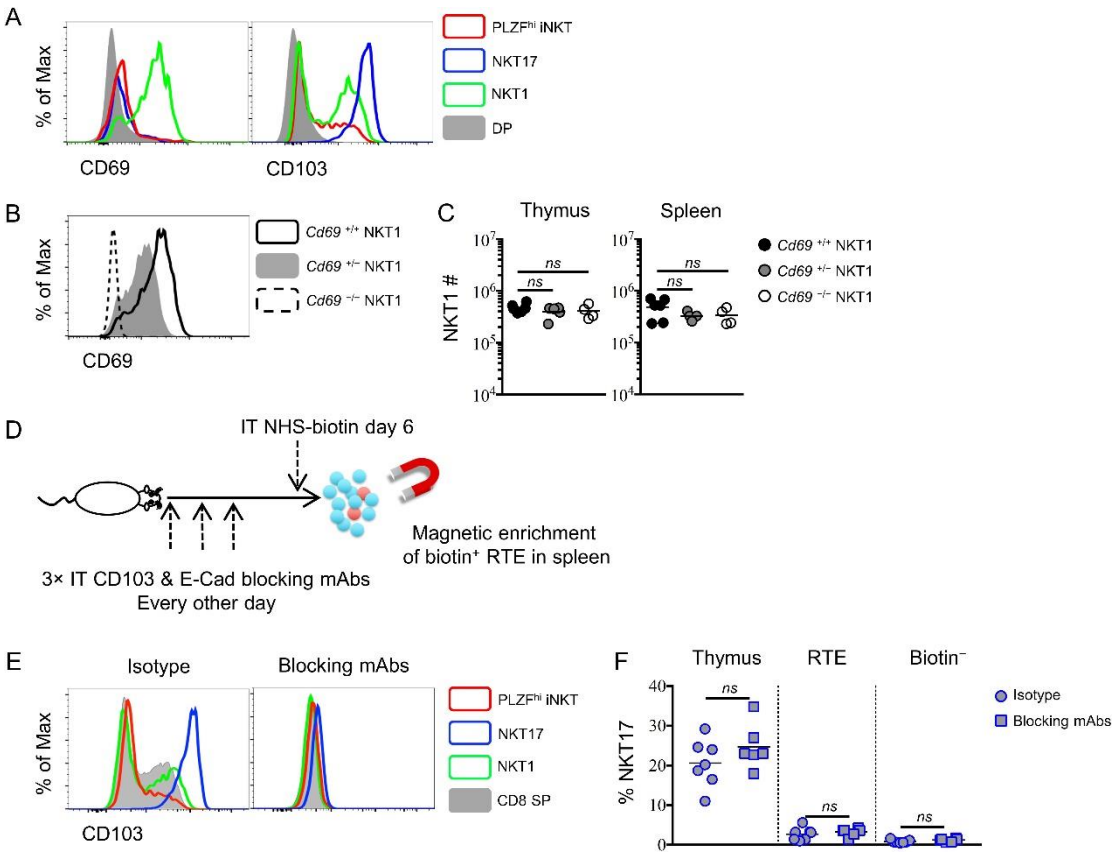

Figure 2-13. NKT1 and NKT17 cells do not rely exclusively on CD69 or CD103 for tissue residency.

(**A**) Expression of CD69 (left column) and CD103 (right column) in thymic PLZF^{hi} iNKT cells, NKT17 cells, NKT1 cells and DP thymocytes. (**B**) Expression of CD69 in thymic NKT1 cells from *Cd69*$^{+/+}$, *Cd69*$^{+/–}$ and *Cd69*$^{–/–}$ mice. (**C**) Number of NKT1 cells in thymus (left column) and spleen (right column) from *Cd69*$^{+/+}$, *Cd69*$^{+/–}$ and *Cd69*$^{–/–}$ mice. Data are pooled from 3 independent experiments, n = 6 (*Cd69*$^{+/+}$), n = 5 (*Cd69*$^{+/–}$), n = 4 (*Cd69*$^{–/–}$). *ns*, not significant, $p>0.05$ (one-way ANOVA). Each symbol represents an individual mouse; small horizontal lines indicate the mean. (**D**) Experimental scheme for blocking CD103 and E-cadherin interaction in thymus. BALB/c mice were intra-thymically injected with CD103 and E-cadherin blocking antibodies or isotype control antibody every other day (at day 0, day 2 and

day 4), mice received intra-thymic labeling with NHS-biotin at day six and enrich biotin^{+} cells in spleen to track RTE 24 hr later. (**E**) CD103 staining in thymic PLZF^{hi} iNKT cells, NKT17 cells, NKT1 cells and CD8 SP thymocytes from mice received isotype control antibody (left column) or blocking antibodies (right column). (**F**) Frequency of NKT17 cells among thymic, RTE and biotin^{-} iNKT cells from mice received isotype control antibody (circle) or blocking antibodies (square). Data are pooled from 2 independent experiments, n = 7 (isotype), n = 6 (blocking mAbs). *ns*, not significant, $p>0.05$ (unpaired two tailed *t*test). Each symbol represents an individual mouse; small horizontal lines indicate the mean.

We also directly tested the retention or emigration of sorted thymic CCR7^{+} iNKT cells (CD4^{+} *Tbx21*$^{GFP-}$ CD24^{-} CD8^{-}) or *Tbx21*$^{GFP+}$ NKT1 (CCR7^{-} CD24^{-} CD8^{-}) cells by transferring them intra-thymically into congenic hosts. In contrast to thymic CCR7^{+}iNKT cells, wherein a substantial number of transferred cells were recovered from spleen 5 days after transfer, the transferred *Tbx21*$^{GFP+}$ NKT1 cells were rarely recovered from spleen (Figure 2-12 D, E), strongly suggest that CCR7^{+} iNKT cells efficiently emigrate thymus while iNKT effector subsets are retained in the thymus. Together, these results show that peripheral iNKT effector subsets are not directly derived from thymic iNKT effector subsets, but rather develop from the CCR7^{+}iNKT progenitors, and indicate that thymic and peripheral pools of iNKT effector subsets do not exchange.

Consistent with their tissue residency, NKT1 and NKT17 cells highly express the classical tissue residency molecules CD69 and CD103, respectively (Figure 2-13 A). To evaluate whether CD69 and CD103 are required for the thymic retention of NKT1 and NKT17 cells, we analyzed *Cd69*$^{+/+}$, *Cd69*$^{+/-}$ and *Cd69*$^{-/-}$ mice. We observed comparable number of NKT1 cells among these mice in both thymus and spleen (Figure 2-13 B, C). To block CD103 interaction with E-Cadherin on epithelial cells, monoclonal antibodies (mAb) against CD103 and E-Cadherin were intra-thymically injected three times (Figure 2-13 D, E). Combined with intra-thymic

biotin labeling to track RTE iNKT, we did not observe loss of thymic NKT17 cells nor increase of NKT17 cells in the RTE and peripheral iNKT cells population (Figure 2-13 F). These data indicate the thymic retention of iNKT effector subsets is unlikely to solely rely on either CD69 or CD103.

That iNKT effector subsets are preferentially retained in the thymus raises the question of their function there. To ask whether NKT1 cells might have effects in the thymus, we investigated if they were producing IFN-γ in the steady state using IFN-γ reporter mice. We observed that ~50% of NKT1 ($NK1.1^+$ $CD44^+$) cells were *Ifn-γ*^{YFP} positive (Figure 2-12 F, G). Furthermore, Qa2 expression on mature thymocytes was recently shown to be interferon dependent (123), and was reduced in absence of iNKT cells (Figure 2-12 H, I), comparable to that observed in IFN-γ receptor-deficient mice (Figure 2-12 I), showing that the IFN-γ produced by NKT1 cells is biologically active, although the functional relevance remains unclear. Lastly, iNKT cells have been shown to regulate mTEC differentiation through the production of RANKL (25). We demonstrate here that NKT2 and NKT17 cells are the exclusive producers of RANKL among iNKT cells (Figure 2-12 J). Consistent with a previous report (25), the absence of iNKT cells resulted in specific reduction of $Aire^+$ medullary thymic epithelial cells (mTEC), while the number of total TEC was not affected (Figure 2-12 K, L). Together these data strongly suggest iNKT cells modulate thymic homeostasis and indicate the possibility that they might

further influence T cell development. Given that different inbred strains have strikingly different ratios of iNKT effector subsets in the thymus, our data imply that retention of lipid specific effector T cells in the thymus fine-tunes T cell development and tissue homeostasis.

Discussion

Previously, PLZF^{hi} iNKT cells have been defined as NKT2 cells, however, our data strongly suggested that CCR7^{+} PLZF^{hi} iNKT cells had multi-lineage potential in both the thymus and periphery. Thus, PLZF^{hi} iNKT cells comprise a mixture of progenitors and mature IL-4 producing NKT2 effector cells. Such heterogeneity was indicated in the previous RNA-Seq analysis of 'bulk PLZF^{hi} NKT2 cells' (28, 29). Moreover, our data demonstrate that CCR7 not only marks the precursors but also directs iNKT cells to localize to the thymic medulla, which plays a critical role in their differentiation to effector subsets. This is consistent with a previous report, which showed that *Ccr7* deficient mice harbor fewer thymic iNKT cells (27). Considering the predominant medullary localization of all three iNKT effector subsets (24), it would seem that medullary factors are crucial for the differentiation and/or maintenance/survival of iNKT effector subsets. Indeed, IL-15 derived from medullary thymic epithelial cells (mTEC) was implicated in the generation of T-bet^{+} NKT1 cells (25, 124). Whether and how medullary factors are required for

differentiation of NKT2 and NKT17 cells remains to be determined.

Another type of innate-like T cells, MAIT cells, which are restricted to MR1 and recognize riboflavin metabolites, have gained interest recently. A number of studies indicated a parallel between these iNKT cells and innate-like T cells in their development and functions (71, 120, 125). For example, both mature iNKT and MAIT cells are poised effector cells, producing large amounts of cytokines upon stimulation; both express and depend on PLZF; and both are composed of effector subsets analogous to CD4 T helper subsets. We show here that, similar to iNKT cells, CCR7 also marks a population of immature MAIT cells after the agonist selection. However, whether CCR7 directs their localization remain to be answered.

Mature iNKT effector subsets, including NKT1, NKT2 and NKT17, exist in both the thymus and peripheral tissues (24). Since iNKT cells originate in the thymus (5, 8), this raises the question whether the peripheral iNKT effector cells directly arise from mature thymic iNKT effector cells or not. Previous work showed that a thymic NK1.1^{-} iNKT cell emigrates (69, 126), but the work was performed before it was appreciated that mature NKT2 and NKT17 effector cells are also NK1.1^{-}. In this study, we demonstrate that all thymic iNKT effector cells are long-term residents that do not emigrate, and that peripheral iNKT effector subsets derive from CCR7^{+} iNKT cells that emigrate from the thymus. iNKT cells can participate in immunity to infection (23), but

they can also regulate tissue homeostasis in the steady state (29, 35, 109, 117). An effect of NKT2 cells on CD8 T cell development in the steady state is well supported by previous data showing their constitutive production of IL-4 drives Eomesodermin (Eomes) expression and a memory-like functional state in CD8 T cells (12, 24). In this report, we further show that thymic resident NKT1 cells produce IFN-γ and promote Qa2 expression in CD4 and CD8 SP thymocytes. T cells up-regulate Qa2 expression during their maturation in the thymus, and type I interferon signaling has been implicated in this process (123). It is possible that IFN-γ might function synergistically with type I interferon to influence Qa2 expression. Lastly, we show both NKT2 and NKT17 cells express RANK ligand, and together could promote Aire expression in mTEC in supporting central tolerance.

It is worth mentioning that a small number of $CCR7^+$ iNKT cells express lower amounts of PLZF, LEF1 or CD4. Indeed, the development of iNKT cells in the thymus is a dynamic process, even though the $CCR7^+$ iNKT cell population is largely immature and maintains precursor potential, it seems likely some of these cells have begun to receive development signals and to differentiate, prior to having completely lost CCR7 expression. Of interest, though CCR7 is critical for optimal differentiation of all three iNKT subsets, NKT17 cells seem to be most affected by CCR7 deficiency. Since NKT1, NKT2 and NKT17 are all localized to the thymic medulla, it is unclear what might cause this effect.

Possibly, the differentiation or maintenance of NKT17 cells is more dependent on as yet undefined factors in the medullary environment.

In summary, we demonstrate here that the sub-population of $CCR7^{+}$ $PLZF^{hi}$ iNKT cells represent a pool of precursor cells for all three iNKT effector subsets in thymus and periphery. Meanwhile, CCR7 not only marks the precursors, but also directs the medullary localization and differentiation of iNKT effector subsets. The thymic and peripheral iNKT effector subsets are resident and do not exchange, therefore depend on $CCR7^{+}$ iNKT progenitors for their establishment.

Material and Methods

Key Resources Table				
Reagent type (species) or resource	**Designation**	**Source or reference**	**Identifiers**	**Additional information**
antibody	anti-CCR7	BD Biosciences	Cat # 562675	(1:50)
antibody	anti-CD4	BD Biosciences	Cat # 563331	(1:400)
antibody	anti-CD8α	BD Biosciences	Cat # 563786	(1:400)
antibody	anti-CD24	BioLegend	Cat # 101824	(1:200)
antibody	anti-NK1.1	BioLegend	Cat # 108718	(1:100)
antibody	anti-CD44	TONBO Biosciences	Cat # 80-0441-U025	(1:200)
antibody	anti-human CD2	BioLegend	Cat # 309218	(1:20)
antibody	anti-TCRβ	BD Biosciences	Cat # 563221	(1:200)
antibody	anti-PD-1	BioLegend	Cat # 135213	(1:100)
antibody	anti-CD45.1	BioLegend	Cat # 110738	(1:200)
antibody	anti-CD45.2	eBioscience	Cat # 11-0454-81	(1:200)
antibody	anti-Qa2	BioLegend	Cat # 121710	(1:200)
antibody	anti-RANKL	eBioscience	Cat # 12-5952-82	(1:100)
antibody	anti-B220	BioLegend	Cat # 103244	(1:200)
antibody	anti-CD11c	eBioscience	Cat # 47-0114-82	(1:200)
antibody	anti-CD11b	eBioscience	Cat # 47-0112-82	(1:200)
antibody	anti-F4/80	eBioscience	Cat # 47-4801-82	(1:200)
antibody	anti-CD122	BD Biosciences	Cat # 562960	(1:100)
antibody	anti-PLZF	BD Biosciences	Cat # 563490	(1:200)
antibody	anti-ROR-γt	BD Biosciences	Cat # 562684	(1:200)
antibody	anti-T-bet	BioLegend	Cat # 644824	(1:200)
antibody	anti-Egr2	eBioscience	Cat # 17-6691-80	(1:100)
antibody	anti-Aire	eBioscience	Cat # 50-5934-82	(1:100)
antibody	anti-LEF1	Cell Signaling Technology	Cat # 2230S	(1:100)
antibody	anti-Rabbit IgG AF488	Invitrogen	Cat # A11034	(1:400)
antibody	anti-IL-17RB	R&D Systems	Cat # FAB10402G	(1:20)
antibody	Goat-anti-R Phycoerythrin (PE)	Abcam	Cat # ab34721	(1:200)
antibody	Donkey-anti-Goat AF555	Abcam	Cat # ab150130	(1:400)
antibody	Rabbit-anti-β5t	MBL International	Cat # PD021	(1:100)
antibody	Goat-anti-Rabbit BV480	BD biosciences	Cat # 564879	(1:400)
antibody	anti-EpCAM	BioLegend	Cat # 118214	(1:200)
Other	streptavidin-PE	BD biosciences	Cat # 554061	(1:400)
Other	streptavidin-BV421	BioLegend	Cat # 405225	(1:400)
Other	Ulex Europaeus Agglutinin I (UEA I)	VECTOR LOBORATORY	FL-1061	(1:200)
commercial assay or kit	Viability dye Ghost Dye™ Red 780	TONBO Biosciences	Cat # 13-0865-T100	(1:500)
commercial assay or kit	anti-biotin MACS beads	Miltenyi	Cat # 130-105-637	
commercial assay or kit	anti-PE microbeads	Miltenyi	Cat # 130-048-801	
chemical compound, drug	Bulsulfan	MP Biomedicals	Cat # 154906	
chemical compound, drug	Streptavidin	Jackson ImmunoResearch	Cat # 016-000-113	
chemical compound, drug	DNase I	Roche	Cat # 10104159001	
chemical compound, drug	Liberase TH	Roche	Cat # 5401127001	
chemical compound, drug	sulfo-NHS-LC biotin	ThermoFisher Scientific	Cat # 21335	
software, algorithm	SPADE	CytoBank	https://www.cytobank.org/	
software, algorithm	Prism 7	GraphPad	https://www.graphpad.com/	
software, algorithm	ImageJ	ImageJ	https://imagej.nih.gov/ij/	
software, algorithm	FlowJo v10	TreeStar - Flowjo	https://www.flowjo.com/solutions/flowjo	

Table 2-1 Key resources table

Mice

B6 (C57BL/6NCr) and B6.SJL (B6-LY5.2/Cr) mice were purchased from the

National Cancer Institute. BALB/c (BALB/cJ or BALB/cBYJ as indicated), congenic CD45.1^{+}BALB/cBYJ (CByJ.SJL(B6)-Ptprca/J), CD4^{Cre} B6, *Ifn-γ*^{YFP} B6 (B6.129S4-Ifng$^{tm3.1Lky/J}$), *Ifn-γR*^{KO} B6 (B6.129S7-Ifngr1$^{tm1Agt/J}$), *Aire*^{KO} B6 (B6.129S2-Aire$^{tm1.1Doi/J}$), *Ccr7*^{KO} B6 (B6.129P2(C)-Ccr7$^{tm1Rfor/J}$), *Cd1d*$^{-/-}$ B6 (B6.129S6-Cd1d1/Cd1d2$^{tm1Spb/J}$) and *Cd1d*$^{-/-}$BALB/c.J (C.129S2-Cd1tm1Gru/J) mice were obtained from the Jackson Laboratory. *Rag2*^{GFP} B6, *Klf2*^{GFP} B6, *Klf2*$^{fl/fl}$ B6, KN2 BALB/cBYJ and B6, *Tbx21*^{GFP} Balb/cBYJ and *Tbx21*^{GFP} KN2 BALB/cBYJ have been previously described (12, 24, 40, 119, 127). *Cd69*$^{-/-}$ B6 (*Cd69* KO) mice were kindly provided by Dr. Linda Cauley at University of Connecticut Health Center. CD4^{Cre} *Klf2*$^{fl/fl}$ (*Klf2* cKO) mice were generated through crossbreeding at University of Minnesota. All animal work was conducted in compliance with the protocols approved by the Institutional Animal Care and Use Committee of the University of Minnesota.

Flow cytometry and antibodies

Single-cell suspensions were prepared from thymus and spleen. Biotinylated PBS57 loaded or unloaded CD1d monomers and MR1–5–OP–RU or control MR1–Ac–6–FP monomers were obtained from the tetramer core of the US National Institutes of Health and tetramerized with streptavidin-PE (invitrogen) or streptavidin-APC (invitrogen) at the ratio of 4:1. For staining of CCR7, cells

were stained with antibody to CCR7 (4B12, BD Biosciences) at 37°C for 45 min. For intracellular staining of transcription factors, cells were stained with antibodies to surface makers, then fixed and permealized with a Foxp3 staining buffer set (eBioscience), and were incubated with antibodies to PLZF (R17-809, BD Biosciences), T-bet (4B10, Biolegend), ROR-γt (Q31-378, BD Biosciences), Egr2 (erongr2, eBioscience) or Aire (5H12, eBioscience). For staining of LEF1, fixed and permealized cells were incubated with antibody to LEF1 (C12A5, Cell Signaling Technology), followed by staining with secondary antibody to Rabbit IgG (A11034, Invitrogen). Antibody to mouse IL-17RB was from R and D Systems (752101, rat IgG1). Ulex Europaeus Agglutinin I (UEA I) was from VECTOR LOBORATORY. Viability dye Ghost Dye Red 780 was from TONBO Biosciences. The complete list of other antibodies used is as follows and were purchased from eBioscience, BD Biosciences or BioLegend, unless otherwise indicated: anti-CD4 (GK1.5 or RM4-4), CD8α (53–6.7), anti-CD24 (M1/69), anti-NK1.1 (PK136), anti-CD44 (IM7), anti-human CD2 (TS1/8 or RPA-2.10), anti-TCRβ (H57-597), anti-PD-1 (29F.1A12), anti-CD45.1 (A20), anti-CD45.2 (104), anti-Qa2 (695H1-9-9), anti-RANKL (IK22/5), anti-B220 (RA3-6B2), anti-CD11c (N418), anti-CD11b (M1/70), anti-F4/80 (BM8), anti-CD122 (TM-β1). See table 2-1 for a list of antibodies and reagents used in this stufy. Cells were analyzed on a BD LSR Fortessa or BD Fortessa X-20 and data were processed with FlowJo

software.

Enrichment of iNKT cells or MAIT cells

Single cell suspensions were prepared from thymus or spleen and incubated with PE-CD1d-PBS57 tetramer at 4°C or with PE-MR1–5–OP–RU tetramer at room temperature. Then anti-PE microbeads (Miltenyi) were used for immunomagnetic enrichment according to the manufacturer's instructions.

SPADE analysis of thymic iNKT cells

Thymic iNKT cells were enriched from B6 KN2 or BALB/c KN2 thymus. Enriched iNKT cells were stained with antibodies to CCR7, TCR-β, IL-17RB, CD1d tetramer, CD24, T-bet, PD-1, PLZF, CD44, Dump (viability dye, B220, F4/80, CD11c), CD8, ROR-γt, human CD2, CD4. Total thymic iNKT cells (TCR-β^+ CD1d tetramer$^+$ $CD24^-$) were subjected to SPADE analysis on Cytobank (www.cytobank.org) based on expression of following surface markers, key transcription factors and IL-4 production: CCR7, IL-17RB, PD-1, CD44, CD4, T-bet, PLZF, ROR-γt, human CD2.

Intra-thymic and intravenous injection

Thymocytes from BALB/c KN2, BALB/c *Tbx21*^{GFP} or BALB/c *Tbx21*^{GFP} KN2 mice were depleted of $CD8^+$ and $CD24^+$ cells (via immunomagnetic selection

[Miltenyi]) to enrich thymic iNKT cells. CCR7^{+} CD4^{+} human CD2$^{–}$, CCR7^{+} *Tbx21*$^{GFP–}$, CCR7^{+} CD4^{+}*Tbx21*$^{GFP–}$ human CD2$^{–}$ cells or CCR7$^{–}$ *Tbx21*$^{GFP+}$ cells were sorted with a FACSAria. Ultrasound imaging guided intra-thymic injections were performed on congenic host mice (BALB/c) using a Vevo 2100 preclinical scanner (VisualSonics) with a MS550 transducer. Ultrasound guided intrathymic injection is described in detail at Bio-protocol (128). Mice received intra-thymic transfer or intravenous injections of cells were analyzed 5 days after injections. For intra-thymic injection of biotin to track RTEs, mice were given ~10 µL of 1 mg/mL solution of sulfo-NHS-LC biotin. At 24 hr or 74 hr later, biotin^{+} RTEs in spleen were enriched by immunomagnetic selection (via anti-biotin MACS beads [Miltenyi]), and stained with streptavidin-PE or streptavidin-BV421, followed by blocking with free streptavidin (Jackson ImmunoResearch) before staining for surface markers and CD1d tetramer.

Bone marrow chimera

Bone marrow cells were prepared from the femurs and tibias of donor mice, and depleted of T cells with CD90.2 MACS beads. Recipient mice (CD45.1^{+} CD45.1^{+}) were lethally irradiated (2 × 500 rads) and received 5 × 10^{6} T-cell-depleted bone marrow cells. Mixed donor cells consisted of 25% of *Klf2* cKO cells (CD45.2^{+} CD45.2^{+}) and 75% of Wt cells

(CD45.1$^+$ CD45.2$^+$) or 50% of *Ccr7* KO cells (CD45.2$^+$ CD45.2$^+$) and 50% of Wt cells (CD45.1$^+$ CD45.2$^+$) or 50% of Wt cells (CD45.2$^+$ CD45.2$^+$) and 50% of Wt cells (CD45.1$^+$ CD45.2$^+$). All chimeras were analyzed 7 or 8 weeks after transplantation unless otherwise indicated. For busulfan induced bone marrow chimeras, recipient mice (CD45.2$^+$ CD45.2$^+$) were injected intraperitoneal with 400 μg of busulfan on two consecutive days, and received 1 × 10^7 T-cell-depleted bone marrow cells (CD45.1$^+$ CD45.1$^+$). Busulfan induced bone marrow chimeras were analyzed at 4 and 5 weeks after transplantation.

Parabiosis surgery

Parabiosis surgeries were performed as previously described (127). Briefly, mice were anesthetized with ketamine, and flank hair was shaved and further removed using Nair. After making lateral incisions, mice were joined with interrupted horizontal mattress sutures with 5–0 NOVAFIL. Additional sutures were placed through the olecranon and knee joints to secure the legs. Parabiotic pairs were analyzed 30 days after surgeries.

Preparation of thymic epithelial cells

The procedure for preparation of thymic epithelial cells have been previously described (129). Briefly, fresh thymus was digested with 0.05% [w/v] of Liberase TH (Roche) and 100 U/ml of DNase I (Roche) and mechanically

disrupted. After complete digestion, flowcytometic analysis was performed, and total thymic epithelial cells were identified as $CD45^{-}$ $EpCAM^{+}$ cells.

Immunofluorescence

The CD1d tetramer immunofluorescence has been described previously (24). Briefly, fresh thymic lobes were incubated with PE-CD1d-PBS57 tetramer at 4°C overnight. The tissues were then washed with PBS and fixed in 4% paraformaldehyde (PFA) for 1 hr and snap frozen in OCT. Five micrometer sections were made and stained with Goat-anti-R Phycoerythrin (PE) (Abcam) followed by Donkey-anti-Goat AF555 (Abcam). The sections were incubated with Rabbit-anti-β5t (MBL International) and anti-CD45.1 AF647 (Biolegend) at 4°C overnight, followed by Goat-anti-Rabbit BV480 (BD biosciences). The sections were counterstained with DAPI covered with Prolong anti-fade mounting medium (Life Technologies). The images were obtained with a Leica DM6000B Epi-Fluorescent microscope.

Histocytometry

The histocytometry analysis was described previously (24, 130). Briefly, the region of interests (ROIs) were identified and the fluorochrome intensities of each ROI were quantified using ImageJ and data were exported into Excel, Prism and FlowJo software for the localization analysis.

Ultrasound imaging guided intra-thymic injection

The intra-thymic injection was guided by ultrasound imaging using the Vevo 2100 preclinical scanner (VisualSonics) with the MS550 transducer, which ranges from 32 to 40 MHz. Briefly, we identified the thymus in the ultrasound imaging, then adjusted and slid the needle under the transducer until it could be clearly visualized above the skin of the chest area. The needle was then inserted into the thymus gland, approaching continuously toward the thymus area while avoiding penetrating any attached blood vessels or going underneath the aorta. Once the needle tip was observed within the thymic area, a 10 μL volume was injected.

Statistical analysis

Prism software (GraphPad) was used for statistical analysis. Unpaired or paired two-tailed t-tests, and one-way ANOVA were used for data analysis and calculation of *p* values. Data sets (in Prism format) are available per request.

Chapter 3

Myeloid cells activate iNKT cells to produce IL-4 in the thymic medulla

Overview

IL-4 is produced by a unique subset of invariant natural killer T (iNKT) cells (NKT2) in the thymus in the steady state, where it conditions $CD8^+$ T cells to become “memory like” amongst other effects. However, the signals that cause NKT2 cells to constitutively produce IL-4 remain poorly defined. Using histocytometry, we observed that IL-4 producing NKT2 cells were localized to the thymic medulla, suggesting medullary signals might instruct NKT2 cells to produce IL-4. Moreover, NKT2 cells receive and require TCR stimulation for continuous IL-4 production at steady state, since NKT2 cells lost IL-4 production when intra-thymically transferred into CD1d deficient recipients. In bone marrow chimeric recipients, only hematopoietic, but not stromal APC, provided such stimulation. Furthermore, using different Cre-recombinase transgenic mouse strains to specifically target CD1d deficiency to various APC, together with the use of diphtheria toxin receptor (DTR) transgenic mouse strains to deplete various APC, we found that macrophages were the predominant cell to stimulate NKT2 IL-4 production. Thus NKT2 cells appear to encounter and require different self-lipid ligands for selection in the cortex and activation in the medulla.

Introduction

The thymus is a primary lymphoid organ that supports T cells development. Nonetheless, even in the steady state, cells of the thymus produce effector cytokines typically associated with acute immune responses, including type I interferon (IFN-α/β), type II cytokines (IL-4/13), and IFN-γ (12, 24, 40, 41, 91, 123, 131-133). These steady state cytokines shape the thymic microenvironment in myriad ways, which affects T cell development and tolerance (12, 24, 40, 41, 91, 123, 131-133). In particular, steady state IL-4 in the thymus drives $CD8^+$ single positive thymocytes to differentiate to a memory-like state through upregulation of eomesodermin (eomes) (12, 24, 40, 41). These IL-4 exposed CD8 T cells display antigen receptor independent survival and effector function due to upregulation of CD122 and IL-12/18R (thus are often referred to as “innate CD8” T cells), and have trafficking properties similar to memory cells due to upregulation of chemokine receptor CXCR3 and CD44 (12, 24, 40, 41). Innate $CD8^+$ T cells were shown to have superior function compared to naïve T cells (40, 41, 92-95) and are thought to play a critical role in defense against infections (40, 41, 92-95). Thymic steady state IL-4 also promotes the development and function of regulatory T cells (T_{regs}), particularly those that arise through the $Foxp3^{low}$ T_{reg} progenitor pathway (134, 135). In addition, thymic dendritic cells (DC) are also influenced, secreting chemokines CCL17 and CCL22 in response to IL-4

signaling (12), which might further affect thymocyte-DC interactions in the organ. Furthermore, thymic B cells undergo class switch recombination, and this process is partially supported by thymic IL-4, as steady state IL-4 promotes class switch into IgE and IgG1 (12)(data not shown). Finally, IL-4 signaling in medullary thymic epithelial cells (mTEC) has been shown to promote the thymic emigration of mature T cells (91). Given all of these effects, it is of interest to understand how IL-4 production is driven in the thymus.

Previous reports showed that steady state IL-4 in the thymus is largely produced by lipid-specific invariant natural killer T (iNKT) cells (12, 41). iNKT cells express a semi-invariant T cell receptor (TCR), characterized by Vα14-Jα18 chains paired to a limited set of Vβ chains in mice (136). iNKT cells specifically recognize lipid antigens presented by the non-polymorphic MHC-like molecule CD1d, which contrasts with conventional $CD4^+$ or $CD8^+$ T cells that recognize peptides presented by highly polymorphic MHC molecules (136). Recent reports showed that mature iNKT cells are composed of three major functionally distinct subsets, termed as NKT1, NKT2 and NKT17, according to their expression of transcription factors and cytokine responses upon activation, analogous to the $CD4^+$ T helper sub-lineages (12, 136). In general, NKT1 cells are positive for T-bet and produce IFN-γ; NKT17 cells are

positive for ROR-γt and produce IL-17; while NKT2 cells express a high level of PLZF and produce IL-4. It is these PLZF^{high} NKT2 cells that were shown to produce IL-4 in the thymus in the steady state (12, 24). Although “self” lipids are implicated in the positive selection of iNKT precursors by CD1d^{+} double positive (DP) thymocyte antigen presenting cells in the thymic cortex (5, 21, 80), it is not known if iNKT cells continue to recognize or respond to self lipids as they differentiate.

In this study, we sought to explore the factors that drive iNKT cells to produce IL-4 in the steady state. Secretion of cytokines by T cells is usually a result of activation by cytokine and/or TCR signaling, and the steady state IL-4 production by iNKT cells in the thymus might very well fall into this scenario. Indeed, recent findings identified a specialized subset of medullary thymic epithelial cells (called thymic tuft cells), with striking similarity to peripheral mucosal tuft cells, which produce IL-25 to further stimulate the differentiation of NKT2 cells (36, 137). Here, we show that NKT2 cells predominantly reside in the thymic medulla. They receive and require TCR stimulation for their IL-4 production in the steady state. Moreover, this TCR stimulation in NKT2 cells is solely mediated by CD1d expressed by hematopoietic antigen presenting cells (APC), and macrophages were the predominant cell that triggered the steady state IL-4 production by NKT2 cells. Collectively, our findings show

that NKT2 cells integrate TCR and cytokine signals for IL-4 production in the thymic medulla in the steady state.

Results

NKT2 cells produce IL-4 in the steady state and are predominantly located in the thymic medulla

To directly investigate the thymic cells that secrete IL-4 in the steady state, we used an IL-4 reporter mouse strain (KN2, wherein a human CD2 reporter gene was introduced into the endogenous *Il-4* locus). In these mice, the IL-4 protein secreting cells can be faithfully detected through the expression of human CD2 (huCD2) on the cell surface (138). In comparison to wild-type (Wt) BALB/c mice, a distinct population of thymocytes expressed huCD2 in BALB/c KN2 mice (Figure 3-1 A). Combined with CD1d tetramer staining to specifically detect invariant natural killer T (iNKT) cells (Figure 3-2 A), we observed that the majority of the IL-4 producing cells were iNKT cells (Figure. 3-1A). We also used transcription factors staining to distinguish different iNKT subsets (Figure 3-2 B), which showed that NKT2 cells were the only cell to express huCD2 highly (Figure 3-1 B, C), suggesting they are the major source of steady state IL-4 in the thymus, consistent with previous studies (12, 42, 91). To track the localization of IL-4 producing NKT2 cells, we performed *in situ* CD1d tetramer incubation followed by immunofluorescent staining for huCD2 in thymic sections (Figure 3-3 A) (24). The majority of IL-4 producing NKT2 cells (huCD2$^+$ CD1d tet$^+$) were found in the UEA-I$^+$ thymic medulla (Figure 3-1 D). We employed quantitative histo-cytometry (Figure 3-1 E),

which showed more than 80% of IL-4 producing NKT2 cells (huCD2^{+} CD1d tet^{+}) localized in the thymic medulla (Figure 3-1 F, G). These results demonstrated that NKT2 cells are the major source of steady state IL-4 in the thymus and predominantly localize to the thymic medulla.

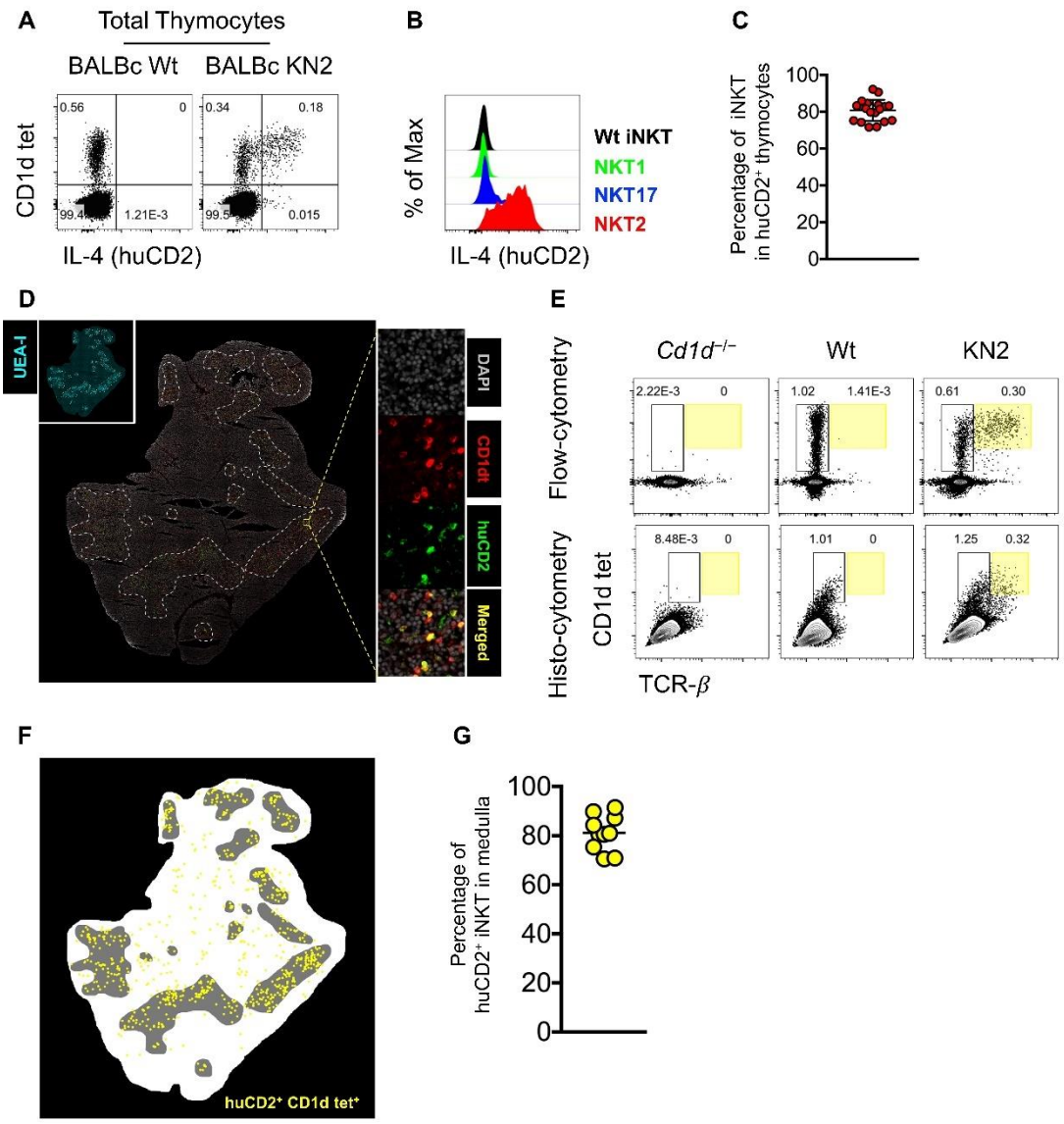

Figure 3-1. NKT2 cells produce IL-4 in the thymic medulla at steady state.

(**A**) Staining of PBS57-CD1d tetramer and human CD2 (huCD2) in *ex vivo* total thymocytes from BALBc wild-type (Wt) and KN2 mice. Gated on live singlets. Data are representative of 4 experiments. (**B**) Expression of huCD2 in NKT2, NKT17, NKT1 cells from BALBc KN2 or total iNKT cell from BALBc Wt mice. Data are representative of 2 experiments. (**C**) Percentage of iNKT cells in huCD2$^+$ thymocytes from BALBc KN2 mice. Data are pooled from 4 experiments. (**D**) Immunofluorescent microcopy of thymic section of BALBc KN2 mice (middle), stained with DAPI, PBS57-CD1d tetramer (CD1dt), huCD2 and UEA-I to identify IL-4

producing iNKT cells (huCD2$^+$ CD1dt$^+$) *in situ*, the white dash lines outlines the medullary region. The yellow square (middle) outlines the magnified region shown in right, single channel of each fluorochrome or merged image. The staining of UEA-I (upper left) was used to distinguish Cortex (UEA-I$^-$) and Medulla (UEA-I$^+$), outlined by the white dash line. Data are representative of 3 experiments. (**E**) Each thymic lobe from BALBc Cd1d$^{-/-}$, Wt or KN2 mouse was subjected to histocytometric analysis after immunofluorescent microscopy or to flow cytometry analysis. Data are representative of 3 experiments. (**F**) Localization of IL-4 producing iNKT cells (huCD2$^+$ CD1dt$^+$) analyzed using histocytometric algorithm. Data are representative of 3 experiments. (**G**) Percentage of huCD2$^+$ iNKT cells localized in thymic medulla. Data are pooled from 3 experiments. Each dot represents an individual mouse and horizontal bars indicate mean values.

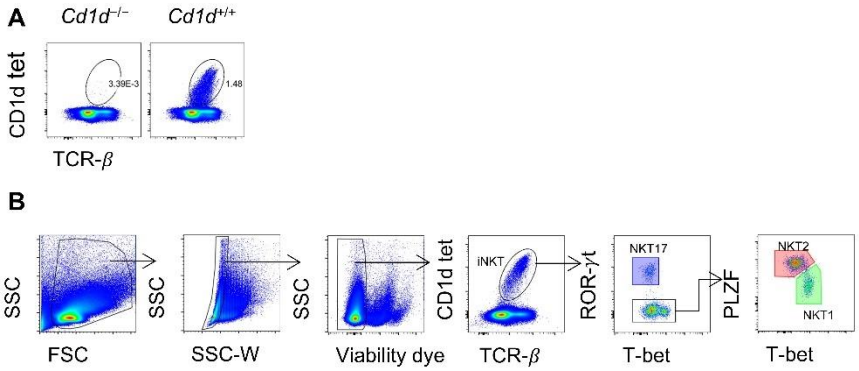

Figure 3-2. Detection and gating strategy of iNKT subsets.

(**A**) Representative flowcytometry plots of PBS57-CD1d tetramer staining in thymocytes from BALBc *Cd1d*$^{-/-}$ and *Cd1d*$^{+/+}$ mouse. (**B**) Flowcytometric gating strategy to identify thymic iNKT cells and iNKT subsets (NKT1, green; NKT2, red; NKT17, blue).

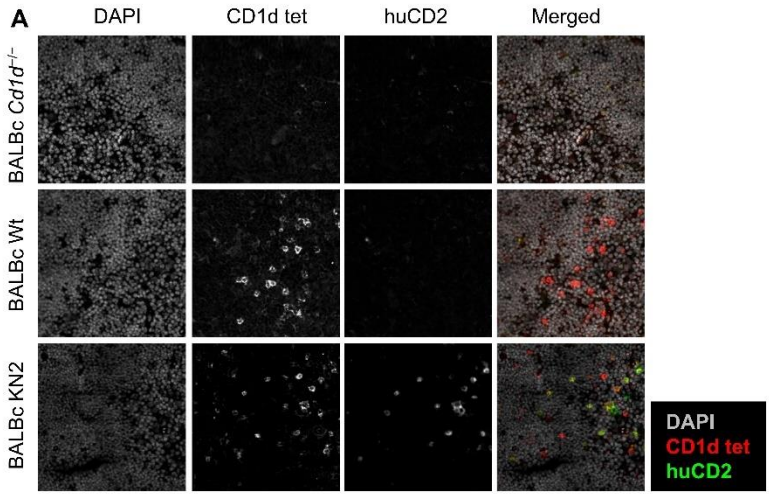

Figure 3-3. Specific detection of IL-4 producing NKT2 cells *in situ*.

(**A**) Immunofluorescent microscopy of thymic sections of BALBc *Cd1d*$^{-/-}$, Wt and KN2 mouse, stained with DAPI, PBS57-CD1d tetramer and huCD2.

NKT2 cells require TCR signal for their production of IL-4 in the steady state

T cells can be activated via stimulation of cytokine and/or TCR signals to produce cytokines (139). A recent report indicated that thymic tuft cell-derived IL-25 promotes the differentiation of NKT2 cells (137). To understand whether NKT2 cells might also receive TCR signals in the steady state, we crossed BALB/c *Nur77*^{GFP} mice with BALB/c KN2 mice to obtain the BALB/c *Nur77*^{GFP}/KN2 mice. In *Nur77*^{GFP} mice, the level of GFP reflects TCR signal strength in T cells and is independent of cytokine or inflammatory signals (21, 140). Interestingly, IL-4 producing NKT2 cells had significantly elevated GFP expression compared to NKT1 and NKT17 cells, though lower than stage 0 iNKT cells (Figure 3-4 A, B), suggesting IL-4 producing NKT2 cells indeed receive TCR stimulation in the steady state. This is consistent with the high level of Egr2 observed in PLZF^{high} iNKT cells (141). We next tested whether steady state IL-4 production was dependent on TCR stimulation by transferring iNKT enriched thymocytes intrathymically into Wt or *Cd1d*$^{-/-}$ hosts (Figure 3-4 C). huCD2^{+} NKT2 cells were dramatically reduced 9 days after intra-thymic transfer into CD1d$^{-/-}$ hosts compared to Wt hosts (Figure 3-4 D, E), while NKT1 and NKT17 cell numbers were not affected (Figure 3-5 A). Altogether, this strongly suggests NKT2 cells receive and require TCR signals for steady state IL-4 production. Considering the majority of IL-4 producing

NKT2 cells were localized in the thymic medulla, it implicates medullary antigen presenting cells (APCs) in CD1d dependent stimulation of NKT2 cells.

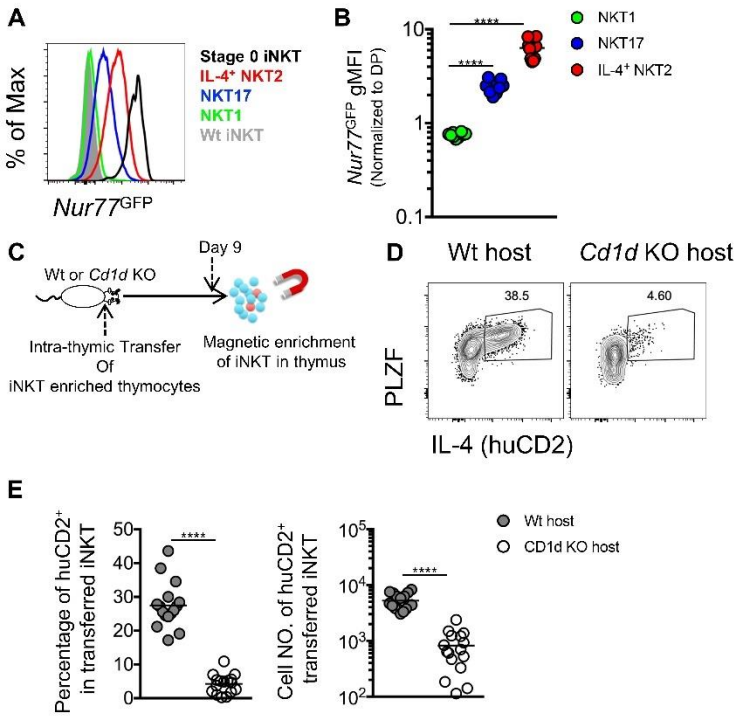

Figure 3-4. NKT2 cells require TCR signal for steady state production of IL-4

(**A**) Representative flowcytometry histogram showing *Nur77*^{GFP} expression of different sub-populations of thymic iNKT cells enriched from BALBc *Nur77*^{GFP} or BALBc Wt mice. Data are representative of 2 experiments. (**B**) Normalized *Nur77*^{GFP} gMFI (to DP) of thymic NKT1, NKT17 and IL-4^{+} NKT2 cells from BALBc *Nur77*^{GFP} mice. Data are pooled from 2 experiments. Each dot represents an individual mouse and horizontal bars indicate mean values. Ordinary one-way ANOVA, ****p<0.0001. (**C**) Experimental scheme showing iNKT enriched thymocytes from CD45.1^{+} CD45.2^{+} BALBc KN2 mice were intra-thymically transferred into BALBc Wt (CD45.2^{+} CD45.2^{+} or CD45.1^{+} CD45.1^{+}) or BALBc Cd1d KO (CD45.2^{+} CD45.2^{+}), 9 days later transferred donor iNKT cells were identified and phenotyped in flowcytometry after magnetic enrichment of total thymic iNKT cells. (**D**) Expression of IL-4 (huCD2) and PLZF in transferred donor iNKT cells 9 days after intra-thymic transfer into BALBc Wt or BALBc *Cd1d* KO host mice. Data are representative of 5 experiments. (**E**)

Percentage (left) and cell number (right) of huCD2^{+} cells in transferred donor iNKT cells 9 days after intra-thymic transfer. Data are pooled from 5 experiments. Each dot represents an individual mouse and horizontal bars indicate mean values. Unpaired t test, ****p<0.0001.

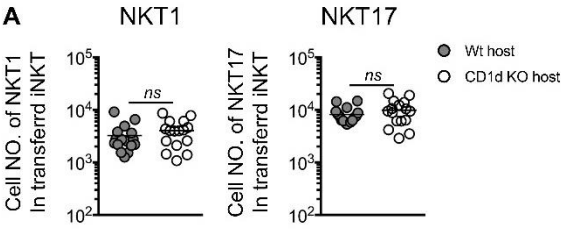

Figure 3-5. Intra-thymic transfer in to *Cd1d*$^{-/-}$ host does NOT affect donor NKT1 & NKT17 in short term

(**A**) Cell number of transferred donors NKT1 (left) and NKT17 (right) cells 9 days after intra-thymic transfer into BALBc Wt or BALBc *Cd1d* KO host mice. Data are pooled from 5 experiments. Each dot represents an individual mouse and horizontal bars indicate mean values. Unpaired t test, ^{ns}p=0.3013 (NKT1) or 0.2534 (NKT17).

NKT2 cells require *Cd1d* in hematopoietic APC to produce IL-4 in the steady state

There are multiple lineages of APCs found in the thymic medulla, including stromal derived APC (thymic epithelial cells) as well as hematopoietic origin APCs (B cells, classical dendritic cells, plasmacytoid dendritic cells and macrophages) (142), all of which express CD1d (Figure 3-7 B, 3-10 A, 3-10 C, data not shown)(143, 144). Therefore, we decided to first distinguish the role of stromal and hematopoietic APCs in supporting NKT2 cells for steady state production of IL-4. For this purpose, we created bone marrow chimeras in which *Cd1d* was selectively deficient in either stromal or hematopoietic APCs (Figure 3-6 A). The bone marrow chimeras were used as hosts for intra-thymic transfer of iNKT enriched thymocytes similar to that described above (Figure 3-6 A, Figure 3-4 C). Strikingly, steady state IL-4 production in NKT2 cells was dramatically decreased upon intra-thymic transfer into chimeras where *Cd1d* was selectively deficient in hematopoietic cells (*Cd1d* KO BM to Wt), while maintained in chimeras where *Cd1d* was selectively deficient in stromal cells (Wt BM to *Cd1d* KO) (Figure 3-6 B, C). These results suggest only hematopoietic APCs stimulate NKT2 cells to produce IL-4 in the steady state.

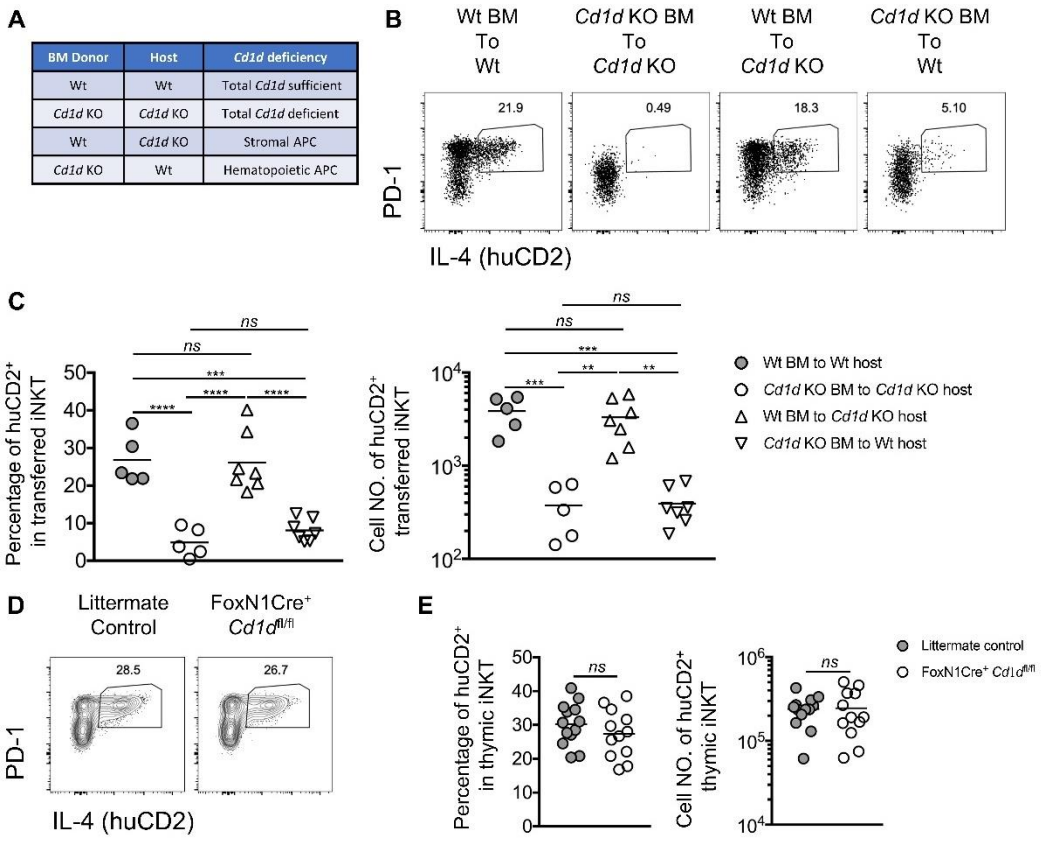

Figure 3-6. Steady state IL-4 production in NKT2 requires Cd1d solely in hematopoietic APC

(**A**) Four type of BALBc bone marrow chimeras were created, including total *Cd1d* sufficiency, total *Cd1d* deficiency, *Cd1d* selectively deficient in Stromal cells and *Cd1d* selectively deficient in hematopoietic cells, to serve as recipient mice for intra-thymic transfer. (**B**) Expression of IL-4 (huCD2) and PD-1 in transferred donor iNKT cells 9 days after intra-thymic transfer into BLABc bone marrow chimeras with total *Cd1d* sufficiency (Wt BM to Wt, far left), total *Cd1d* deficiency (*Cd1d* KO BM to *Cd1d* KO, middle left), *Cd1d* selectively deficient in Stromal cells (Wt BM to *Cd1d* KO, middle right) and *Cd1d* selectively deficient in hematopoietic cells (*Cd1d* KO BM to Wt, far right), respectively. Data are representative of 3 experiments. (**C**) Percentage (left) and cell number (right) of huCD2$^+$ cells in transferred donor

iNKT cells 9 days after intra-thymic transfer. Ordinary one-way ANOVA; ^{ns}p=0.9967 (left, A-C) or 0.7751 (left, B-D) or 0.8656 (right, A-C) or >0.9999 (right, B-D), **p=0.0024 (right, B-C) or 0.0010 (right, C-D), ***p=0.0001 (left) or 0.0009 (right, A-B) or 0.0004 (right, A-D), ****p<0.0001. (**D**) Expression of IL-4 (huCD2) and PD-1 in thymic iNKT cells from F1 littermate control (left) or F1 FoxN1Cre^{+} Cd1d$^{fl/fl}$ (right) mice. Data are representative of 5 experiments. (**E**) Percentage (left) and cell number (right) of huCD2^{+} cells in thymic iNKT cells from F1 littermate control or F1 FoxN1Cre^{+} Cd1d$^{fl/fl}$ mice. Data are pooled from 5 experiments. Each dot represents an individual mouse and horizontal bars indicate mean values. Unpaired t test, ^{ns}p=0.2994 (left) or 0.9180 (right).

To confirm this result, we sought to target *Cd1d* deficiency specifically in thymic epithelial cells (TECs) using FoxN1Cre. However, NKT2 and NKT17 cells are scarce in B6 mice (12), thus it was desirable to do this and further tissue specific gene deletion experiments in BALB/c mice. However, *Cd1d*$^{fl/fl}$ mice and Cre-recombinase transgenic mice are most readily available on the B6 background. Interestingly, the thymic iNKT cells in B6 × BALB/c F1 mice resemble that of in BALB/c mice (Figure 3-8 A-C). Thus, we developed a strategy to achieve conditional CD1d deficiency in B6 × BALB/c F1 mice. Briefly, we backcrossed B6 *Cd1d*$^{fl/fl}$ to BALB/c KN2 for at least 10 generations to obtain BALB/c *Cd1d*$^{fl/fl}$-KN2. B6 Cre-recombinase transgenic mice were first crossed to B6 *Cd1d*$^{fl/fl}$ mice to obtain B6 Cre-*Cd1d*$^{fl/fl}$ mice. Then the B6 Cre-*Cd1d*$^{fl/fl}$ mice were further crossed with BALB/c *Cd1d*$^{fl/fl}$-KN2 mice to generate F1 Cre-*Cd1d*$^{fl/fl}$ (Figure 3-7 A). Using this experimental strategy, we generated F1 FoxN1Cre-*Cd1d*$^{fl/fl}$-KN2 to efficiently target *Cd1d* deficiency in TECs (Figure 3-7 B, C). huCD2 expression was comparable in iNKT cells between F1 FoxN1Cre-*Cd1d*$^{fl/fl}$-KN2 and littermate controls (Figure 3-6 D, E). This is consistent with the results we showed above in intra-thymic transfer of BM chimeras (Figure 3-6 A-C), suggesting that CD1d in TECs is dispensable for stimulating NKT2 cells to produce IL-4 in the steady state.

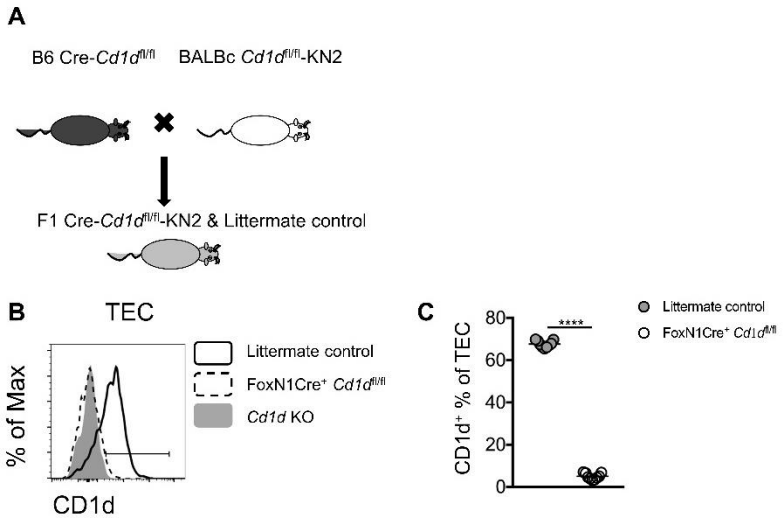

Figure 3-7. Experimental strategy of generating F1 Cre-CD1dfl/fl-KN2 mouse & targeting of Cd1d with FoxN1Cre

(**A**) Experimental scheme showing generation of F1 Cre-Cd1d$^{fl/fl}$-KN2 or Littermate control mice through cross breeding of B6 Cre-Cd1d$^{fl/fl}$ with BALBc Cd1d$^{fl/fl}$-KN2 mice. (**B**) Representative flowcytometry histogram showing expression of CD1d in thymic epithelial cells (TECs, EpCAM^{+} CD45^{-}) from F1 littermate control, F1 FoxN1Cre Cd1d$^{fl/fl}$ and BALBc Cd1d KO mice. (**C**) Frequency of CD1d^{+} cells of TECs from F1 littermate control or F1 FoxN1Cre^{+} Cd1d$^{fl/fl}$ mice.

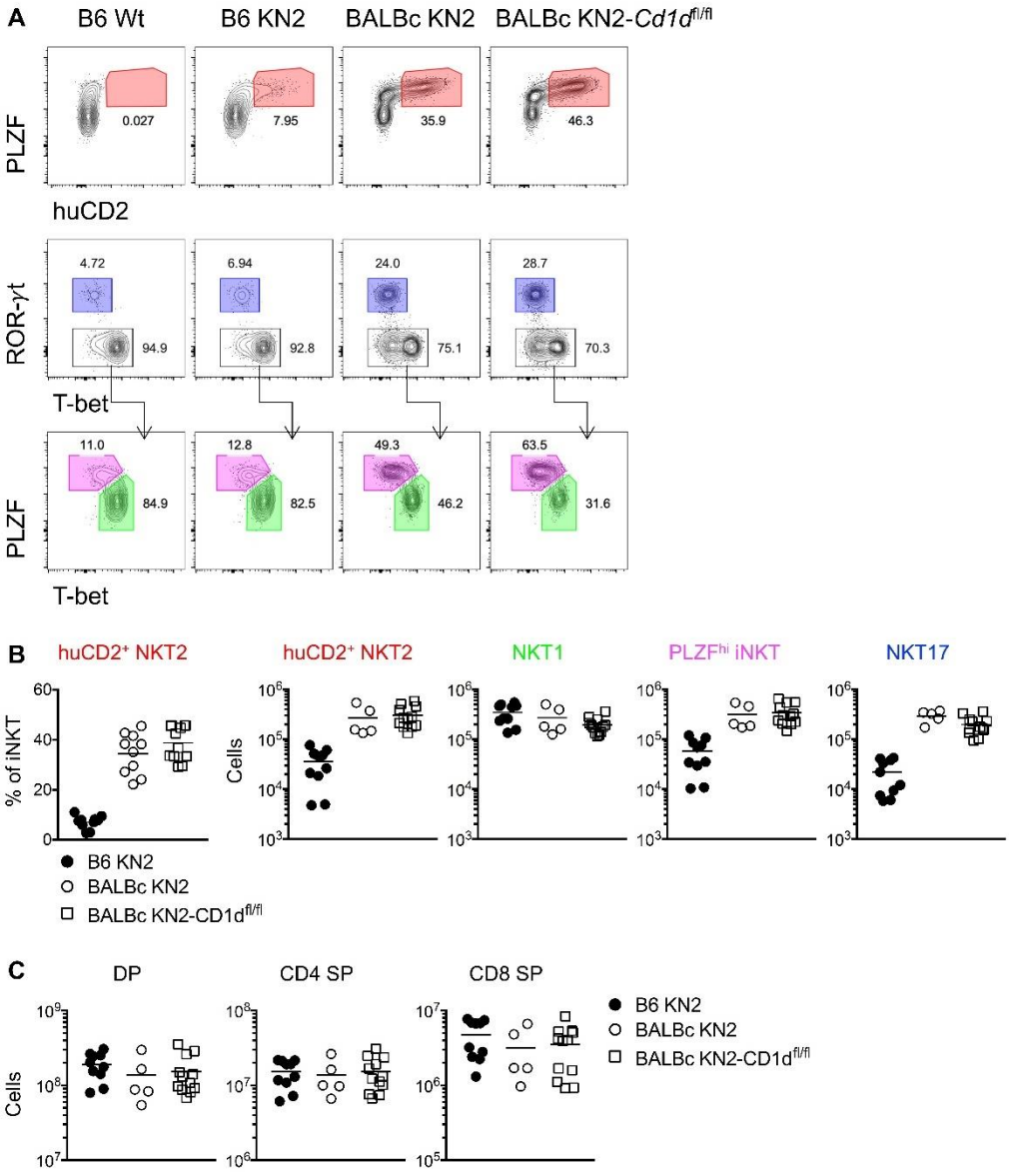

Figure 3-8. B6 *Cd1d*$^{fl/fl}$ mouse backcrossed to BALBc KN2 mouse.

(**A**) Expression of huCD2 and PLZF (upper row), T-bet and ROR-γt (middle row) in thymic iNKT cells, and expression of T-bet and PLZF in ROR-γt^{-} (lower row) thymic iNKT cells from B6 Wt, B6 KN2, BALBc KN2 and BALBc Cd1d$^{fl/fl}$-KN2 mice. (**B**) Frequency of huCD2^{+} cells (far left panel 1, red) and cell number of huCD2^{+} cells (panel 2, red), NKT1 cells (panel 3, green), PLZF^{high} cells (panel 4, pink) and NKT17 cells (panel 5, blue) in thymic iNKT cells from B6 KN2, BLABc KN2 or BALBc Cd1d$^{fl/fl}$-KN2 mice. (**C**) Cell number of double positive

(DP) (far left), CD4 single positive (SP) (middle) and CD8 single positive (SP) (far right) thymocytes from B6 KN2, BLABc KN2 or BALBc $Cd1d^{fl/fl}$-KN2 mice.

CD11c$^+$ APCs support steady state IL-4 production in NKT2 cells in CD1d dependent manner

To define the hematopoietic APC in the thymus that is required to stimulate NKT2 cells to produce IL-4 in the steady state, we expanded our F1 Cre-*Cd1d*$^{fl/fl}$ strategy (Figure 3-7 A). CD1d expression was specifically abrogated in different antigen presenting cells using animals expressing Cre under various tissue specific promoters. Effective depletion of CD1d was observed in thymic B cells in F1 MB1Cre-*Cd1d*$^{fl/fl}$ mice (Suppl. 6A-B). However, the frequency and cell number of huCD2$^+$ iNKT cells was not affected by CD1d deficiency in B cells (Figure 3-9 A, B). However, in F1 CD11cCre-*Cd1d*$^{fl/fl}$ mice, we observed a substantial decrease of huCD2 expression in iNKT cells (Figure 3-9 C, D), indicating an essential role for CD11c$^+$ APCs in induction of steady state IL-4.

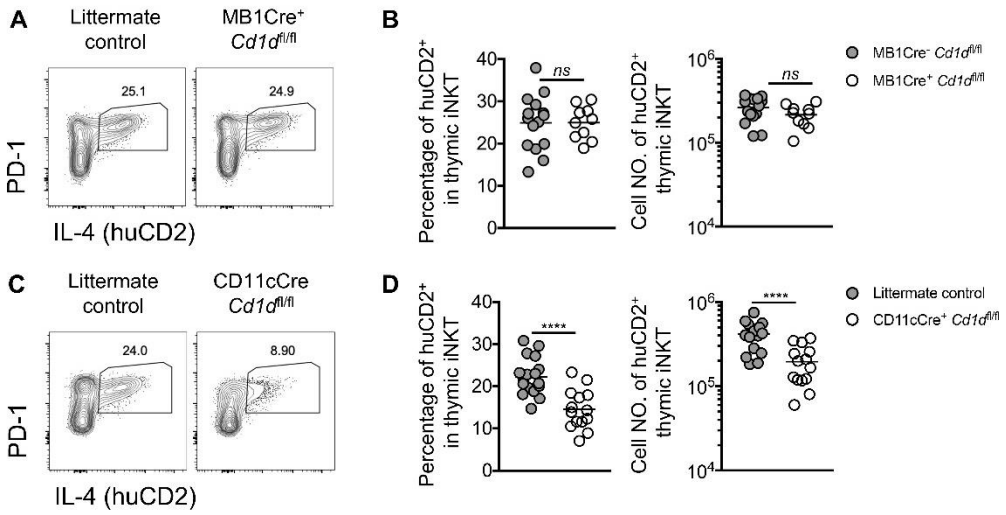

Figure 3-9. Steady state IL-4 production relies on CD1d in CD11c expressing APCs.

(**A**) Expression of IL-4 (huCD2) and PD-1 in thymic iNKT cells from F1 littermate control (left) or F1 MB1Cre^{+} *Cd1d*$^{fl/fl}$ (right) mice. Data are representative of 5 experiments. (**B**) Percentage (left) and cell number (right) of huCD2^{+} cells in thymic iNKT cells from F1 littermate control or F1 MB1Cre^{+} *Cd1d*$^{fl/fl}$ mice. Data are pooled from 5 experiments. Each dot represents an individual mouse and horizontal bars indicate mean values. Unpaired t test, ^{ns}p=0.9852 (left) or 0.1456 (right). (**C**) Expression of IL-4 (huCD2) and PD-1 in thymic iNKT cells from F1 littermate control (left) or F1 CD11cCre^{+} *Cd1d*$^{fl/fl}$ (right) mice. Data are representative of 7 experiments. (**D**) Percentage (left) and cell number (right) of huCD2^{+} cells in thymic iNKT cells from F1 littermate control or F1 CD11cCre^{+} *Cd1d*$^{fl/fl}$ mice. Data are pooled from 7 experiments. Each dot represents an individual mouse and horizontal bars indicate mean values. Unpaired t test, ****p<0.0001.

Although CD11c is an important marker for dendritic cells, it was previously shown, and we confirmed here, that CD11cCre targets multiple lineages of myeloid cells, including classical dendritic cells (cDC), plasmacytoid dendritic cells (pDC) and macrophages (suppl. 6C-D) (145-147). So, although this result strongly suggests that $CD11c^+$ APCs are essential for the steady state NKT2 IL-4 production, either cDC, pDC or macrophages ($F4/80^+$ $Mertk^+$ cells) might be involved.

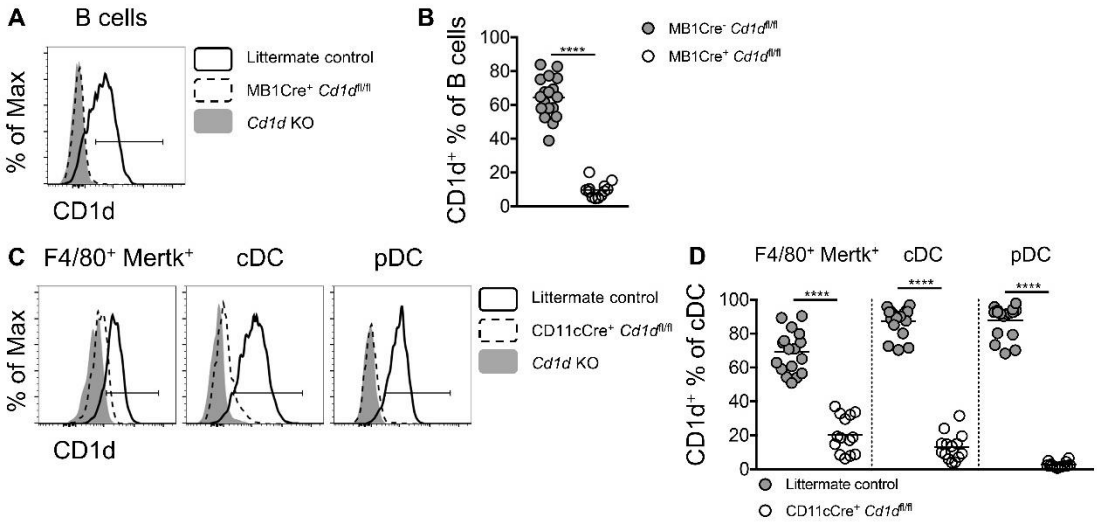

Figure 3-10. Targeting of Cd1d with MB1Cre & CD11cCre, respectively.

(**A**) Representative flowcytometry histogram showing expression of CD1d in thymic B cells from F1 littermate control, F1 MB1Cre Cd1d$^{fl/fl}$ and BALBc Cd1d KO mice. (**B**) Frequency of CD1d^{+} cells of thymic B cells from F1 littermate control or F1 MB1Cre^{+} Cd1d$^{fl/fl}$ mice. (**C**) Representative flowcytometry histogram showing expression of CD1d in thymic macrophages (F4/80^{+} Mertk^{+}, far left), cDC (middle) and pDC (far right) from F1 littermate control, F1 CD11cCre Cd1d$^{fl/fl}$ and BALBc Cd1d KO mice. (**D**) Frequency of CD1d^{+} cells of thymic macrophages (F4/80^{+} Mertk^{+}, far left), cDC (middle) and pDC (far right) from F1 littermate control or F1 MB1Cre^{+} Cd1d$^{fl/fl}$ mice.

F4/80^{+} Mertk^{+} Macrophages are essential for steady state IL-4 production in NKT2 cells

We sought to further distinguish the role of cDC, pDC and macrophages in the CD1d mediated induction of IL-4 by NKT2 cells. For this purpose, we generated F1 *Zbtb46*Cre-CD1d$^{fl/fl}$ mice and observed a specific loss of CD1d in cDC (Figure 3-11 A, B) (145). Nonetheless, the frequency and number of huCD2^{+} iNKT cells in the thymus was not affected upon the depletion of *Cd1d* in cDC (Figure 3-12 A, B), suggesting the CD1d mediated interaction between cDC and iNKT cells is not required for NKT2 steady state IL-4 production. To evaluate the impact of pDC on steady state IL-4, pDC were effectively depleted using the F1 BDCA2-DTR mice with repeated injection of diphtheria toxin (DT) every other day (Figure 3-13 A-C). After 9 days of DT administration, we observed a mild decrease of huCD2^{+} iNKT cells in the pDC-depleted F1 BDCA2-DTR mice compared to F1 littermate control mice. This indicates pDC may play a supportive role in steady state IL-4 production.

Finally, we examined the role of macrophages by generating LysMCre-*Csf1r*$^{LsL\text{-}DTR}$ mice (148) on an F1 background. F4/80^{+} Mertk^{+} macrophages were effectively ablated with a 9-day course of DT administration every other day in these mice (Figure 3-13 D, E). Moreover, flow cytometric analysis of various myeloid cells and lymphocytes in the thymus (Figure 3-14 A) showed

cells of other lineages were not affected (Figure 3-13 E). Strikingly, depletion of the relatively small population of F4/80$^+$ Mertk$^+$ macrophages in the thymus led to a substantial decrease of IL-4 production by NKT2 cells (Figure 3-12 E). NKT2 derived IL-4 was previously shown to condition CD8$^+$ T cells to become memory phenotype, characterized by the expression of the transcription factor Eomes (12, 41). Consistent with a loss of NKT2 derived IL-4, we observed a marked decrease in Eomes$^+$ CD8$^+$ T cells after depletion of macrophages (Figure 3-12 G, H). Together, these results show that thymic macrophages (F4/80$^+$ Mertk$^+$ cells) are critical for stimulating thymic NKT2 cells to produce IL-4 in the steady state.

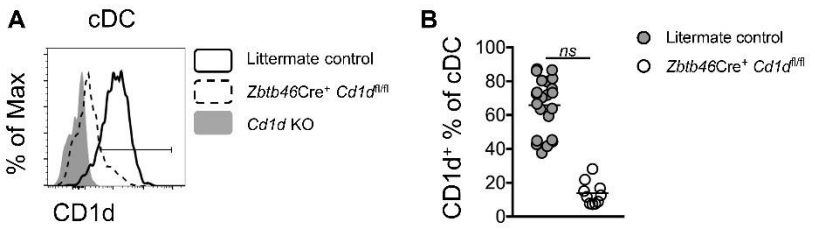

Figure 3-11. Targeting of Cd1d with *Zbtb46*Cre.

(**A**) Representative flowcytometry histogram showing expression of CD1d in thymic cDC from F1 littermate control, F1 *Zbtb46*Cre^{+} Cd1d$^{fl/fl}$ and BALBc Cd1d KO mice. (**B**) Frequency of CD1d^{+} cells of thymic cDC from F1 littermate control or F1 *Zbtb46*Cre^{+} Cd1d$^{fl/fl}$ mice.

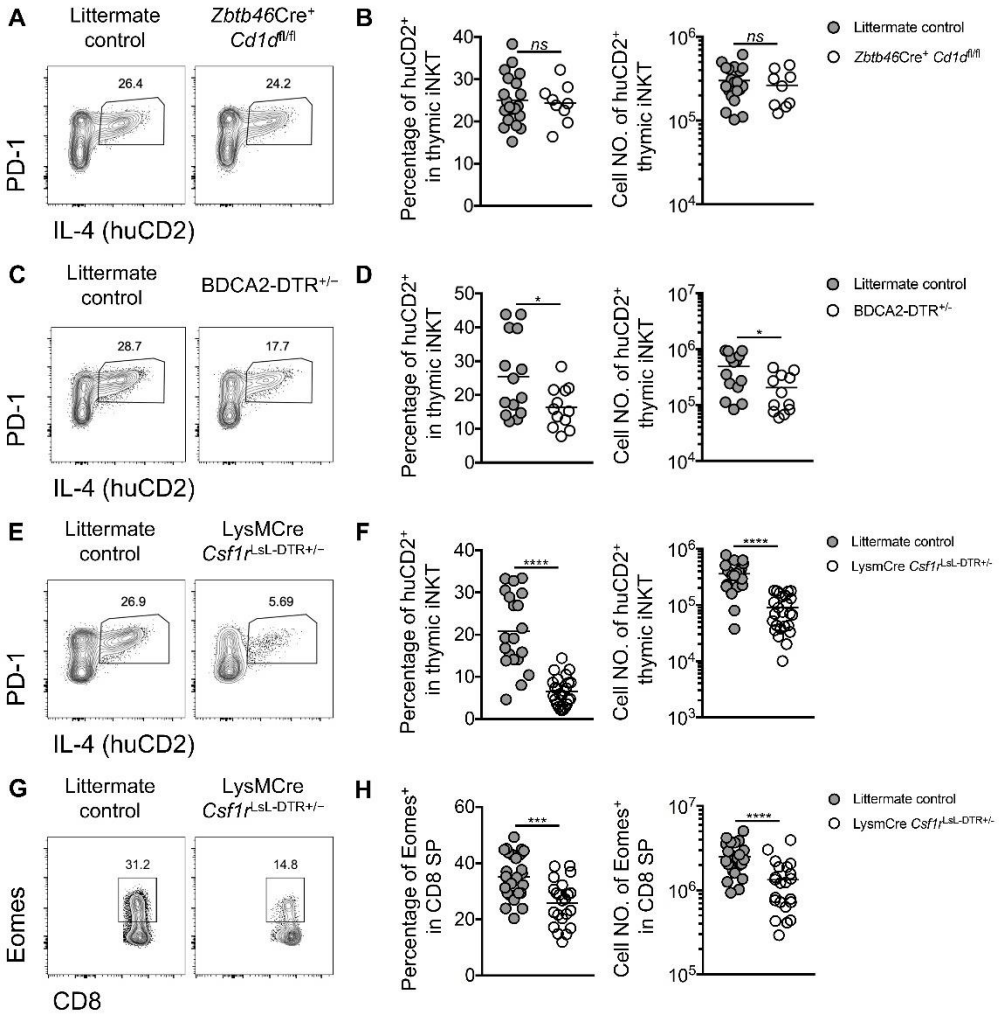

Figure 3-12. Macrophages/phagocytes are essential for steady state IL-4 production in

NKT2 cells.

(**A**) Expression of IL-4 (huCD2) and PD-1 in thymic iNKT cells from F1 littermate control (left) or F1 *Zbtb46*Cre^{+} *Cd1d*$^{fl/fl}$ (right) mice. Data are representative of 7 experiments. (**B**) Percentage (left) and cell number (right) of huCD2^{+} cells in thymic iNKT cells from F1 littermate control or F1 *Zbtb46*Cre^{+} *Cd1d*$^{fl/fl}$ mice. Data are pooled from 7 experiments. Each dot represents an individual mouse and horizontal bars indicate mean values. Unpaired t test, ^{ns}p=0.7468 (left) or 0.5010 (right). (**C**) Expression of IL-4 (huCD2) and PD-1 in thymic iNKT cells from F1 littermate control (left) or F1 BDCA2-DTR$^{+/-}$ (right) mice after a 9-day course of DT treatment. Data are representative of 3 experiments. (**D**) Percentage (left) and cell number (right) of huCD2^{+} cells in thymic iNKT cells from F1 littermate control or F1 BDCA2-DTR$^{+/-}$ mice after a 9-day course of DT treatment. Data are pooled from 3 experiments. Each dot represents an individual mouse and horizontal bars indicate mean values. Unpaired t test, *p=0.0249 (left) or 0.011 (right). (**E**) Expression of IL-4 (huCD2) and PD-1 in thymic iNKT cells from F1 littermate control (left) or F1 LysMCre^{+} *Csf1r*$^{LsL\text{-}DTR+/-}$ (right) mice after a 9-day course of DT treatment. Data are representative of 7 experiments. (**F**) Percentage (left) and cell number (right) of huCD2^{+} cells in thymic iNKT cells from F1 littermate control or F1 LysMCre^{+} *Csf1r*$^{LsL\text{-}DTR+/-}$ mice after a 9-day course of DT treatment. Data are pooled from 7 experiments. Each dot represents an individual mouse and horizontal bars indicate mean values. Unpaired t test, ****p<0.0001. (**G**) Expression of Eomes in thymic CD8 SP from F1 littermate control (left) or F1 LysMCre^{+} *Csf1r*$^{LsL\text{-}DTR+/-}$ (right) mice after a 9-day course of DT treatment. Data are representative of 6 experiments. (**H**) Percentage (left) and cell number (right) of Eomes^{+} cells in thymic CD8 SP from F1 littermate control or F1 LysMCre^{+} *Csf1r*$^{LsL\text{-}DTR+/-}$ mice after a 9-day

course of DT treatment. Data are pooled from 6 experiments. Each dot represents an individual mouse and horizontal bars indicate mean values. Unpaired t test, ***p=0.0002 (left), ****p<0.0001 (right).

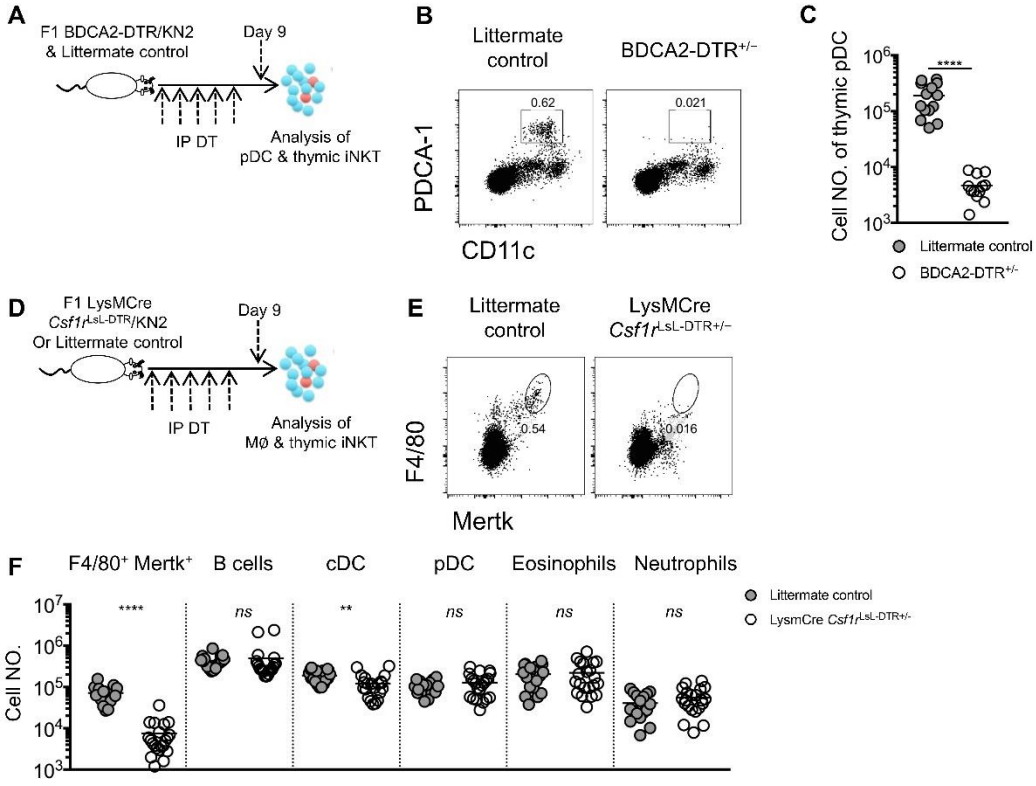

Figure 3-13. Depletion of pDC and macrophages/phagocytes in respective transgenic mouse models.

(**A**) Experimental scheme showing the F1 littermate control and F1 BDCA2-DTR KN2 mice were injected intraperitoneally (i.p.) with DT every other day for 5 times in a 9-day course, and the thymic iNKT cells and pDC were analyzed at day 9. (**B**) Expression of CD11c and PDCA-1 in thymic cells and gating of pDC ($CD11c^{intermediate}$ $PDCA\text{-}1^{+}$) from F1 littermate control and F1 $BDCA2\text{-}DTR^{+/-}$ KN2 mice after a 9-day course of DT treatment. (**C**) Cell number of thymic pDC in F1 littermate control and F1 $BDCA2\text{-}DTR^{+/-}$ KN2 mice after a 9-day course of DT

treatment. (**D**) Experimental scheme showing the F1 littermate control and F1 BDCA2-DTR KN2 mice were injected intraperitoneally (i.p.) with DT every other day for 5 times in a 9-day course, and the thymic iNKT cells and myeloid cells were analyzed at day 9. (**E**) Expression of Mertk and F4/80 in thymic cells and gating of macrophages/phagocytes (F4/80$^+$ Mertk$^+$) from F1 littermate control and F1 LysMCre$^+$ Csf1r$^{LsL\text{-}DTR+/-}$ KN2 mice after a 9-day course of DT treatment. (**F**) Cell number of thymic F4/80$^+$ Mertk$^+$ macrophages/phagocytes, B cells, cDC, pDC, eosinophils and neutrophils in F1 littermate control and F1 LysMCre$^+$ Csf1r$^{LsL\text{-}DTR+/-}$ KN2 mice after a 9-day course of DT treatment.

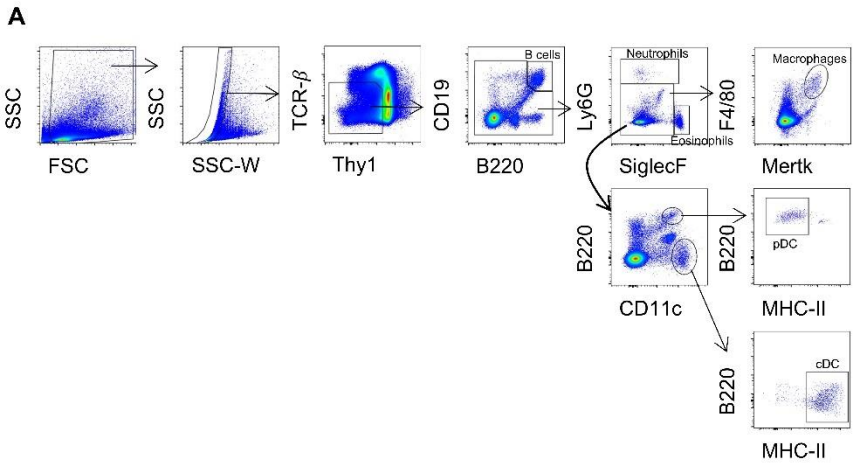

Figure 3-14. Gating strategy of myeloid cell populations in the thymus.

(**A**) Flowcytometric gating strategy to identify thymic B cells (CD19$^+$ B220$^+$), neutrophils (Ly6G$^+$ SiglecF$^-$), eosinophils (Ly6G$^-$, SiglecF$^+$), cDC (CD11c^{high}, MHC-II^{high}), pDC (CD11c^{intermediate}, B220$^+$, MHC-II^{low}) and macrophages/phagocytes (F4/80$^+$ Mertk$^+$).

Discussion

This and previous studies collectively showed that NKT2 cells are the major source of IL-4 in the thymus in the steady state (12, 41, 91). This type II cytokine-enriched thymic environment strongly influences thymocyte development through the induction of large numbers of innate CD8 T cells (12, 41), although the biological rationale for this is not yet clear. It may enhance neonatal immunity, as thymic IL-4 is more abundant early in life (12). Alternatively, thymic IL-4 may enhance tolerance of conventional T cells to self-antigens that are uniquely produced during type II immune responses, especially those derived from IL-4 induced genes.

In this study we further demonstrated that IL-4 producing NKT2 cells reside in the thymic medulla and require continuous TCR signal for their steady state production of IL-4, suggesting a cognate interaction between NKT2 cells and thymic antigen presenting cells (APC) in the medulla in the steady state. Both the selective activation of a subset of iNKT cells and the medullary location are surprising findings that raise additional questions.

The medulla is an important site of iNKT cell differentiation

iNKT cells are initially selected at the most immature “stage 0” state, through the interactions among DP thymocytes in the thymic cortex (5, 7, 8).

Nonetheless, the thymic medulla is crucial for the continued development of iNKT cells, as mature thymic iNKT cells ($CD44^+$) were greatly reduced in *Relb*$^{-/-}$ thymic epithelial cell (TEC) kidney capsule grafts, which specifically lack medullary thymic epithelial cells (mTEC) (25). In line with this, we recently showed that $CCR7^+$ iNKT cells represent a multipotent precursor for all three iNKT effector subsets (NKT1, NKT2 and NKT17) and CCR7 facilitates migration of this precursor from the cortex to the medulla (132). Collectively, these findings put forward the notion that initial selection happens in cortex while further differentiation into thymic effector subsets is reinforced in the medulla. Indeed, IL-15 produced by medullary thymic epithelial cells was essential for the generation of T-bet^+ NKT1 cells (25, 124) and medullary thymic tuft cells were shown to influence the differentiation of thymic NKT2 cells, possibly through production of IL-25 (137).

Medullary macrophages activate iNKT cells

In addition to providing cytokines that impact the differentiation or retention of iNKT cells, we here showed that NKT2 cells in particular were activated by CD1d expressing APC in the medulla. This is consistent with an earlier study that showed that CD1d was required for maturation of thymic iNKT cells beyond the positive selection of “stage 0 iNKT cells” (87), albeit not for their retention. We further demonstrated that thymic macrophages were the

predominant APC required for NKT2 cells to produce IL-4 through a CD1d mediated interaction. Thymic macrophages are distributed throughout the cortex and medulla (149, 150) (data not shown), and are believed to serve as scavengers that play an essential role in clearing apoptotic thymocytes. However, previous reports also showed thymic macrophages express both MHC-I and MHC-II and may possess antigen presenting activity (149-152) (data not shown). Interestingly, macrophages are enriched in genes involved in lipid metabolism (153). Moreover, recent studies showed that macrophages were required to stimulate iNKT cells to produce IL-4 in context of sterile liver injury (106) and influenza infection (154). Those CD1d dependent interactions facilitated recovery from injury and optimal B cell immunity, respectively. Collectively, these data indicate that macrophages can serve as important APC to present lipid antigens to iNKT cells under certain circumstances. However, the nature of these lipid antigens, and whether they are distinct from the lipid antigens that mediate positive selection of iNKT cells in the thymic cortex, remains to be elucidated,

NKT2 cells are selectively activated in the thymus

Not only do NKT2 cells produce the highest levels of IL-4 amongst thymic iNKT, they also expressed the highest level of *Nur77*^{GFP}, indicating they are perceiving stronger TCR signaling. This is consistent with the elevated Egr2

level in PLZF^{high} iNKT cells (141). This TCR signal is essential for IL-4 production, as it ceased after adoptive transfer in *Cd1d* KO hosts. High TCR signal strength also favors the differentiation of thymic NKT2 cells (PLZF^{high} iNKT), as such cells were substantially decreased in mice with weakened TCR signaling (SKG, YYAA mice) (141, 155). How do NKT2 cells perceive CD1d/self-lipid ligands differently than NKT1 and NKT17 when they all utilize a “semi-invariant” TCR? One possibility is that Vβ usage alters the fine specificity of the iNKT cells. Indeed, the three iNKT subsets have distinct and stable Vβ repertoires (12, 88, 141) with NKT2 cells (PLZF^{high} iNKT) showing higher TCR density and a preferential usage of Vβ7 (12, 141). In a model system where retrogenic mice expressed various iNKT TCR β chains, it was demonstrated that the frequency of different iNKT subsets was governed by the half-life of TCR-Ag-CD1d interaction (90). Similarly, another study using somatic nuclear transfer to generate mouse strains bearing different monoclonal iNKT TCRs showed higher TCR avidity correlates with higher frequency of PLZF^{high} iNKT cells (88). Earlier study suggests Vβ7^{+} iNKT cells might have a higher avidity for CD1d/self-lipid ligands than iNKT cells bearing other Vβs (89). Thus, it is possible that biased TCR Vβ gene usage led to differential TCR signaling events that further impacted the differentiation of iNKT subsets. Another possibility is that TCR level dictate the perceived stimulus. NKT2 cells express the highest level of surface TCR, followed by

NKT17, and NKT1 have quite low levels. Indeed, TCR density was directly shown to influence the differentiation of iNKT subsets (156). It was recently suggested that SLAM family receptors (SFR) facilitate NKT development by reducing TCR strength after position selection, and SFR deficiency skewed the subset distribution, most strongly affecting NKT1 cells (157).

In conclusion, we showed IL-4 producing NKT2 cells reside in thymic medulla are the major source of steady state IL-4 in the thymus. The steady state production of IL-4 in NKT2 cells depends on continuous TCR signal mediated by hematopoietic APC, predominantly by thymic macrophages. Moreover, considering previous reports discussed above, all these data suggest a model for the differentiation steps of thymic iNKT cells that, 1) the initial positive selection among DP thymocytes generates the most immature “stage 0 iNKT cells” in the thymic cortex; 2) with the upregulation of PLZF and CCR7, the iNKT multi-potent precursors migrate from cortex to medulla; 3) The differentiation into effector subsets (NKT1, NKT2 and NKT17) from $PLZF^{+}$ $CCR7^{+}$ iNKT precursors is influenced by various factors in thymic medulla.

Material and Methods

Key Resources Table				
Reagent type (species) or resource	**Designation**	**Source or reference**	**Identifiers**	**Additional information**
antibody	anti-CD4	BD Biosciences	Cat # 563331	(1:400)
antibody	anti-CD8α	BD Biosciences	Cat # 563786	(1:400)
antibody	anti-CD24	BioLegend	Cat # 101824	(1:200)
antibody	anti-CD44	TONBO Biosciences	Cat # 80-0441-U025	(1:200)
antibody	anti-human CD2	BioLegend	Cat # 309218	5μL/test
antibody	anti-TCRβ	BD Biosciences	Cat # 563221	(1:200)
antibody	anti-PD-1	BioLegend	Cat # 135213	(1:100)
antibody	anti-CD45.1	BioLegend	Cat # 110738	(1:200)
antibody	anti-CD45.2	eBioscience	Cat # 11-0454-81	(1:200)
antibody	anti-CD45	eBioscience	Cat # 25-0451-82	(1:200)
antibody	anti-B220	BioLegend	Cat # 103244	(1:200)
antibody	anti-CD11c	eBioscience	Cat # 47-0114-82	(1:200)
antibody	anti-CD11b	eBioscience	Cat # 47-0112-82	(1:200)
antibody	anti-F4/80	eBioscience	Cat # 47-4801-82	(1:200)
antibody	anti-CD122	BD Biosciences	Cat # 562960	(1:100)
antibody	anti-PLZF	BD Biosciences	Cat # 563490	(1:200)
antibody	anti-ROR-γt	BD Biosciences	Cat # 562684	(1:200)
antibody	anti-T-bet	BioLegend	Cat # 644824	(1:200)
antibody	anti-Mertk	BioLegend	Cat # 151504	(1:200)
antibody	anti-CD1d	eBioscience & BD Biosciences	Cat # 12-0011-81 & 553846	(1:200)
antibody	anti-CD19	TONBO Biosciences	Cat # 60-0193-U100	(1:200)
antibody	anti-PDCA-1	BioLegend	Cat # 127106	(1:200)
antibody	anti-Thy1.2	eBiosiences	Cat # 47-0902-82	(1:400)
antibody	anti-SiglecF	BD Biosciences	Cat # 740280	(1:200)
antibody	anti-Ly6G	BioLegend	Cat # 127610	(1:200)
antibody	anti-MHC-II	BioLegend	Cat # 107653	(1:1000)
antibody	anti-EpCAM	BioLegend	Cat # 118214	(1:200)
antibody	Goat-anti-R Phycoerythrin (PE)	Abcam	Cat # ab34721	(1:200)
antibody	w hole rabbit sera anti-R Phycoerythin (PE)	Novus Biologicals	Cat # NB120-7011	(1:200)
antibody	Donkey-anti-Rabbit AF555 & Goat-anti-Rabbit AF555	Invitrogen	Cat # A31572 & A21429	(1:400)
antibody	Donkey-anti-Goat AF555	Invitrogen	Cat # A21432	(1:400)
Other	Ulex Europaeus Agglutinin I (UEA I)	VECTOR LOBORATORY	FL-1061	(1:200)
Other	Strepavidin PE	Invitrogen	Cat # S21388	
commercial assay or kit	Viability dye Ghost Dye™ Red 780	TONBO Biosciences	Cat # 13-0865-T100	(1:500)
commercial assay or kit	Magnetic columns	Miltenyi	Cat # 130-042-401	
commercial assay or kit	anti-PE microbeads	Miltenyi	Cat # 130-048-801	
commercial assay or kit	tyramide amplification kit	PerkinElmer	Cat # NEL745001KT	
chemical compound, drug	Collagenase D	Roche	Cat # 11088882001	1mg/mL
chemical compound, drug	Mouse serum	Jackson ImmunoResearch	Cat # 015-000-120	5μL/test
chemical compound, drug	DNase I	Roche	Cat # 10104159001	100 U/ml
chemical compound, drug	Liberase TH	Roche	Cat # 5401127001	0.05% [w /v]
chemical compound, drug	Diptherial toxin	Sigma-Aldrich	Cat # D0564	Diluted in PBS
softw are, algorithm	Prism 7	GraphPad	https://w w w .graphpad.com/	
softw are, algorithm	ImageJ	ImageJ	https://imagej.nih.gov/ij/	
softw are, algorithm	Flow Jo v10	TreeStar - Flow jo	https://w w w .flow jo.com/solutions/flow jo	

Table 3-1 Key resources table

Mice

B6 (C57BL/6NCr) mice were purchased from the National Cancer Institute. BALB/cBYJ, CD45.1^{+} BALB/cBYJ (CByJ.SJL(B6)-Ptprca/J), Cd1d$^{-/-}$ BALB/c. (C.129S2-Cd1tm1Gru/J), *Cd1d*$^{fl/fl}$ B6, FoxN1Cre B6, MB1Cre B6, CD11cCre B6, *Zbtb46*Cre B6, BDCA2-DTR B6 mice were obtained from the Jackson Laboratory. KN2 BALB/cBYJ, *Nur77*^{GFP} BALBc and KN2 B6 mice have been previously described (12). LysMCre-*Csf1r*$^{LsL\text{-}DTR}$ B6 mice were kindly provided by Dr. Marc Jenkins at University of Minnesota. CD45.1^{+} CD45.2^{+} KN2 BALB/cBYJ, Nur77^{GFP} KN2 BALBc, FoxN1Cre *Cd1d*$^{fl/fl}$ KN2 F1, MB1Cre *Cd1d*$^{fl/fl}$ KN2 F1, CD11cCre *Cd1d*$^{fl/fl}$ KN2 F1, *Zbtb46*Cre *Cd1d*$^{fl/fl}$ KN2 F1, BDCA2-DTR KN2 F1, LysMCre *Csfr1*$^{LsL\text{-}DTR}$ KN2 F1, LysMCre *Csfr1*$^{LsL\text{-}DTR}$ F1 mice as well as littermate control mice for each strain were generated through crossbreeding at University of Minnesota. *Cd1d*$^{fl/fl}$ KN2 BALB/c mice were generated through using *Cd1d*$^{fl/fl}$ B6 mice backcrossed to KN2 BALB/c mice for at least 10 generations at University of Minnesota. All animal work was conducted in compliance with the protocols approved by the Institutional Animal Care and Use Committee of the University of Minnesota.

Diphtherial toxin treatment

BDCA2-DTR F1 and littermate control mice were injected intraperitoneally (i.p.) with diphtherial toxin (DT) every other day for 9 days (5 injections in total, 500ng of DT in 100μL PBS for the 1st injection on 1st day, 100ng of DT in

100µL PBS for all subsequent injections). LysMCre *Csfr1*$^{LsL\text{-}DTR}$ F1 and littermate control mice were injected i.p. with diphtherial toxin (DT) every other day for 9 days (5 injections in total, 100ng of DT in 100µL PBS for the all 5 injections). Mice were used the day after the last injections.

Intra-thymic transfer

iNKT enriched thymocytes were prepared through depletion of $CD8^+$ and $CD24^+$ cells (via immunomagnetic selection [Miltenyi]) in thymocytes from $CD45.1^+$ $CD45.2^+$ KN2 BALB/cBYJ mice. Intra-thymic transfers were performed on congenic host mice through ultrasound imaging guidance. Ultrasound imaging guided intra-thymic transfer is described in detail previously (128).

Bone marrow chimera

Bone marrow cells were directly flushed out from the femurs and tibias of donor mice (BALB/c Wt or BALB/c *Cd1d*$^{-/-}$) and depleted of T cells via immunomagnetic depletion (Miltenyi) of $CD8^+$ and $CD3^+$ cells. Recipient mice (BALB/c Wt or BALB/c *Cd1d*$^{-/-}$) received a total lethal dose of 600 rads. Irradiations were done in 2 doses (300 rads each) separated by a period of 3-4 hours. 2 hours after last irradiation, recipient mouse received at least 4×10^6 of T-cell-depleted bone marrow donor cells through intravenous injection via

tail vein. Bone marrow chimeras were used at 8 weeks after introduction of bone marrow donor cells.

Enrichment of iNKT cells

Thymocytes were prepared in single cell suspension and incubated with PE-CD1d-PBS57 tetramer at 4℃ for 30 min followed by immunomagnetic enrichment using anti-PE microbeads per manufacturer's instructions (Miltenyi).

Preparation of lymphocytes and flow cytometric analysis

Thymocytes were prepared in single cell suspension through mashing thymi and filtering through 70 μM cell strainers (FALCON), or digestion with collagenase D (concentration?) at 37℃ for 30 min before mashing and filtration through 70 μM cell strainers. The thymic epithelial cells were prepared as previously described (Ref). Cells were incubated with Fc block (Tonbo) and mouse serum (Jackson ImmunoResearch) for 15 min at 4℃ before staining with antibodies to surface markers and viability dye (Tonbo) for 45 min at 4℃. For intracellular staining of transcription factors, cells were fixed and permealized with a Foxp3 staining buffer set (eBioscience) after staining with antibodies to surface markers, then were incubated with antibodies to transcription factors in permealization buffer for 45 min at 4℃.

Biotinylated PBS57 loaded or unloaded CD1d monomers were from the tetramer core of the US National Institutes of Health and tetramerized with streptavidin-PE at the ratio of 4:1. All antibodies were purchased from eBioscience, BD Biosciences or BioLegend, unless otherwise indicated. See table 3-1 for a list of antibodies and other reagents used in this study. Samples were acquired on a BD LSR Fortessa or BD Fortessa X-20 and data were analyzed with FlowJo 10 (Treestar). Samples were SSC-A/FSC-A gated to exclude debris, SSC-A/SSC-W gated to select single cells, then gated to exclude viability dye^{+} dead cells.

Immunofluorescence and histocytometric analysis

For CD1d tetramer based immunofluorescence, the fresh thymic lobe was incubated PE-CD1d-PBS57 tetramer (50 μL of 1×PBS containing 2% FBS + 2 μL of CD1d tetramer in 96 well plate) at 4℃ overnight, then washed with PBS for 3 times, then fixed in 4% paraformaldehyde (PFA) at 4℃ for 1 hour followed by incubation in 30% (w/v) sucrose for overnight. Tissues were further snap frozen in Optimal Cutting Temperature Compound (Tissue-Tek) and stored at -80℃ before sectioning (5-7 μm) on a Cryostat (Leica). The immunofluorescence was performed in CAS block solution (Invitrogen) as follows: 1 hour blocking in CAS block solution at room temperature (RT), 2 hours incubation at RT with primary antibodies mixture including anti-PE

antibody (Goat polyclonal to R Phycoerythrin, Abcam; or rabbit whole antisera, Novus Biologicals) and other antibodies, wash 3 times, 1 hour incubation at RT with secondary antibodies mixture (Donkey anti Goat AF555, Invitrogen; or Goat-anti-Rabbit-AF555, Invitrogen), wash 3 times, mount overnight in mounting media containing DAPI (ProLong® Diamond Antifade Mountant with DAPI).

For human CD2 (huCD2) immunofluorescence, the tissue was stained with anti-huCD2 (RPA2) antibody followed by tyramide-based amplification per manufacturer's instructions (PerkinElmer). The images were collected on a Leica DM6000B Epi-Fluorescent microscope. The histocytometric analysis to quantify localization was performed in ImageJ, Flowjo and Prism as previously described (24, 130).

Statistical analysis

Unpaired two-tailed t-tests, and one-way ANOVA were used for data analysis and calculation of *p* values in Prism software (GraphPad).

Chapter 4

ARTC2.2/P2RX7 Signaling during Cell Isolation Distorts Function and Quantification of iNKT subsets.

Overview

Peripheral invariant natural killer T (iNKT) cells express high levels of the extracellular ATP receptor P2RX7 in mice. High extracellular ATP concentrations or NAD-mediated P2RX7 ribosylation by the enzyme ARTC2.2 can induce P2RX7 pore formation and cell death. Because both ATP and NAD are released during tissue preparation for analysis, cell death through these pathways may compromise the analysis of iNKT. Indeed, ARTC2.2 blockade enhanced recovery of viable liver iNKT. The expression of ARTC2.2 and P2RX7 on distinct iNKT subsets is unclear, however, as is the impact of recovery from other nonlymphoid sites. In this study, we performed a comprehensive analysis of ARTC2.2 and P2RX7 expression in iNKT cells in diverse tissues, at steady-state. NKT1 cells express high levels of both ARTC2.2 and P2RX7 compared with NKT2, NKT17, and $CD8^+$ circulating memory subsets. Using nanobody-mediated ARTC2.2 antagonism, we showed that ARTC2.2 blockade enhanced NKT1 recovery from nonlymphoid tissues during cell preparation. Moreover, blockade of this pathway was essential to preserve functionality, viability, and proliferation of iNKT cells. In summary, our data show that short-term in vivo blockade of the ARTC2.2/P2RX7 axis permits much improved flow cytometry–based phenotyping and enumeration of murine iNKT from nonlymphoid tissues, and it represents a crucial step for functional studies of this population.

Introduction

During preparation of ex vivo cell suspensions or in response to microbial infections, inflammation, or tumor growth, high concentrations of the nucleotides ATP and NAD can be released from apoptotic, necroptotic, or stressed cells (158). Extracellular ATP (eATP) stimulates P2RX7, which is a nonselective ligand-gated ion channel expressed by several immune cell types. Prior research focused on myeloid cells (159, 160), but P2RX7 is also expressed by lymphocyte populations (161-164). When activated by high concentrations of eATP, P2RX7 forms reversible nonselective pores that can mediate activation signals but can ultimately lead to cell death if eATP exposure persists (159, 165). ADP-ribosylation of P2RX7 by the ectoenzyme ARTC2.2, in contrast, induces irreversible pore formation and subsequent cell death. ARTC2.2 is activated by extracellular NAD (166). Importantly, ARTC2.2 activation-induced P2RX7 pore formation occurs at much lower concentrations of NAD compared with that of eATP (167). ARTC2.2 is catalytically active even when cells are at 4°C (158). The subsequent formation of P2RX7 pores, however, only happens at temperatures above 24°C, suggesting the effects of ARTC2.2-mediated ribosylation could be manifested during tissue processing that involves incubation at room temperature or 37°C—such as the steps necessary for lymphocyte isolation from nonlymphoid tissues (168, 169). Indeed, previous studies have shown

extensive cell death of T cell populations under these circumstances, especially cells expressing high levels of ARTC2.2 and P2RX7, like $CD4^+$ T regulatory cells (T_{reg}) (158). Moreover, even cells that survive isolation steps may be compromised for in vitro functional assays (170).

To tackle this issue, ARTC2.2-specific antagonist nanobodies to block the ARTC2.2/P2RX7 signaling axis were developed (166). Previous studies successfully used this strategy to recover lymphocytes with high expression of ARTC2.2, including T_{reg} and invariant natural killer T (iNKT) cells (170). Two recent reports showed that ARTC2.2 blockade also prevents the death of liver $CD8^+$ tissue-resident memory T cells (T_{RM}) during tissue preparation (171, 172). Overall, this indicates that T lymphocytes in nonlymphoid tissues are sensitive to death induced by activation of ARTC2.2 and P2RX7. Despite the pioneering nature of these reports, several questions remain. First, these studies focused on elevated frequency of live cells and short-term functional assays, rather than numeric comparisons of cells in the tissues. This made it hard to quantify to what extent ARTC2.2 blockade prevented loss of iNKT cells.

Second, iNKT cells are not homogeneous populations, with potential differences dictated both by differentiation state and tissue-specific microenvironmental signals. iNKT cells are composed of functionally and transcriptionally distinct effector subsets that include T-bet^+ $PLZF^{low}$ NKT1,

PLZF^{high} NKT2, and RORγt^{+} PLZF^{intermediate} NKT17 cells (12, 24, 136). Notably, the previous ARTC2.2 blockade studies focused on liver and spleen iNKT, most of which are NKT1 cells. Whether other iNKT subsets co-express ARTC2.2 and P2RX7 and whether blockade of this pathway can rescue these cells is unexplored.

In this study, we provide an analysis of co-expression of ARTC2.2 and P2RX7 in different iNKT subsets, in lymphoid and nonlymphoid tissues. In summary, we show that high expression of both molecules correlated with high susceptibility to *ex vivo* cell death during harvest procedures. Moreover, we found that blocking ARTC2.2 using nanobodies preserved the cell viability and in vitro function, favoring a more precise description of the numeric proportions of different subsets, as well as their exact functionality. Finally, we explored the possibility of using direct P2RX7 inhibition for the preservation of T cell numbers.

Results

ARTC2.2 and P2RX7 are preferentially co-expressed in peripheral NKT1 cells in lymphoid and nonlymphoid tissues

We first sought to evaluate the expression of P2RX7 and ARTC2.2 in subsets of iNKT cells from an array of lymphoid and nonlymphoid tissues. Previous studies indicate that ARTC2.2/P2RX7 activation strongly affects the viability of liver iNKT (173). Liver iNKT are predominantly NKT1, and we confirmed that liver NKT1 cells express high levels of both ARTC2.2 and P2RX7 (Figure 4-1 A). Similar expression was seen on NKT1 from other nonlymphoid tissues and in the spleen and mLN, whereas mature NKT1 in the thymus showed low expression of both ARTC2.2 and P2RX7 (Figure 4-1 B, C). Examination of NKT2 and NKT17 cell subsets (12), however, showed distinct expression patterns: NKT2 cells expressed high ARTC2.2 and P2RX7 in all sites, including the thymus, whereas NKT17 cells expressed low levels of both molecules, whether recovered from thymus, LN, or lung (Figure 4-1 B and data not shown).

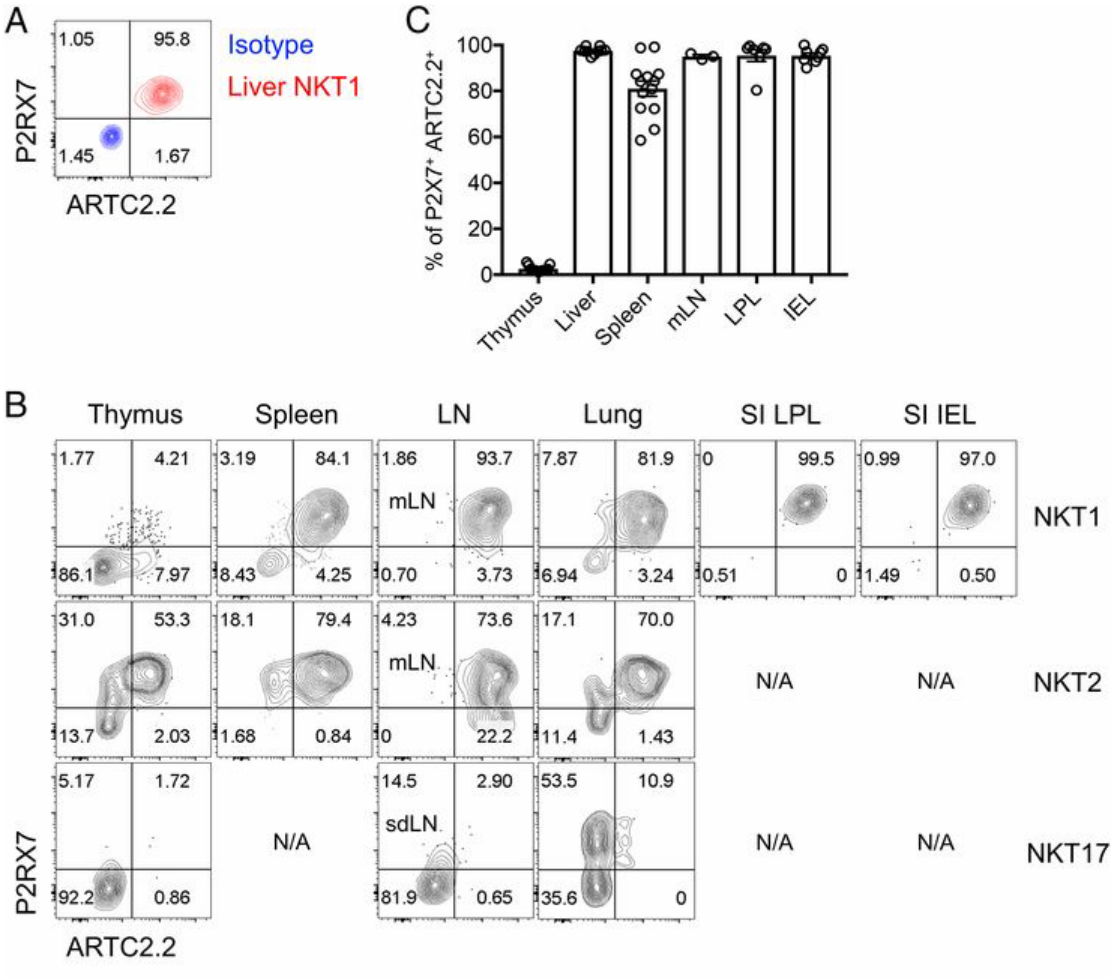

Figure 4-1. Expression of ARTC2.2 and P2RX7 in iNKT and CD8⁺ T cell subsets.

(**A**) Representative flow cytometry plot showing expression of ARTC2.2 and P2RX7 or isotype control in liver iNKT. (**B**) Representative plots showing expression of ARTC2.2 and P2RX7 in NKT1, NKT2, or NKT17 cell subsets from the indicated tissues. "N/A" means not analyzed (because of a paucity of cells of that subset in the tissue). (**C**) Percentage of NKT1 cells that are ARTC2.2⁺P2RX7⁺ [as defined by the quadrants in (A)]. (**D**) Expression of ARTC2.2 and P2RX7 in polyclonal CD8⁺ T cells from the indicated tissues (above) and in virus-specific CD8⁺ T cells 4 wk postinfection (below). For the virus-specific CD8⁺ T cell analysis, P14 CD8⁺ T cells were adoptively transferred into congenic recipient mice (2.5×10^4cells per mouse), followed by infection with LCMV Armstrong (2×10^5 PFU, i.p.). After 4 wk, cells were

isolated from the indicated tissues. (**E**) The percentages of ARTC2.2^{+}P2RX7^{+} cells are shown for polyclonal CD8^{+} T cells in the thymus and spleen, as well as splenic memory P14 cell subsets (T_{CM}, T_{EM}, SLO T_{RM}). (**F**) Percentages of memory P14 cells that were ARTC2.2^{+}P2RX7^{+} in the different organs are shown, as well as polyclonal SI-resident CD8^{+} T cells. (A–F) Data are from three independent experiments, *n* = 5–6 mice per experimental group.

ARTC2.2 blockade improves the yield of NKT1 cells in nonlymphoid tissues

Considering the high expression of both ARTC2.2 and P2XR7 in NKT1 cells, especially those residing in the nonlymphoid tissues (liver and small intestine), we asked whether tissue harvest and processing led to loss of NKT1 cells in an ARTC2.2-dependent pathway. To test this, we used a nanobody specific to ARTC2.2, previously shown to inhibit this enzyme's function in T_{reg} cells (173). In keeping with previous reports (170, 173), we observed a significantly higher yield of NKT1 cells in liver of mice treated with intravenous injection (i.v.) of anti-ARTC2.2 30 min prior to sacrifice (Figure 4-2). The action of the ARTC2.2 blockade was not limited to the liver because we observed a notably higher yield (5-fold) of NKT1 cells in the intraepithelial lymphocyte (IEL) of treated mice (Figure 4-2). Although not statistically significant, there was also a clear trend of higher yield of NKT1 cells in lamina propria (LPL) by pretreatment with anti-ARTC2.2 nanobody (Figure 4-2). Importantly, ARTC2.2 blockade led to increased numbers of NKT1 cells recovered, which was not specifically reported in previous studies (170, 173). In contrast, we did not observe any difference in the recovery of NKT1 cells in thymus, spleen, or mLN between mice injected with anti-ARTC2.2 nanobody or PBS (Figure 4-2). It is important to note that tissue processing of liver and intestines (but not of thymus, spleen, or LNs) requires short-term (20–60 min) incubations at room

temperature (25°C) or 37°C, conditions that permit ARTC2.2-mediated P2RX7 pore formation. Together, our data suggest that nonlymphoid tissue processing might result in ARTC2.2-mediated loss of NKT1 cells, and blockade of this pathway is a crucial step for the recovery of optimal numbers of this cell population.

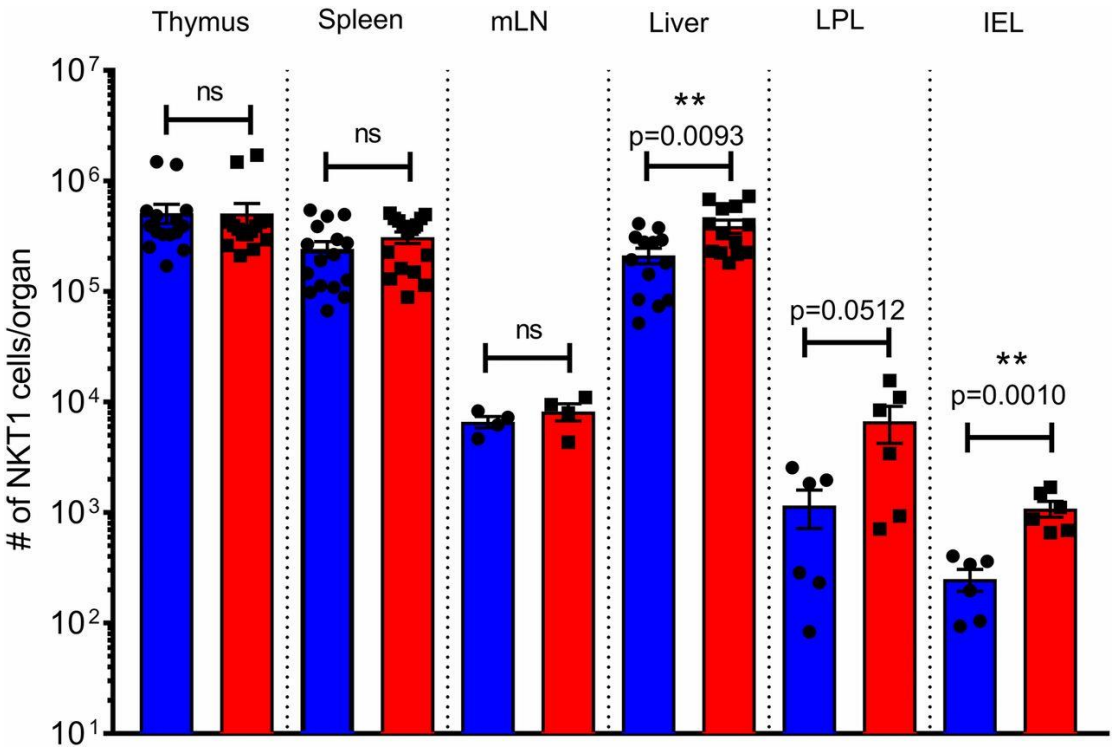

Figure 4-2. Blockade of the ARTC2.2/P2RX7 axis improves recovery of NKT1 cells in nonlymphoid tissues.

Number of NKT1 cells recovered in the indicated tissues from mice treated with anti-ARTC2.2 nanobody or PBS prior to tissue harvest. NKT1 cells are defined as TCRβ$^+$ CD1d tetramer$^+$ T-bet$^+$. Blue bars represent cells from mice that received PBS, red bars represent cells from mice that received anti-ARTC2.2 nanobody. Data are from eight independent experiments with two to six mice in each experiment. $^{**}p < 0.01$.

Anti-ARTC2.2 nanobody blockade preserves phenotype, functionality, and viability of iNKT

Activation of the ARTC2.2/P2RX7 signaling axis also induces the loss of other cell surface molecules (166). Consistent with a previous study (173), we observed that in vivo treatment with anti-ARTC2.2 nanobody prevented loss of CD27 in both splenic and liver iNKT (Figure 4-3 A). Furthermore, we evaluated other surface markers that have been used for phenotyping of iNKT and $CD8^+$ T cells. We observed that cell surface levels of CD69 and P2RX7 in iNKT were substantially preserved by in vivo treatment of anti-ARTC2.2 nanobody, whereas expression of ARTC2.2 itself, CD122, and CD4 was not affected (Figure 4-3 A). To our knowledge, the nanobody-mediated preservation of CD69 and P2RX7 expression in iNKT is a novel finding and suggests that some previous studies of iNKT may not faithfully describe their phenotype ex vivo. Whether ARTC2.2 activation alters other surface markers in iNKT is still unclear and will be a focus of future research.

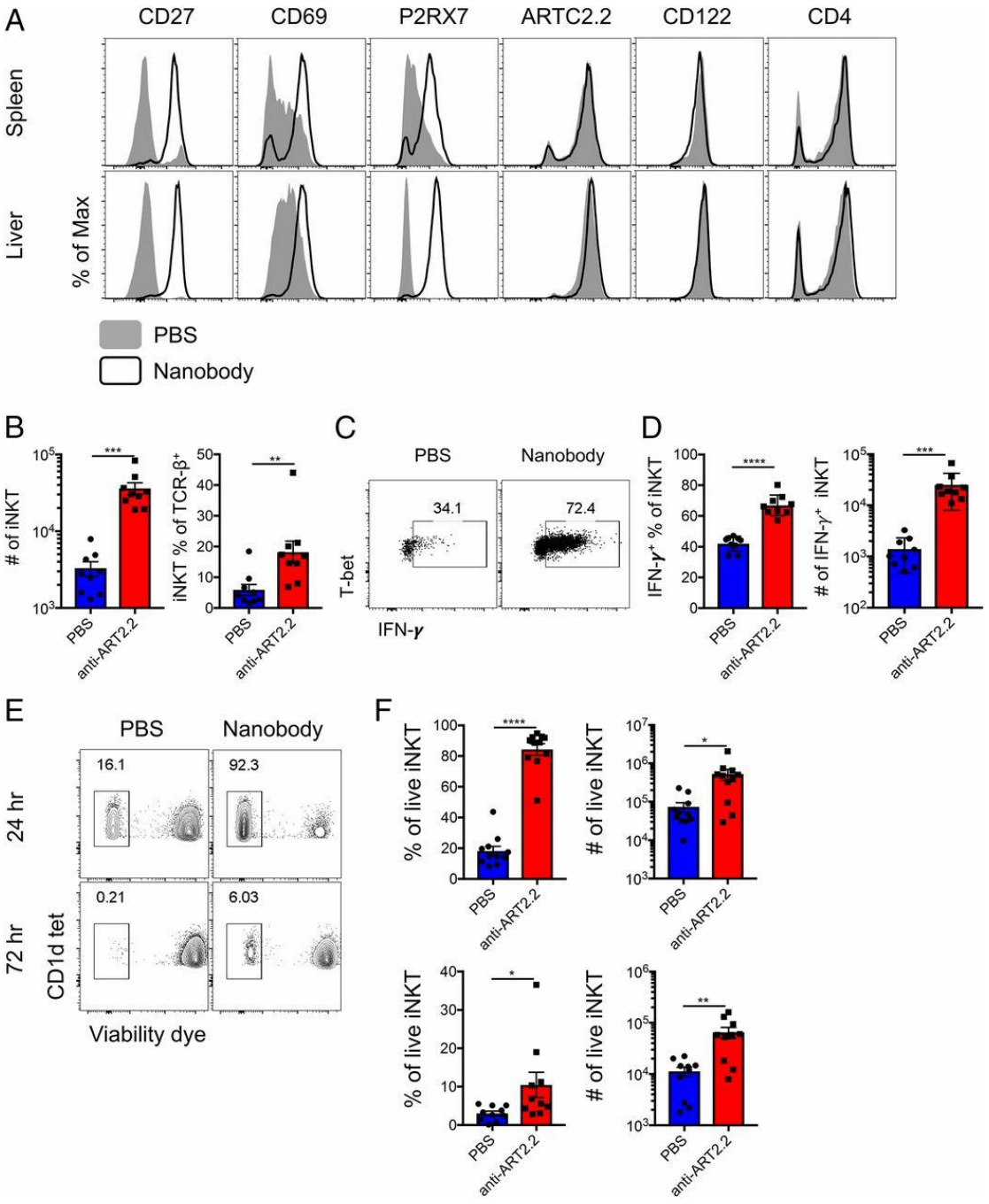

Figure 4-3. Blockade of the ARTC2.2/P2RX7 axis preserves surface molecules, cytokine production, and viability of iNKT.

Blue bars represent cells from mice that received PBS, and red bars represent cells from mice that received anti-ARTC2.2 nanobody. (**A**) Representative flow cytometry plots for surface expression of CD27, CD69, P2RX7, ARTC2.2, CD122, and CD4 in spleen and liver

NKT1 cells from mice treated with anti-ARTC2.2 nanobody or PBS. (**B**–**D**) Liver mononuclear cells isolated from mice treated with anti-ARTC2.2 nanobody or PBS were stimulated in vitro with presence of PMA/ionomycin for 4 h. (B) Numbers (left column) and frequency of NKT1 cells among total T cells ($TCR\beta^+$) (right column) after in vitro stimulation. (C) Representative flow cytometry plots for IFN-γ production in NKT1 cells after in vitro stimulation. (D) Frequency (left column) and number (right column) of IFN-γ^+ NKT1 cells after in vitro stimulation. (**E** and **F**) Liver mononuclear cells isolated from mice treated with anti-ARTC2.2 nanobody or PBS were cultured in vitro for 24 or 72 h. (E) Frequency of live iNKT (viability dye negative) after in vitro culture for 24 h (upper row) or 72 h (bottom row). (F) Frequency (left column) and number (right column) of live iNKT after in vitro culture for 24 h (upper row) or 72 h (bottom row). Data are from four independent experiments, n = 2–10 mice per experiment. *$p < 0.05$, **$p < 0.01$, ***$p < 0.001$, ****$p < 0.0001$.

Next, we asked whether blockade of the ARTC2.2/P2RX7 signaling axis would improve functional properties of iNKT after *in vitro* stimulation. Liver mononuclear cells from mice treated with PBS or anti-ARTC2.2 nanobody were cultured *in vitro* with the presence of PMA/ionomycin for 4 hrs. The treatment of anti-ARTC2.2 nanobody prior to tissue harvest not only led to much better recovery of iNKT after short-term *in vitro* stimulation (Figure 4-3 B) but also to a substantially higher frequency of IFN-γ production by those NKT1 cells (Figure 4-3 C, D).

Recently, there has been an increasing interest in harnessing iNKT for immunotherapy, which usually requires prolonged *in vitro* culture for transduction and/or expansion. Therefore, we tested the possibility that blockade with anti-ARTC2.2 nanobody might enhance the feasibility of culturing iNKT *in vitro*. Indeed, we observed that *in vivo* treatment of mice with anti-ARTC2.2 nanobody enhanced the number and viability of iNKT after short-term *in vitro* culture by ~5-fold (Figure 4-3 E, F). Taken together, these data show that in vivo treatment of anti-ARTC2.2 nanobody to block the ARTC2.2/P2RX7 signaling pathway prior to isolation significantly improves viability and functionality of iNKT for in vitro stimulation and cell culture.

Discussion

Early studies indicated that the activation of the ARTC2.2/P2RX7 pathway during *ex vivo* preparation of a single-cell suspension could lead to profound apoptosis and dysfunction in T_{reg} and liver iNKT (170). However, the expression of ARTC2.2 and P2RX7 in iNKT in tissues other than liver has not been extensively evaluated. Moreover, whether ARTC2.2/P2RX7 signaling might lead to disproportionate changes in cell number, phenotype, or function of specific subsets of iNKT during tissue processing had not been evaluated. In the current study, we established a detailed analysis of P2RX7 and ARTC2.2 expression in iNKT cells and short-term blockade of this ARTC2.2/P2RX7 axis shortly before tissue harvest could significantly improve the recovery and *ex vivo* function of iNKT. Our results suggest that both ARTC2.2 and P2RX7 are highly expressed in peripheral but not thymic NKT1 cells. This might be due to the environmental cues present only in periphery. Retinoic acid reportedly induces P2RX7 expression in intestinal lymphocytes (174), being a potential factor that influences the expression of ARTC2.2 and P2RX7 in iNKT cells residing in nonlymphoid tissues. Whether retinoic acid itself or similar molecules drive expression in other tissues is still unknown and will certainly be a subject of future studies. Moreover, it is worth mentioning that cell-intrinsic factors might also contribute to this phenomenon, as NKT2 cells seem to express high levels of ARTC2.2 and P2RX7 regardless

in the thymus or periphery, whereas NKT17 cells do not express these receptors in either the thymus or periphery. Altogether, these results demonstrate considerable heterogeneity in the expression of P2RX7 and ARTC2.2 across various subpopulations of T cells (even among iNKT subsets), suggesting differential susceptibility to NAD-induced and ATP-induced cell death and signaling. In the future, it will be important to determine whether iNKT differentiation signals override local environmental cues for expression of P2RX7 and ARTC2.2 and whether activation of these receptors is involved in shaping the representation of distinct iNKT subsets.

The physiological role of P2RX7 in T cell function and homeostasis is still the subject of intense investigation. It has been reported that P2RX7 activation can favor mouse $CD4^+$ T cell IL-2 production following re-stimulation and the differentiation of Th17 cells but restrains generation of T_{reg} and T follicular helper cells (162, 175, 176). Moreover, we recently reported that P2RX7 is crucial for establishment of long-lived memory $CD8^+$ T cell populations, including T_{RM} (164). Interestingly, our data presented in this article suggest a "Jekyll and Hyde" function of this receptor for T_{RM} biology, in which high expression of P2RX7 can be beneficial in most cases (e.g., for memory establishment) but potentially detrimental if these cells encounter situations (such as highly inflammatory environments) in which ARTC2.2 activation by NAD may be anticipated. Indeed, a recent report showed P2RX7 to be

detrimental for liver and SI IEL T_{RM} in the presence of sterile inflammation (177). It will be important to expand these studies and determine how long-term survival of various tissue-resident T cell populations, as well as their in vivo function, is affected by inflammatory challenge in a P2RX7/ARTC2.2-dependent way. Likewise, ARTC2.2 and P2RX7 are highly expressed by some subsets of iNKT, yet the impact of this expression on differentiation and function of these populations is unclear. Furthermore, it will be interesting to explore the role of P2RX7 and ARTC2.2 in mucosal-associated invariant T cells (71, 120, 132, 136, 178, 179), another innate-like T cell population, in future studies.

Taken together, our results help cement the notion that high expression of ARTC2.2 and P2RX7 act as biomarkers for susceptibility to cell death during tissue isolation in murine models. This was confirmed by our comprehensive ARTC2.2 blockade study. Beyond the scope of previous reports, we showed in this study that inhibition of ARTC2.2-mediated cell death not only preserves viability of nonlymphoid tissue T cell populations but allows a more accurate representation of different subsets among those recovered lymphocytes. Moreover, we show this blockade permits the accurate assessment of functionality of tissue-resident T cells in vitro, which opens several future possibilities—for example, metabolism assays and transduction of T cell populations isolated from nonlymphoid sites, both of which have been

technically challenging. In summary, we report that short-term blockade of ARTC2.2/P2RX7 activation during cell isolation is a crucial technical step for the optimal study of the biological characteristics of iNKT in nonlymphoid tissues and should be used when practical.

Materials and Methods

Mice

Six- to ten-week-old C57BL/6 (B6) and B6.SJL (expressing the CD45.1 allele) mice were purchased from Charles River Laboratories (via the National Cancer Institute). Animals were maintained under specific pathogen-free conditions at the University of Minnesota. All experimental procedures were approved by the institutional animal care and use committee at the University of Minnesota.

Anti-ARTC2.2 nanobody treatments

To prevent ADP-ribosylation of P2RX7 during harvest procedures, experimental mice were injected i.v. with 50 μg of the ARTC2.2 blocking nanobody (S+16a; Treg Protector, BioLegend) diluted in 200 μl of PBS, 30 min prior to sacrifice (171). Control mice received 200 μl of vehicle (PBS) at the same time.

Flow cytometry

Lymphocytes were isolated from tissues, including spleen, skin-draining lymph nodes (LN), mesenteric LN (mLN), thymus, blood, lung, small intestine (SI) intestinal epithelium, SI lamina propria (LPL), and liver, as previously described (127, 180) with the indicated mouse pretreatments (vehicle,

ARTC.2.2 nanobody). Briefly, this involved digestion at 37°C for 30 min in DTE (SI intestinal epithelial lymphocyte [IEL]) or 30–45 min in Type I Collagenase (SI LPL, lung), with stirring, followed by Percoll gradient centrifugation at room temperature. For secondary lymphoid organs (SLO), processing was followed by RBC lysis with ACK lysis buffer, at room temperature. Direct *ex vivo* staining and intracellular cytokine staining were performed as described previously (93, 127). Foxp3 Fix/Perm kit (eBioscience) was used for intracellular detection. Fluorochrome-conjugated Abs were purchased from BD Biosciences, BioLegend, eBioscience, Cell Signaling Technology, Tonbo, or Thermo Fisher Scientific. iNKT were detected using CD1d tetramers loaded with PBS-57 (provided by the National Institutes of Health Tetramer Facility) and TCRβ staining, and the distinct iNKT subsets were distinguished as described previously (12, 24); briefly, the NKT1 cells were defined as PLZF^{low} T-bet^{+}, NKT2 cells were defined as PLZF^{high} ROR-γt^{-} T-bet^{-}, and NKT17 cells were defined as PLZF^{intermediate} ROR-γt^{+}. For survival assessment, cells were stained with Live/Dead dye (Tonbo Biosciences). Flow cytometric analysis was performed on an LSR II or LSR Fortessa (BD Biosciences), and data were analyzed using FlowJo software (Tree Star).

In vitro culture experiments

To measure the proliferation, survival, and cytokine production of liver iNKT and spleen/SI memory (P14) $CD8^+$ T cells, cells from experimental mice were isolated as described above and stimulated in vitro with vehicle (RPMI 1640), PMA (20 ng/ml) plus ionomycin (1 μM). Cells were cultured for 4, 24 and 72 hrs. For all experiments, complete RPMI media (RPMI 1640 supplemented with 10% FBS, 100 U/ml penicillin/streptomycin, 2 mM l-glutamine) was used.

Statistical analysis

Statistical differences were calculated by using unpaired two-tailed Student *t* test or one-way ANOVA with Tukey posttest, where indicated. All experiments were analyzed using Prism 5 (GraphPad Software). The *p* values <0.05 (*), <0.01 (**), <0.001 (***), or <0.0001 (****) indicated significant differences between groups, and nonsignificant differences were indicated with “ns”.

Bibliography

1. Ohteki, T. and H.R. MacDonald, *Major histocompatibility complex class I related molecules control the development of CD4+8- and CD4-8- subsets of natural killer 1.1+ T cell receptor-alpha/beta+ cells in the liver of mice.* J Exp Med, 1994. **180**(2): p. 699-704.
2. Makino, Y., et al., *Predominant expression of invariant V alpha 14+ TCR alpha chain in NK1.1+ T cell populations.* Int Immunol, 1995. **7**(7): p. 1157-61.
3. Lantz, O. and A. Bendelac, *An invariant T cell receptor alpha chain is used by a unique subset of major histocompatibility complex class I-specific CD4+ and CD4-8- T cells in mice and humans.* J Exp Med, 1994. **180**(3): p. 1097-106.
4. Godfrey, D.I., S. Stankovic, and A.G. Baxter, *Raising the NKT cell family.* Nat Immunol, 2010. **11**(3): p. 197-206.
5. Egawa, T., et al., *Genetic evidence supporting selection of the Valpha14i NKT cell lineage from double-positive thymocyte precursors.* Immunity, 2005. **22**(6): p. 705-16.
6. Benlagha, K., et al., *Characterization of the early stages of thymic NKT cell development.* J Exp Med, 2005. **202**(4): p. 485-92.
7. Bendelac, A., *Positive selection of mouse NK1+ T cells by CD1-expressing cortical thymocytes.* J Exp Med, 1995. **182**(6): p. 2091-6.
8. Gapin, L., et al., *NKT cells derive from double-positive thymocytes that are positively selected by CD1d.* Nat Immunol, 2001. **2**(10): p. 971-8.
9. Kovalovsky, D., et al., *The BTB-zinc finger transcriptional regulator PLZF controls the development of invariant natural killer T cell effector functions.* Nat Immunol, 2008. **9**(9): p. 1055-64.
10. Savage, A.K., et al., *The transcription factor PLZF directs the effector program of the NKT cell lineage.* Immunity, 2008. **29**(3): p. 391-403.
11. Thomas, S.Y., et al., *PLZF induces an intravascular surveillance program mediated by long-lived LFA-1-ICAM-1 interactions.* J Exp Med, 2011. **208**(6): p. 1179-88.
12. Lee, Y.J., et al., *Steady-state production of IL-4 modulates immunity in mouse strains and is determined by lineage diversity of iNKT cells.* Nat Immunol, 2013. **14**(11): p. 1146-54.
13. Michel, M.L., et al., *Critical role of ROR-gammat in a new thymic pathway leading to IL-17-producing invariant NKT cell differentiation.* Proc Natl Acad Sci U S A, 2008. **105**(50): p. 19845-50.
14. Watarai, H., et al., *Development and function of invariant natural killer T cells producing T(h)2- and T(h)17-cytokines.* PLoS Biol, 2012. **10**(2): p. e1001255.
15. Dashtsoodol, N., et al., *Alternative pathway for the development of Valpha14(+) NKT cells directly from CD4(-)CD8(-) thymocytes that*

bypasses the CD4(+)CD8(+) stage. Nat Immunol, 2017. **18**(3): p. 274-282.
16. Bezbradica, J.S., et al., *Commitment toward the natural T (iNKT) cell lineage occurs at the CD4+8+ stage of thymic ontogeny.* Proc Natl Acad Sci U S A, 2005. **102**(14): p. 5114-9.
17. D'Cruz, L.M., et al., *An essential role for the transcription factor HEB in thymocyte survival, Tcra rearrangement and the development of natural killer T cells.* Nat Immunol, 2010. **11**(3): p. 240-9.
18. Dose, M., et al., *Intrathymic proliferation wave essential for Valpha14+ natural killer T cell development depends on c-Myc.* Proc Natl Acad Sci U S A, 2009. **106**(21): p. 8641-6.
19. Mycko, M.P., et al., *Selective requirement for c-Myc at an early stage of V(alpha)14i NKT cell development.* J Immunol, 2009. **182**(8): p. 4641-8.
20. Hu, T., et al., *The transcription factor c-Myb primes CD4+CD8+ immature thymocytes for selection into the iNKT lineage.* Nat Immunol, 2010. **11**(5): p. 435-41.
21. Moran, A.E., et al., *T cell receptor signal strength in Treg and iNKT cell development demonstrated by a novel fluorescent reporter mouse.* J Exp Med, 2011. **208**(6): p. 1279-89.
22. Griewank, K., et al., *Homotypic interactions mediated by Slamf1 and Slamf6 receptors control NKT cell lineage development.* Immunity, 2007. **27**(5): p. 751-62.
23. Bendelac, A., P.B. Savage, and L. Teyton, *The biology of NKT cells.* Annu Rev Immunol, 2007. **25**: p. 297-336.
24. Lee, Y.J., et al., *Tissue-Specific Distribution of iNKT Cells Impacts Their Cytokine Response.* Immunity, 2015. **43**(3): p. 566-78.
25. White, A.J., et al., *An essential role for medullary thymic epithelial cells during the intrathymic development of invariant NKT cells.* J Immunol, 2014. **192**(6): p. 2659-66.
26. Kozai, M., et al., *Essential role of CCL21 in establishment of central self-tolerance in T cells.* J Exp Med, 2017. **214**(7): p. 1925-1935.
27. Cowan, J.E., et al., *Differential requirement for CCR4 and CCR7 during the development of innate and adaptive alphabetaT cells in the adult thymus.* J Immunol, 2014. **193**(3): p. 1204-12.
28. Engel, I., et al., *Innate-like functions of natural killer T cell subsets result from highly divergent gene programs.* Nat Immunol, 2016. **17**(6): p. 728-39.
29. Lee, Y.J., et al., *Lineage-Specific Effector Signatures of Invariant NKT Cells Are Shared amongst gammadelta T, Innate Lymphoid, and Th Cells.* J Immunol, 2016. **197**(4): p. 1460-70.
30. Zhu, J., H. Yamane, and W.E. Paul, *Differentiation of effector CD4 T cell populations (*).* Annu Rev Immunol, 2010. **28**: p. 445-89.

31. Gordy, L.E., et al., *IL-15 regulates homeostasis and terminal maturation of NKT cells.* J Immunol, 2011. **187**(12): p. 6335-45.
32. Havenar-Daughton, C., et al., *Development and function of murine RORgammat+ iNKT cells are under TGF-beta signaling control.* Blood, 2012. **119**(15): p. 3486-94.
33. Motomura, Y., et al., *The transcription factor E4BP4 regulates the production of IL-10 and IL-13 in CD4+ T cells.* Nat Immunol, 2011. **12**(5): p. 450-9.
34. Sag, D., et al., *IL-10-producing NKT10 cells are a distinct regulatory invariant NKT cell subset.* J Clin Invest, 2014. **124**(9): p. 3725-40.
35. Lynch, L., et al., *Regulatory iNKT cells lack expression of the transcription factor PLZF and control the homeostasis of T(reg) cells and macrophages in adipose tissue.* Nat Immunol, 2015. **16**(1): p. 85-95.
36. von Moltke, J., et al., *Tuft-cell-derived IL-25 regulates an intestinal ILC2-epithelial response circuit.* Nature, 2016. **529**(7585): p. 221-5.
37. Seiler, M.P., et al., *Elevated and sustained expression of the transcription factors Egr1 and Egr2 controls NKT lineage differentiation in response to TCR signaling.* Nat Immunol, 2012. **13**(3): p. 264-71.
38. O'Hagan, K.L., et al., *Pak2 Controls Acquisition of NKT Cell Fate by Regulating Expression of the Transcription Factors PLZF and Egr2.* J Immunol, 2015. **195**(11): p. 5272-84.
39. Carlson, C.M., et al., *Kruppel-like factor 2 regulates thymocyte and T-cell migration.* Nature, 2006. **442**(7100): p. 299-302.
40. Weinreich, M.A., et al., *KLF2 transcription-factor deficiency in T cells results in unrestrained cytokine production and upregulation of bystander chemokine receptors.* Immunity, 2009. **31**(1): p. 122-30.
41. Weinreich, M.A., et al., *T cells expressing the transcription factor PLZF regulate the development of memory-like CD8+ T cells.* Nat Immunol, 2010. **11**(8): p. 709-16.
42. Lai, D., et al., *KLF13 sustains thymic memory-like CD8(+) T cells in BALB/c mice by regulating IL-4-generating invariant natural killer T cells.* J Exp Med, 2011. **208**(5): p. 1093-103.
43. Mackay, L.K., et al., *Hobit and Blimp1 instruct a universal transcriptional program of tissue residency in lymphocytes.* Science, 2016. **352**(6284): p. 459-63.
44. van Gisbergen, K.P., et al., *Mouse Hobit is a homolog of the transcriptional repressor Blimp-1 that regulates NKT cell effector differentiation.* Nat Immunol, 2012. **13**(9): p. 864-71.
45. Steinke, F.C. and H.H. Xue, *From inception to output, Tcf1 and Lef1 safeguard development of T cells and innate immune cells.* Immunol Res, 2014. **59**(1-3): p. 45-55.
46. Berga-Bolanos, R., et al., *Cell-autonomous requirement for TCF1 and*

LEF1 in the development of Natural Killer T cells. Mol Immunol, 2015. **68**(2 Pt B): p. 484-9.
47. Carr, T., et al., *The transcription factor lymphoid enhancer factor 1 controls invariant natural killer T cell expansion and Th2-type effector differentiation.* J Exp Med, 2015. **212**(5): p. 793-807.
48. Tahiliani, M., et al., *Conversion of 5-methylcytosine to 5-hydroxymethylcytosine in mammalian DNA by MLL partner TET1.* Science, 2009. **324**(5929): p. 930-5.
49. Ito, S., et al., *Tet proteins can convert 5-methylcytosine to 5-formylcytosine and 5-carboxylcytosine.* Science, 2011. **333**(6047): p. 1300-3.
50. He, Y.F., et al., *Tet-mediated formation of 5-carboxylcytosine and its excision by TDG in mammalian DNA.* Science, 2011. **333**(6047): p. 1303-7.
51. Tsagaratou, A., et al., *TET proteins regulate the lineage specification and TCR-mediated expansion of iNKT cells.* Nat Immunol, 2017. **18**(1): p. 45-53.
52. Pereira, R.M., et al., *Jarid2 is induced by TCR signalling and controls iNKT cell maturation.* Nat Commun, 2014. **5**: p. 4540.
53. Thapa, P., et al., *The transcriptional repressor NKAP is required for the development of iNKT cells.* Nat Commun, 2013. **4**: p. 1582.
54. Thapa, P., et al., *Histone deacetylase 3 is required for iNKT cell development.* Sci Rep, 2017. **7**(1): p. 5784.
55. Beyaz, S., et al., *The histone demethylase UTX regulates the lineage-specific epigenetic program of invariant natural killer T cells.* Nat Immunol, 2017. **18**(2): p. 184-195.
56. Bartel, D.P., *MicroRNAs: genomics, biogenesis, mechanism, and function.* Cell, 2004. **116**(2): p. 281-97.
57. Fedeli, M., et al., *Dicer-dependent microRNA pathway controls invariant NKT cell development.* J Immunol, 2009. **183**(4): p. 2506-12.
58. Li, Q.J., et al., *miR-181a is an intrinsic modulator of T cell sensitivity and selection.* Cell, 2007. **129**(1): p. 147-61.
59. Zietara, N., et al., *Critical role for miR-181a/b-1 in agonist selection of invariant natural killer T cells.* Proc Natl Acad Sci U S A, 2013. **110**(18): p. 7407-12.
60. Fedeli, M., et al., *miR-17 approximately 92 family clusters control iNKT cell ontogenesis via modulation of TGF-beta signaling.* Proc Natl Acad Sci U S A, 2016. **113**(51): p. E8286-e8295.
61. Yuan, J., et al., *Lin28b reprograms adult bone marrow hematopoietic progenitors to mediate fetal-like lymphopoiesis.* Science, 2012. **335**(6073): p. 1195-200.
62. Pobezinsky, L.A., et al., *Let-7 microRNAs target the lineage-specific transcription factor PLZF to regulate terminal NKT cell differentiation*

and effector function. Nat Immunol, 2015. **16**(5): p. 517-24.
63. Bezman, N.A., et al., *miR-150 regulates the development of NK and iNKT cells.* J Exp Med, 2011. **208**(13): p. 2717-31.
64. Zheng, Q., L. Zhou, and Q.S. Mi, *MicroRNA miR-150 is involved in Valpha14 invariant NKT cell development and function.* J Immunol, 2012. **188**(5): p. 2118-26.
65. Mao, A.P., et al., *A shared Runx1-bound Zbtb16 enhancer directs innate and innate-like lymphoid lineage development.* Nat Commun, 2017. **8**(1): p. 863.
66. Mao, A.P., et al., *Multiple layers of transcriptional regulation by PLZF in NKT-cell development.* Proc Natl Acad Sci U S A, 2016. **113**(27): p. 7602-7.
67. Mathew, R., et al., *BTB-ZF factors recruit the E3 ligase cullin 3 to regulate lymphoid effector programs.* Nature, 2012. **491**(7425): p. 618-21.
68. Vasanthakumar, A., et al., *A non-canonical function of Ezh2 preserves immune homeostasis.* EMBO Rep, 2017. **18**(4): p. 619-631.
69. Pellicci, D.G., et al., *A natural killer T (NKT) cell developmental pathway iInvolving a thymus-dependent NK1.1(-)CD4(+) CD1d-dependent precursor stage.* J Exp Med, 2002. **195**(7): p. 835-44.
70. Olszak, T., et al., *Microbial exposure during early life has persistent effects on natural killer T cell function.* Science, 2012. **336**(6080): p. 489-93.
71. Koay, H.F., et al., *A three-stage intrathymic development pathway for the mucosal-associated invariant T cell lineage.* Nat Immunol, 2016. **17**(11): p. 1300-1311.
72. Albu, D.I., et al., *Transcription factor Bcl11b controls selection of invariant natural killer T-cells by regulating glycolipid presentation in double-positive thymocytes.* Proc Natl Acad Sci U S A, 2011. **108**(15): p. 6211-6.
73. Jayawardena-Wolf, J., et al., *CD1d endosomal trafficking is independently regulated by an intrinsic CD1d-encoded tyrosine motif and by the invariant chain.* Immunity, 2001. **15**(6): p. 897-908.
74. Chiu, Y.H., et al., *Multiple defects in antigen presentation and T cell development by mice expressing cytoplasmic tail-truncated CD1d.* Nat Immunol, 2002. **3**(1): p. 55-60.
75. Mori, L., M. Lepore, and G. De Libero, *The Immunology of CD1- and MR1-Restricted T Cells.* Annu Rev Immunol, 2016. **34**: p. 479-510.
76. Salio, M., et al., *Biology of CD1- and MR1-restricted T cells.* Annu Rev Immunol, 2014. **32**: p. 323-66.
77. Mattner, J., et al., *Exogenous and endogenous glycolipid antigens activate NKT cells during microbial infections.* Nature, 2005. **434**(7032): p. 525-9.

78. Porubsky, S., et al., *Normal development and function of invariant natural killer T cells in mice with isoglobotrihexosylceramide (iGb3) deficiency.* Proc Natl Acad Sci U S A, 2007. **104**(14): p. 5977-82.
79. Popovic, Z.V., et al., *Glucosylceramide Synthase Is Involved in Development of Invariant Natural Killer T Cells.* Front Immunol, 2017. **8**: p. 848.
80. Kain, L., et al., *The identification of the endogenous ligands of natural killer T cells reveals the presence of mammalian alpha-linked glycosylceramides.* Immunity, 2014. **41**(4): p. 543-54.
81. Lairson, L.L., et al., *Glycosyltransferases: structures, functions, and mechanisms.* Annu Rev Biochem, 2008. **77**: p. 521-55.
82. Brennan, P.J., et al., *Invariant natural killer T cells recognize lipid self antigen induced by microbial danger signals.* Nat Immunol, 2011. **12**(12): p. 1202-11.
83. Brennan, P.J., et al., *Activation of iNKT cells by a distinct constituent of the endogenous glucosylceramide fraction.* Proc Natl Acad Sci U S A, 2014. **111**(37): p. 13433-8.
84. Kain, L., et al., *Endogenous ligands of natural killer T cells are alpha-linked glycosylceramides.* Mol Immunol, 2015. **68**(2 Pt A): p. 94-7.
85. Facciotti, F., et al., *Peroxisome-derived lipids are self antigens that stimulate invariant natural killer T cells in the thymus.* Nat Immunol, 2012. **13**(5): p. 474-80.
86. Paduraru, C., et al., *Role for lysosomal phospholipase A2 in iNKT cell-mediated CD1d recognition.* Proc Natl Acad Sci U S A, 2013. **110**(13): p. 5097-102.
87. McNab, F.W., et al., *The influence of CD1d in postselection NKT cell maturation and homeostasis.* J Immunol, 2005. **175**(6): p. 3762-8.
88. Clancy-Thompson, E., et al., *Monoclonal Invariant NKT (iNKT) Cell Mice Reveal a Role for Both Tissue of Origin and the TCR in Development of iNKT Functional Subsets.* J Immunol, 2017. **199**(1): p. 159-171.
89. Schumann, J., et al., *Cutting edge: influence of the TCR Vbeta domain on the selection of semi-invariant NKT cells by endogenous ligands.* J Immunol, 2006. **176**(4): p. 2064-8.
90. Cruz Tleugabulova, M., et al., *Discrete TCR Binding Kinetics Control Invariant NKT Cell Selection and Central Priming.* J Immunol, 2016. **197**(10): p. 3959-3969.
91. White, A.J., et al., *A type 2 cytokine axis for thymus emigration.* J Exp Med, 2017. **214**(8): p. 2205-2216.
92. Jameson, S.C., Y.J. Lee, and K.A. Hogquist, *Innate memory T cells.* Adv Immunol, 2015. **126**: p. 173-213.
93. Renkema, K.R., et al., *IL-4 sensitivity shapes the peripheral CD8+ T cell pool and response to infection.* J Exp Med, 2016. **213**(7): p. 1319-

29.
94. Lee, A., et al., *IL-4 Induced Innate CD8+ T Cells Control Persistent Viral Infection.* PLoS Pathog, 2015. **11**(10): p. e1005193.
95. White, J.T., E.W. Cross, and R.M. Kedl, *Antigen-inexperienced memory CD8(+) T cells: where they come from and why we need them.* Nat Rev Immunol, 2017. **17**(6): p. 391-400.
96. Wilson, S.B., et al., *Extreme Th1 bias of invariant Valpha24JalphaQ T cells in type 1 diabetes.* Nature, 1998. **391**(6663): p. 177-81.
97. Wang, B., Y.B. Geng, and C.R. Wang, *CD1-restricted NK T cells protect nonobese diabetic mice from developing diabetes.* J Exp Med, 2001. **194**(3): p. 313-20.
98. Mi, Q.S., et al., *Interleukin-4 but not interleukin-10 protects against spontaneous and recurrent type 1 diabetes by activated CD1d-restricted invariant natural killer T-cells.* Diabetes, 2004. **53**(5): p. 1303-10.
99. Kent, S.C., et al., *Loss of IL-4 secretion from human type 1a diabetic pancreatic draining lymph node NKT cells.* J Immunol, 2005. **175**(7): p. 4458-64.
100. Hong, S., et al., *The natural killer T-cell ligand alpha-galactosylceramide prevents autoimmune diabetes in non-obese diabetic mice.* Nat Med, 2001. **7**(9): p. 1052-6.
101. Sharif, S., et al., *Activation of natural killer T cells by alpha-galactosylceramide treatment prevents the onset and recurrence of autoimmune Type 1 diabetes.* Nat Med, 2001. **7**(9): p. 1057-62.
102. Blazar, B.R., W.J. Murphy, and M. Abedi, *Advances in graft-versus-host disease biology and therapy.* Nat Rev Immunol, 2012. **12**(6): p. 443-58.
103. Mavers, M., K. Maas-Bauer, and R.S. Negrin, *Invariant Natural Killer T Cells As Suppressors of Graft-versus-Host Disease in Allogeneic Hematopoietic Stem Cell Transplantation.* Front Immunol, 2017. **8**: p. 900.
104. Hashimoto, D., et al., *Stimulation of host NKT cells by synthetic glycolipid regulates acute graft-versus-host disease by inducing Th2 polarization of donor T cells.* J Immunol, 2005. **174**(1): p. 551-6.
105. Du, J., et al., *Invariant natural killer T cells ameliorate murine chronic GVHD by expanding donor regulatory T cells.* Blood, 2017. **129**(23): p. 3121-3125.
106. Liew, P.X., W.Y. Lee, and P. Kubes, *iNKT Cells Orchestrate a Switch from Inflammation to Resolution of Sterile Liver Injury.* Immunity, 2017. **47**(4): p. 752-765.e5.
107. Geissmann, F., et al., *Intravascular immune surveillance by CXCR6+ NKT cells patrolling liver sinusoids.* PLoS Biol, 2005. **3**(4): p. e113.
108. Akiyama, T., et al., *The tumor necrosis factor family receptors RANK and CD40 cooperatively establish the thymic medullary*

microenvironment and self-tolerance. Immunity, 2008. **29**(3): p. 423-37.
109. Lynch, L., et al., *Adipose tissue invariant NKT cells protect against diet-induced obesity and metabolic disorder through regulatory cytokine production.* Immunity, 2012. **37**(3): p. 574-87.
110. Engel, I. and M. Kronenberg, *Transcriptional control of the development and function of Valpha14i NKT cells.* Curr Top Microbiol Immunol, 2014. **381**: p. 51-81.
111. Coquet, J.M., et al., *Diverse cytokine production by NKT cell subsets and identification of an IL-17-producing CD4-NK1.1- NKT cell population.* Proc Natl Acad Sci U S A, 2008. **105**(32): p. 11287-92.
112. Doisne, J.M., et al., *Skin and peripheral lymph node invariant NKT cells are mainly retinoic acid receptor-related orphan receptor (gamma)t+ and respond preferentially under inflammatory conditions.* J Immunol, 2009. **183**(3): p. 2142-9.
113. Doisne, J.M., et al., *Cutting edge: crucial role of IL-1 and IL-23 in the innate IL-17 response of peripheral lymph node NK1.1- invariant NKT cells to bacteria.* J Immunol, 2011. **186**(2): p. 662-6.
114. Michel, M.L., et al., *Identification of an IL-17-producing NK1.1(neg) iNKT cell population involved in airway neutrophilia.* J Exp Med, 2007. **204**(5): p. 995-1001.
115. Terashima, A., et al., *A novel subset of mouse NKT cells bearing the IL-17 receptor B responds to IL-25 and contributes to airway hyperreactivity.* J Exp Med, 2008. **205**(12): p. 2727-33.
116. Gapin, L., *Development of invariant natural killer T cells.* Curr Opin Immunol, 2016. **39**: p. 68-74.
117. Lynch, L., et al., *iNKT Cells Induce FGF21 for Thermogenesis and Are Required for Maximal Weight Loss in GLP1 Therapy.* Cell Metab, 2016. **24**(3): p. 510-519.
118. Boursalian, T.E., et al., *Continued maturation of thymic emigrants in the periphery.* Nat Immunol, 2004. **5**(4): p. 418-25.
119. McCaughtry, T.M., M.S. Wilken, and K.A. Hogquist, *Thymic emigration revisited.* J Exp Med, 2007. **204**(11): p. 2513-20.
120. Wang, H. and K.A. Hogquist, *How MAIT cells get their start.* Nat Immunol, 2016. **17**(11): p. 1238-1240.
121. Allende, M.L., et al., *S1P1 receptor expression regulates emergence of NKT cells in peripheral tissues.* Faseb j, 2008. **22**(1): p. 307-15.
122. Berzins, S.P., et al., *Long-term retention of mature NK1.1+ NKT cells in the thymus.* J Immunol, 2006. **176**(7): p. 4059-65.
123. Xing, Y., et al., *Late stages of T cell maturation in the thymus involve NF-kappaB and tonic type I interferon signaling.* Nat Immunol, 2016. **17**(5): p. 565-73.
124. Cui, G., et al., *Characterization of the IL-15 niche in primary and secondary lymphoid organs in vivo.* Proc Natl Acad Sci U S A, 2014.

111(5): p. 1915-20.
125. Rahimpour, A., et al., *Identification of phenotypically and functionally heterogeneous mouse mucosal-associated invariant T cells using MR1 tetramers.* J Exp Med, 2015. **212**(7): p. 1095-108.
126. Benlagha, K., et al., *A thymic precursor to the NK T cell lineage.* Science, 2002. **296**(5567): p. 553-5.
127. Skon, C.N., et al., *Transcriptional downregulation of S1pr1 is required for the establishment of resident memory CD8+ T cells.* Nat Immunol, 2013. **14**(12): p. 1285-93.
128. Wang, H., et al., *Ultrasound Guided Intra-thymic Injection to Track Recent Thymic Emigrants and Investigate T Cell Development.* Bio-protocol, 2018. **8**(23): p. e3107.
129. Xing, Y. and K.A. Hogquist, *Isolation, identification, and purification of murine thymic epithelial cells.* J Vis Exp, 2014(90): p. e51780.
130. Gerner, M.Y., et al., *Histo-cytometry: a method for highly multiplex quantitative tissue imaging analysis applied to dendritic cell subset microanatomy in lymph nodes.* Immunity, 2012. **37**(2): p. 364-76.
131. Lienenklaus, S., et al., *Novel reporter mouse reveals constitutive and inflammatory expression of IFN-beta in vivo.* J Immunol, 2009. **183**(5): p. 3229-36.
132. Wang, H. and K.A. Hogquist, *CCR7 defines a precursor for murine iNKT cells in thymus and periphery.* Elife, 2018. **7**.
133. Reynolds, C.J., et al., *Bioluminescent Reporting of In Vivo IFN-gamma Immune Responses during Infection and Autoimmunity.* J Immunol, 2019. **202**(8): p. 2502-2510.
134. Owen, D.L., et al., *Thymic regulatory T cells arise via two distinct developmental programs.* Nat Immunol, 2019. **20**(2): p. 195-205.
135. Kang, B.H., et al., *PLZF(+) Innate T Cells Support the TGF-beta-Dependent Generation of Activated/Memory-Like Regulatory T Cells.* Mol Cells, 2016. **39**(6): p. 468-76.
136. Wang, H. and K.A. Hogquist, *How Lipid-Specific T Cells Become Effectors: The Differentiation of iNKT Subsets.* Front Immunol, 2018. **9**: p. 1450.
137. Miller, C.N., et al., *Thymic tuft cells promote an IL-4-enriched medulla and shape thymocyte development.* Nature, 2018. **559**(7715): p. 627-631.
138. Mohrs, K., et al., *A two-step process for cytokine production revealed by IL-4 dual-reporter mice.* Immunity, 2005. **23**(4): p. 419-29.
139. Jenkins, M.K., et al., *In vivo activation of antigen-specific CD4 T cells.* Annu Rev Immunol, 2001. **19**: p. 23-45.
140. Au-Yeung, B.B., et al., *A sharp T-cell antigen receptor signaling threshold for T-cell proliferation.* Proc Natl Acad Sci U S A, 2014. **111**(35): p. E3679-88.

141. Tuttle, K.D., et al., *TCR signal strength controls thymic differentiation of iNKT cell subsets.* Nat Commun, 2018. **9**(1): p. 2650.
142. Breed, E.R., S.T. Lee, and K.A. Hogquist, *Directing T cell fate: How thymic antigen presenting cells coordinate thymocyte selection.* Semin Cell Dev Biol, 2018. **84**: p. 2-10.
143. Zimmer, M.I., et al., *A cell-type specific CD1d expression program modulates invariant NKT cell development and function.* J Immunol, 2006. **176**(3): p. 1421-30.
144. Forestier, C., et al., *T cell development in mice expressing CD1d directed by a classical MHC class II promoter.* J Immunol, 2003. **171**(8): p. 4096-104.
145. Loschko, J., et al., *Absence of MHC class II on cDCs results in microbial-dependent intestinal inflammation.* J Exp Med, 2016. **213**(4): p. 517-34.
146. Bai, L., et al., *Distinct APCs explain the cytokine bias of alpha-galactosylceramide variants in vivo.* J Immunol, 2012. **188**(7): p. 3053-61.
147. Abram, C.L., et al., *Comparative analysis of the efficiency and specificity of myeloid-Cre deleting strains using ROSA-EYFP reporter mice.* J Immunol Methods, 2014. **408**: p. 89-100.
148. Schreiber, H.A., et al., *Intestinal monocytes and macrophages are required for T cell polarization in response to Citrobacter rodentium.* J Exp Med, 2013. **210**(10): p. 2025-39.
149. Wood, G.W., *Macrophages in the thymus.* Surv Immunol Res, 1985. **4**(3): p. 179-91.
150. Soga, H., et al., *Heterogeneity of mouse thymic macrophages: I. Immunohistochemical analysis.* Arch Histol Cytol, 1997. **60**(1): p. 53-63.
151. Esashi, E., et al., *Cutting Edge: A possible role for CD4+ thymic macrophages as professional scavengers of apoptotic thymocytes.* J Immunol, 2003. **171**(6): p. 2773-7.
152. Unanue, E.R., *Antigen-presenting function of the macrophage.* Annu Rev Immunol, 1984. **2**: p. 395-428.
153. Remmerie, A. and C.L. Scott, *Macrophages and lipid metabolism.* Cell Immunol, 2018. **330**: p. 27-42.
154. Gaya, M., et al., *Initiation of Antiviral B Cell Immunity Relies on Innate Signals from Spatially Positioned NKT Cells.* Cell, 2018. **172**(3): p. 517-533.e20.
155. Zhao, M., et al., *Altered thymic differentiation and modulation of arthritis by invariant NKT cells expressing mutant ZAP70.* Nat Commun, 2018. **9**(1): p. 2627.
156. Joseph, C., et al., *TCR density in early iNKT cell precursors regulates agonist selection and subset differentiation in mice.* Eur J Immunol,

2019.
157. Lu, Y., et al., *SLAM receptors foster iNKT cell development by reducing TCR signal strength after positive selection.* Nat Immunol, 2019. **20**(4): p. 447-457.
158. Scheuplein, F., et al., *NAD+ and ATP released from injured cells induce P2X7-dependent shedding of CD62L and externalization of phosphatidylserine by murine T cells.* J Immunol, 2009. **182**(5): p. 2898-908.
159. Di Virgilio, F., et al., *The P2X7 Receptor in Infection and Inflammation.* Immunity, 2017. **47**(1): p. 15-31.
160. Bartlett, R., L. Stokes, and R. Sluyter, *The P2X7 receptor channel: recent developments and the use of P2X7 antagonists in models of disease.* Pharmacol Rev, 2014. **66**(3): p. 638-75.
161. Kawamura, H., et al., *P2X7 receptors regulate NKT cells in autoimmune hepatitis.* J Immunol, 2006. **176**(4): p. 2152-60.
162. Proietti, M., et al., *ATP-gated ionotropic P2X7 receptor controls follicular T helper cell numbers in Peyer's patches to promote host-microbiota mutualism.* Immunity, 2014. **41**(5): p. 789-801.
163. Heiss, K., et al., *High sensitivity of intestinal CD8+ T cells to nucleotides indicates P2X7 as a regulator for intestinal T cell responses.* J Immunol, 2008. **181**(6): p. 3861-9.
164. Borges da Silva, H., et al., *The purinergic receptor P2RX7 directs metabolic fitness of long-lived memory CD8(+) T cells.* Nature, 2018. **559**(7713): p. 264-268.
165. Di Virgilio, F., G. Schmalzing, and F. Markwardt, *The Elusive P2X7 Macropore.* Trends Cell Biol, 2018. **28**(5): p. 392-404.
166. Rissiek, B., et al., *P2X7 on Mouse T Cells: One Channel, Many Functions.* Front Immunol, 2015. **6**: p. 204.
167. Adriouch, S., et al., *ADP-ribosylation at R125 gates the P2X7 ion channel by presenting a covalent ligand to its nucleotide binding site.* Faseb j, 2008. **22**(3): p. 861-9.
168. Masopust, D., et al., *Preferential localization of effector memory cells in nonlymphoid tissue.* Science, 2001. **291**(5512): p. 2413-7.
169. Kim, S.K., K.S. Schluns, and L. Lefrancois, *Induction and visualization of mucosal memory CD8 T cells following systemic virus infection.* J Immunol, 1999. **163**(8): p. 4125-32.
170. Rissiek, B., et al., *ADP-ribosylation of P2X7: a matter of life and death for regulatory T cells and natural killer T cells.* Curr Top Microbiol Immunol, 2015. **384**: p. 107-26.
171. Rissiek, B., et al., *In Vivo Blockade of Murine ARTC2.2 During Cell Preparation Preserves the Vitality and Function of Liver Tissue-Resident Memory T Cells.* Front Immunol, 2018. **9**: p. 1580.
172. Fernandez-Ruiz, D., et al., *Liver-Resident Memory CD8(+) T Cells*

Form a Front-Line Defense against Malaria Liver-Stage Infection. Immunity, 2016. **45**(4): p. 889-902.
173. Rissiek, B., et al., *Technical Advance: a new cell preparation strategy that greatly improves the yield of vital and functional Tregs and NKT cells.* J Leukoc Biol, 2014. **95**(3): p. 543-9.
174. Hashimoto-Hill, S., et al., *Contraction of intestinal effector T cells by retinoic acid-induced purinergic receptor P2X7.* Mucosal Immunol, 2017. **10**(4): p. 912-923.
175. Schenk, U., et al., *Purinergic control of T cell activation by ATP released through pannexin-1 hemichannels.* Sci Signal, 2008. **1**(39): p. ra6.
176. Schenk, U., et al., *ATP inhibits the generation and function of regulatory T cells through the activation of purinergic P2X receptors.* Sci Signal, 2011. **4**(162): p. ra12.
177. Stark, R., et al., *T RM maintenance is regulated by tissue damage via P2RX7.* Sci Immunol, 2018. **3**(30).
178. Garner, L.C., P. Klenerman, and N.M. Provine, *Insights Into Mucosal-Associated Invariant T Cell Biology From Studies of Invariant Natural Killer T Cells.* Front Immunol, 2018. **9**: p. 1478.
179. Salou, M., et al., *A common transcriptomic program acquired in the thymus defines tissue residency of MAIT and NKT subsets.* J Exp Med, 2019. **216**(1): p. 133-151.
180. Steinert, E.M., et al., *Quantifying Memory CD8 T Cells Reveals Regionalization of Immunosurveillance.* Cell, 2015. **161**(4): p. 737-49.